School of Civil & Mechanical Engineering

Design and Development of a 1-Degree-of-Freedom Leg Exoskeleton for Rehabilitation

Zefang Shen

This thesis is presented for the degree of Doctor in Philosophy

of

Curtin University

May 2019

Declaration

To the best of my knowledge and belief this thesis contains no material previously published by any other person except where due acknowledgement has been made.

This thesis contains no material which has been accepted for the award of any other degree or diploma in any university.

Signature:

Date: 21/05/2019

Acknowledgement

First of all, I would like to express my sincere gratitude to my supervisor Dr. Lei Cui for his continuous guidance and insightful instructions that he has provided during my PhD study. I am also grateful for his encouragement when I had difficulties in my research and patience that he has extended on me along the way. I would also like to thank my co-supervisor Prof. Tele Tan for his insightful comments on my papers and valuable suggestions on my research and thesis.

I thank my fellow colleagues in Biorobotics Lab, Ke Wang, Hamed Rahimi Nohooji, Thibault Rouillard, Pratik Pandya, and Ngoc Tam Lam, for the assistance they have given to my work and the stimulating discussions we had together. I learned a lot from their presentations and discussions with them, which have helped me develop a great interest in research.

I am also grateful to my friends who have shared my joys and sorrows during my PhD study. I thank them for the personal caring they have given to me in the time of difficulties and sickness. Without their friendship and help, my time here would not be so enjoyable.

I would like to extend my gratitude to my family. I thank my parents and my brother for their support and encouragement in my endeavours.

Finally, I would like to thank Department of Mechanical Engineering for the CIPRS scholarship that funds my PhD study.

Abstract

Background

Robotic rehabilitation can assist leg-function recovery for patients after stroke or spinal cord injury. A great number of leg exoskeletons have been developed in the past decades to replace labour-based rehabilitation. However, such exoskeletons are mostly bulky and heavy, confining their applications in clinical settings. Portable exoskeletons are preferred for outside hospital applications.

Portable leg exoskeletons driven by built-in batteries have limited working hours due to low energy efficiency, which hinders their applications beyond clinical settings. Studies in human locomotion energetics have shown that springs with controlled on/off timings, mimicking elastic elements in human legs, can improve the energy efficiency of walking. Such clutched-spring mechanisms (CSMs) may be embedded into leg exoskeletons for longer working hours.

Aims

This thesis was aimed to develop a lightweight and portable leg exoskeleton with a long lasting battery life. We explored planar 1-DOF linkages for their compactness and CSMs for their potential in energy efficiency.

Methods

This thesis proposed a methodology to develop planar 1-DOF linkages for exoskeletons. Problem definition specifies design requirements on the linkages; type synthesis generates candidate designs via an Assur Group based method; dimensional synthesis adopts optimization techniques to obtain linkage parameters. The methodology was used to design a 1-DOF leg exoskeleton for continuous passive motion (CPM) based rehabilitation. CSM studies first examined the mechanisms in a simulation environment, OpenSim, to test their effectiveness at hip and knee joints. Predictive dynamics (PD) was then employed to optimize the stiffness and on/off timings of CSMs embedded in the 1-DOF leg exoskeleton.

Results

The 1-DOF leg exoskeleton was able to closely regenerate a reference gait with maximal errors of 0.09 and 0.12 radians at hip and knee respectively. The leg skeleton has no singularity and its joint ranges of motion (ROM) are safe for users. In the OpenSim simulation studies, CSMs reduced walking metabolic cost by 4.85% and 7.63% when applied at hip and knee joints respectively. CSMs in the 1-DOF leg exoskeleton reduced the motor energy consumption by 17.59% and 15.26% when added at hip and knee joints independently, whereas an energy saving of 30.87% was achieved when applied at both joints.

Conclusions

We proposed a methodology integrating type synthesis and dimensional synthesis for designing planar 1-DOF linkages with multiple outputs. This methodology was used to design a leg exoskeleton driven by one motor, where the hip and knee joint displacement profiles followed closely the given reference motions.

We validated that CSMs could reduce walking metabolic cost when applied at hip and knee joints in OpenSim and applied PD to optimize the stiffness and on/off timings of CSMs embedded in the 1-DOF leg exoskeleton at hip and knee joints to reduce motor energy consumption. A total saving of 30.87% was achieved in the device.

This thesis has shown that a combination of a planar 1-DOF linkage-based design and CSMs can lead to compact and portable leg exoskeletons with long working hours. As a result, such devices can facilitate lower limb rehabilitation beyond clinical settings.

Contents

List of Symbols

θ_i	The i^{th} angular output of in a 1-DOF linkage
θ_{Hip}	Hip joint angular displacement
θ_{Knee}	Knee joint angular displacement
l_i	Lengths of the link sides
φ_i	Angular displacement of the link sides
J	Objective of optimization problems
α_i	Ternary link angles
${}^{H}\theta_j^i$	The i^{th} reference motion point from the j^{th} human joint.
${}^{H}\theta_{hip}^i$	The i^{th} reference motion point from the human hip joint.
${}^{H}\theta_{knee}^i$	The i^{th} reference motion point from the human knee joint.
${}^{E}\theta_j^i$	The i^{th} motion point from the corresponding j^{th} human joint in exoskeleton
${}^{E}\theta_{hip}^i$	The i^{th} motion point from the leg exoskeleton hip joint
${}^{E}\theta_{knee}^i$	The i^{th} motion point from the leg exoskeleton knee joint
r_{hip}	Hip joint motion range
r_{knee}	Knee joint motion range
β_0	Initial displacement of the motor
β_T	Finial displacement of the motor
t_{on}	Turning on timing of springs/actuator
t_{off}	Turning on timing of springs/actuator

F_{ref}	Virtual muscle force
k	Spring stiffness
Δl	Spring stretching length
Δl_{hip}	Hip spring stretching length
Δl_{knee}	Knee spring stretching length
Δl_{Ankle}	Ankle spring stretching length
d_{AB}	Distance between spring connecting points A and B
d_{CD}	Distance between spring connecting points C and D
d_{EF}	Distance between spring connecting points E and F
$\boldsymbol{q}$	Link sates
τ	Joint torques
$C(u)$	B-spline curve
P_i	The i^{th} control points of a B-spline
m_i	Mass of the i^{th} link
I_i	Moment of inertia of the i^{th} link
$\dot{\varphi}_i$	Angular velocity
$\ddot{\varphi}_i$	Angular acceleration
R_i	Arm of centre-of-mass position in the i^{th} link's local frame
γ_i	Angle of R_i in the i^{th} link's local frame
T_{spring}^{hip}	Hip spring torque
T_{spring}^{knee}	Knee spring torque

t_{on}^{hip} Hip spring turning on time

t_{on}^{knee} Knee spring turning on time

t_{off}^{hip} Hip spring turning off time

t_{off}^{knee} Hip spring turning off time

k_{hip} Hip spring stiffness

k_{knee} Knee spring stiffness

List of Figures

List of Tables

Part I Introduction

Chapter 1 Introduction

1.1 Motivations

Stroke happens when a shortage of blood flow occurs in the brain. This can affect the functionality of parts of the brain, leading to loss of movement. In 2016, 13.7 million people suffered from stroke, and about 79.6 million people had previously encountered a stroke [1]. People over 65 years old are more vulnerable to stroke, accounting for nearly three quarters of stroke patients [2].

The aging population may further worsen the situation [2, 3]. People greater than 60 years will consist of 23% of the global population by 2050, whereas the numbers will reach 30% in China and Europe. As stroke and osteoarthritis are more prevalent in elderly individuals, aging population projects an increased number of stroke patients.

Stroke can affect the functions of sensation, motor, and cognition [4]. Motor impairment is the common consequence of stroke, which can affect the patient's daily activities. There exists a neuroplasticity widow after a stroke, utilizing which can greatly improve the motor function recovery. Rehabilitation is, therefore, used to boost patients' regain of motor skills after stroke. Studies show that task-oriented training is able to acceleration functional recovery [5]. Such trainings are considered more effective with high-intensity and repetitive training task [5, 6]. Constrained-induced movement therapy is able to

reduce disability in the arms after stroke [7]; Gait-oriented training can improve walking competency after stroke [8].

In addition to stroke patients, 250,000 to 500,000 people suffer from spinal cord injury every year. Spinal cord injury (SCI) can lead to premature death and loss of mobility. Damage to the spinal cord, resulting from physical trauma (accidents) or non-physical trauma (infection or tumours), can cause symptoms such as muscle atrophy, loss of sensation function, etc. [9]. SCI also brings about secondary complicates such as muscle atrophy, pressure sores, infections and breathing problems [10, 11].

Relearning of walking enables the patients to ambulate and conduct daily activities independently, improving living quality and reducing the risk of secondary complicates. Patients would, otherwise, be wheelchair-bounded. Rehabilitation programs develop compensation strategies to develop alternative movement patterns and utilize the neural plasticity of the spinal cord to reorganize the neural circuits for functional recovery [12, 13]. Repetitive task practice is usually employed to assist spinal cord injury patients for improving speed and accuracy of walking [9, 14]. Such practices are accomplished via over ground training, treadmill training, or body weight supported training [15]. Studies have demonstrated improvements in walking through those rehabilitation programs [12].

For stroke and SCI patients, locomotion remains the top priority to complete daily tasks, reducing dependence and ensuring a good quality of life. Considering the great number of patients suffering stroke and spinal cord injury, increasing access to rehabilitation services is of significance.

Conventional rehabilitation requires at least 2 therapists to guide a patient in walk training. The reference gait is, therefore, unstable, and the intensity of the gaits training is limited. Robotic rehabilitation has then been introduced to tackle such issues. Rehabilitation robots can fully support the motion of the user and generate highly repetitive gait patterns. Robots can also increase the intensity of training easily. These advantages have greatly encouraged the development of rehabilitative robots.

A great number of rehabilitation devices for leg training have been developed in the past decades to exploit the benefits of robotic rehabilitation. However, many of the devices are limited to hospital or therapy centres due to their complexity, bulkiness and high energy consumption. To enable outside hospital application, portable devices are preferred. In addition, energy efficiency also needs to be considered for long working hours. However, current portable systems only allow continuous operation for several hours.

1.2 Aims and Objectives

This thesis focuses on developing a portable leg exoskeleton based on a planar 1-DOF linkage for reproducing a human-like gait pattern at the hip and knee joints. It also attempts to improve the energy efficiency of the leg exoskeleton by implementing CSMs at hip and knee joints.

The following objectives have been proposed to fulfil the aims of the thesis.

a) Proposing a design methodology of designing planar 1-DOF linkages with only revolute joints for multiple successive function generation outputs.
b) Developing a 1-DOF planar linkage-based leg exoskeleton design for reproducing human-like gait pattern at hip and knee joints.
c) Exploiting clutched-spring mechanisms at the hip and knee joints for saving walking metabolic cost.
d) Proposing a method for obtaining optimal clutched-spring mechanism parameters.
e) Implementing the clutched-spring mechanism in the leg exoskeleton for a better energetic performance.

1.3 Thesis Outline

The thesis includes four parts with 8 chapters; details are given as follows.

Part I Introduction

Part I states the motivations, aims and objectives of this thesis. It also provides background knowledge and review of related work.

Chapter 1 begins with the motivations of developing portable and energy efficient leg exoskeletons. Aims and objectives are then proposed to achieve such a leg exoskeleton design. The chapter ends with a description of the structure of the thesis.

Chapter 2 first introduces robotic rehabilitation in comparison with conventional rehabilitative programs, where the benefits of robot-based rehabilitation are reviewed. A literature review on lower-limb-rehabilitation devices follows to sum up and categorize the current robotic rehabilitation devices. Exoskeleton type rehabilitative robots are further reviewed in detail with their pros and cons discussed. The chapter then investigates 1-DOF linkage for leg exoskeleton design. The chapter also reviews attempts to reduce human locomotion energy, which may benefit the energy performance of the proposed leg exoskeleton.

Part II Leg exoskeleton development – linkage design focused

Part II introduces a design methodology of developing 1-DOF linkage-based exoskeletons. This part also presents the development of a 1-DOF linkage-based leg exoskeleton based on the proposed method.

Chapter 3 proposes an integrated type and dimensional synthesis method to generate and optimize linkages for multiple successive angular outputs. Its application on exoskeleton devices is also discussed in detail. First, design requirements on developing 1-DOF linkage for rehabilitation exoskeletons have been discussed. Secondly, a type synthesis method is proposed to generate candidate linkages. Dimensional synthesis, adopting optimization techniques, then examines the candidate linkages for reproducing human-like motions.

Chapter 4 presents the development of the leg exoskeleton in terms of linkage design, actuation design and control system development. Following the design method in Chapter 3, the chapter first details the design of a 1-DOF linkage for reproducing human-like walking gait at hip and knee joints. Modelling for manufacture, simulation for actuation design, and open-loop control system for easy operation are then presented. The chapter ends with the evaluation of the leg exoskeleton prototype.

Part III Clutched-spring mechanisms for energy efficiency

Part III focuses on the energy saving effects of CSMs in human walking and in the proposed 1-DOF leg exoskeleton.

Chapter 5 examines clutched-spring mechanisms for saving walking energy cost when applied at the hip or knee joint. The chapter first introduces a human motion simulation platform, OpenSim, for the simulation study. It then presents the method to approximately obtain the optimal parameters of the clutched-spring mechanisms. The optimal parameters are then evaluated.

Chapter 6 employs another method, PD, to obtain optimal CSM parameters. The chapter first introduces the preliminaries of the method. A study on a pendulum leg is then presented to test the PD method for optimal CSM design. The study tests the effectiveness of the PD method and investigates the energy saving capability of the CSMs.

Chapter 7 introduces CSMs into the leg exoskeleton at hip and knee joints. The chapter first gives the kinematic and dynamic analysis of the human-exoskeleton model for the establishment of the PD optimization problem. The chapter then compares the energy saving effects of the clutched-spring mechanisms when applied at the hip, knee, or both joints.

Part IV Conclusions

Chapter 8 concludes the work on 1-DOF linkage design method, the development of the 1-DOF linkage-based leg exoskeleton, the clutched-spring mechanism studies and its application in the leg exoskeleton. Further work is also presented.

Chapter 2 Literature Review

2.1 Introduction

Literature review on the effectiveness of robotic rehabilitation is first conducted, as it is the foundation for developing rehabilitative robots. Robotic rehabilitation in stroke and SCI patients is then presented. The current devices are classified to analysis their advantage and limitations and to identify challenges in rehabilitation robots design: portable design and energy efficiency.

One-DOF linkages in exoskeleton applications and leg mechanisms are investigated for their potential for leg exoskeleton designs. The possibility of a combination of 1-DOF leg exoskeleton and CPM is also examined. To improve leg exoskeleton's energy efficiency, studies on saving human walking energy have been reviews in search of a solution.

2.2 Lower Limb Robotic Rehabilitation

2.2.1 Introduction

With the enormous development of in robotics, robot-based rehabilitation has been adopted to boost recovery after stroke and spinal cord injury. Robot-assisted gait training after stroke facilitates independent walking learning [16]. Individuals who are in their first 3 months after stroke benefit the most from such devices when they are not able to walk.

Electromechanical devices can also assist upper limb function recovery in terms of arm and hand function, and arm and hand muscle strength [17]. For incomplete SCI patients, robotic exoskeletons retrain them to walk at modest speeds [9]. Patients who undergo robotic gait training achieve better mobility outcomes compared with those received conventional over ground training [15].

A number of inherent advantages of robotic device accounts for the proliferation of robots in rehabilitation, and would continue to contribute in the future. In comparison with conventional training programs, robotic rehabilitation features continuous, natural and highly reproducible movements in the limbs. Rehabilitation robots can also increase doses and prolong duration. Moreover, robotic training provides the possibility for assessing the patients' performance. Other benefits may include reduced labour burden on therapists and early intervention for patients with severe dependence.

2.2.2 Lower Limb Rehabilitation Devices

The capacity of robots to deliver therapy programs with high intensity and repeatability has encouraged development of rehabilitation robots. As a result, a great number of robots have been created to assist therapistsi in boosting patient recovery after stroke and spinal cord injury [18-21]. Such devices adopt various design schemes, such as foot plate type, cable driven, exosuit and exoskeleton type. These different design schemes bring them various functionalities.

Foot-plate-based training robots utilize a pair of preprogramed moving foot plates to delivery gait training for its simplicity [22-25]. With additional support for body weight and balancing, a patient fastens his/her feet on the foot palates to follow the movements provided by the robots. As these devices only focus on the motion of the feet, this requires the patient's musculoskeletal system to be intact. Moreover, precise assistance at the leg joints are absent in foot-plate-based devices.

In recent years, there is an increasing interest in cable-driven parallel robots for its light weight and elimination of joint alignment problem. These devices use cables connected to human lower limbs to guide the leg motions. In [26], the robot exercises the patient's leg at hip and knee joints while the patient remains laying down. Cable-driven parallel robots for walking assistance has also been proposed [27-29]. However, such devices require fixed frames for mounting the motors and supporting the patient. This makes them unsuitable for portable designs.

Recent studies also attempt to use soft exposits for rehabilitation. Soft exosuits try to eliminate the mass and rigidity of mechanical structure. They use textiles to transit tension forces to assist joint movements. Such devices are popular for assisting healthy individuals for less energy consumption [30-33]. These devices seem promising for light weigh rehabilitation devices. However, such devices can only generate tension forces to compensate the human muscles, and they are restricted to providing a small amount of

assistance [28]. They cannot assist a patient through an entire walking cycle. Their application is limited to patents who have major functionalities left after an illness.

The commonly adopted design with successful application in a great number of devices is the exoskeleton type [2, 34, 35]. Leg exoskeletons mimic the human musculoskeletal system, where mechanical structure resembles the human leg skeleton and motor actuation replaces muscle power. Due to its similarity to the human leg, such a device can be easily attached to the leg and operate in synchronization with the human leg.

Ether foot-plate or cable-driven platforms requires a bulking structure to support the patients and guide the leg motions. This restricts their application in clinical settings. Exosuits might provide a light-weight and compact solution. However, as exosuits employ tendons which can only exert tensile forces, they can only provide a small amount of assistance. Fully support for leg movements is not practical. Therefore, their application suits best for patients sustaining leg functions. On the contrary, portable leg exoskeletons, not only enable outside hospital training but also provide full support at the leg joints. They may provide a solution for rehabilitation beyond hospitals, e.g. at home.

2.2.3 Leg Exoskeletons

The first creation of a leg exoskeleton dates back to 1980s when GE developed the first exoskeleton which attempted to combine human intelligence and robot power [36]. This has triggered enormous interest in developing exoskeleton devices for human strength augmentation, locomotion assistance, and rehabilitation.

Leg exoskeletons for strength augmentation combine mechanical structures and motor power to enhance the user's capability for lifting, carrying loads, walking longer distances, etc. [37-41]. Such devices resemble the human leg and provide actuations at the various joints (ankle, knee and hip joint). They can be used by factory workers transporting heavy loads constantly.

Leg exoskeletons for locomotion assistance are developed for patients who have partially or fully lost functionalities in their legs [42-48].These devices provide functions that enable a patient to complete daily locomotion tasks, such as level ground walking, sit-to-stand transition, stand-to-sit transition, stair climbing and descending, etc. The use of such devices encourages the patients' independence and increases their quality of life.

Leg exoskeletons has also been developed to facilitate rehabilitation after stroke, spinal cord injury, and surgery. In the 1990s, scientists started to develop exoskeleton-based devices to relief labour burdens on physiotherapist. Many exoskeleton-based

rehabilitation systems have been proposed ever since. Rehabilitation leg exoskeletons generally occur in three major categories according to their training scheme: treadmill-based systems, level ground training platforms, and portable devices.

Treadmill based systems [49-51] combines a treadmill, a pair of leg exoskeletons, and a weight-support system, which allows such systems to deliver intensive rehabilitative trainings. They also enable monitoring the rehabilitative effect. This facilitates the design of rehabilitation programs that maximize outcome. However, the treadmill-based design does not truly reflect the real level-ground walking, and the complex configuration limits their application in hospital and clinical settings.

Level ground training robots [52-55] replace the treadmill with a moving platform to enable level ground walking practice. These robots also employ a weight support system to balance the patient during walking, which limits the training programs to level-ground walking. Similar to the treadmill-base system, such robots are either portable.

More recently, a number of portable leg exoskeletons [48, 56], previously developed for paralysed individuals, have been tailored for rehabilitation purposes. Such exoskeletons feature a built-in battery supply and a control system. Wearing such an exoskeleton, a patient can walk independently with the help of crutches for balancing. Such portable leg

exoskeleton may bring rehabilitation outside clinical settings. However, such leg exoskeletons still suffer from a high weights and a short battery life.

Current robotic rehabilitation programs are only available in hospitals and rehabilitation centres due to complexity, bulkiness and high cost of the devices. This has limited the access to rehabilitation services for patients in need. Ideally, patients should access rehabilitation service easily when they need. Compact and portable leg exoskeletons may provide rehabilitation beyond hospitals and increase access to rehabilitation service. However, improvements in portability and battery life are still required.

Though the current portable leg exoskeletons may provide rehabilitation outside hospitals, they are still cumbersome, and the systems still lack long duration power supply solutions [57]. Therefore, developing compact and portable leg exoskeletons and improving energy their efficiency is of significance.

2.3 Planar 1-DOF Linkages for Leg Exoskeleton Design

2.3.1 Planar 1-DOF Linkages with Only Revolute Joints

Planar linkages have various applications in life and engineering, without exception in exoskeletons. Due to their simplicity, planar linkages can be found in upper limb exoskeletons [58-61], hand/finger exoskeletons [62-64] and leg exoskeletons [65-67]. Planar linkages in upper limb exoskeletons serve to create virtual rotation centres that

aligns with the human shoulder joint [58, 59], to assist reaching tasks [60], and to support the weight of exoskeleton and human arm [61]. Linkage-based designs are especially popular in finger/hand exoskeletons due to the limited space around the fingers for mounting motors for serial-chain-based design. Combined with cable actuation, linkage-based design relocates the motors to a base, resulting in compact and lightweight exoskeletons. Some leg exoskeletons also involve planar linkages. Banala et.al adopted linkage for a gravity-balancing leg orthosis [65]; Kim et.al developed a knee exoskeleton using linkage that aligns the exoskeleton joint with the human knee joints [66]; Copilusi et.al presented a planar linkage that can drive the human leg [67].

Current linkages in exoskeletons are usually used for joint alignment, weight supporting and relocating actuators in assistance of other designs. Only limited attempts have been made for reproducing human-like motion using a pure linkage-based design [60, 67]. Until recent years, a number of finger exoskeletons exploited 1-DOF linkage to regenerate finger curling motion [68-71]. These devices introduce simplicity in mechanical design, sensing, and control, which results in compact and easy to operate devices. Such designs may hint the future of portable exoskeleton devices for outside hospital applications.

Single-DOF planar linkages bring about several benefits for exoskeletons designs. As 1-DOF planar linkages have a closed structure, motions provide by such devices can be highly stable and repetitive. The closed loop structure also comes with safety features, as the motion is rigidly predefined by the linkage structure. Using a single motor also

simplifies the actuation design significantly, which can lead to compact control and sensing systems. The simplicity in mechanism, sensing, and control system can make the overall device compact and lightweight.

Though 1-DOF linkages have been successfully applied for finger exoskeletons, no attempts have been made for leg exoskeleton designs. On the contrary, a great number of 1-DOF leg mechanisms have been proposed in the literature [72-85], which indicates their feasibility for leg exoskeleton designs. Many of these linkages were built for legged robots, in which the linkages are required to generate certain motion patterns at the foot end to enable desired motions, e.g. walking. Several linkages even resemble a human-leg-like morphology [72, 80, 82]. Such linkages indicate 1-DOF linkages' potential for wearable linkage-based leg exoskeleton.

The targeted to 1-DOF linkage aims to provide planar motion at the hip and knee joints. It is important to investigate whether such a motion is suitable for the human leg. Human hip joints have three DOFs, namely flexion/extension, abduction/adduction, and internal/external rotation, while knee joint is usually simplified as 1-DOF for flexion/extension. For human walking, hip flexion/extension and knee flexion and extension are the dominating motions which reside in the sagittal plane. Therefore, a 1-DOF planar linkage is possible to assist such planar motions.

2.3.2 Planar 1-DOF Linkage Design Method

Applying single DOF linkages to exoskeleton designs challenges such mechanisms to produce multiple successive function generation outputs with a single input. This question has not been addressed in the literature. A typical mechanisms design problem involves 3 major steps: problem definition, type and dimensional synthesis. In the current studies [68, 70], problem definition has not been fully discussed, for example, important issues like a human morphology, joint range of motion (ROM) and singularity conditions are not fully considered. Type synthesis is ignored, and dimensional synthesis fails to take care of several issues due to a lack of inclusive discussion on problem definition.

Problem definition concerns the functional requirements on the exoskeletons. Above all safety should be guaranteed during the training, where ROM and singularities are considered. They also need to reproduce the human movement pattern to deliver rehabilitation practices. In addition, the devices should also be easy to don and doff.

Type synthesis proposes mechanisms that can satisfy the functional requirements. A great number of approaches have been developed to solve the problem for planar chains [86, 87]. Two groups of methods are frequently involved. One group which has been exploited intensively is based on graph theory [88-92], in which linkages are represented by graphs. By enumerating the graphs and ruling out isomorphic designs, these methods can propose all the linkage types topologically with a given number of links and DOFs. Another group is based on a concept named Assur Group [91]. These approaches build up linkages by

adding Assur Group elements onto the previous links or the base to introduce additional loops.

Both methods are able to propose candidate linkages. However, the graph-theory-based methods mainly focus on enumerating the linkage types topologically. When converting the topological graphs into functional linkages, additional efforts are needed to tackle the design requirements. As the requirements increase, these methods become difficult to implement. By comparison, Assur Group based methods adopt a more straightforward scheme to build up linkages. Design requirements can be taken care of easily while constructing the linkages.

Dimensional synthesis aims at finding the optimal linkage parameters. Available methods fall into three categories: graphical, analytical and optimization-based methods. In the early stages, graphical methods were developed to find feasible dimensions for given tasks [92-95]. Such methods are helpful to obtain insights into the design problem and find approximate dimensions for linkages with a small number of links. The methods become less feasible when accurate dimensions of a linkage are required. Moreover, the methods become difficult to implement as the link number increase.

Analytical methods adopt a number of precision points to achieve accurate linkage dimensions [96, 97]. These methods have been intensively used to design four-bar linkages tracking several precision points [94, 98-100]. The methods were later developed for more complex linkages [71, 101-105].

These methods are able to obtain accurate linkage dimensions that let the linkage restrictively pass through several precision points. Algebraic formulations are required to implement such methods on a linkage. This is become difficult to carry out as the number of links increases. Therefore, such methods are suitable for linkage with a small number of links, such as four-bar, six-bar, and eight-bar linkages.

In the context of exoskeleton design, the general shapes of the outputs are considered over the accuracy at certain points. The general shapes of the linkage output resemble a human-like motion. Tracking precision points using analytical methods may violate the generation of a human-like motion.

Modern methods for linkage design often involve optimization techniques. A great number of optimization methods have been developed with two major groups being studied intensively [95]. Gradient-based methods [106-108] use gradient information of the objective function to search for a minimum. These methods rely on the supplied initial population which leads to local minima.

In recent decades, evolutionary algorithms [109-113], especially genetic algorithms [114, 115], have been studied for linkage synthesis intensively with promising results. These algorithms can effectively explore the solution space for a global optimum. They can also

tackle geometric constraints easily. In a word, these algorithms lend themselves well for designing complex mechanisms with constraints.

2.3.3 Continuous Passive Motion in Rehabilitation

Continuous passive motion (CPM) delivers repetitive and slow motions to a human joint (e.g. knee joint) to boost rehabilitation, which is carried out by a CPM machine in a hospital or rehabilitation centre. It can assist the recovery the range of motion at the aimed joint, prevent muscle degeneration, and reduce pain. This makes CPM a popular rehabilitation scheme after a total knee replacement, an excision of scar tissue, and fracture in the arm or leg.

The concept was first introduced in 1970 by Robert B. Salter [116, 117]. The author, together with his colleagues, latter conducted experiment on rabbits using CPM for the healing of full-thickness articular cartilage defects penetrating the subchondral bone of rabbit knee joints [116]. Their study reported superior outcomes of CPM group compared with immobilization and intermittent active motion group. CPM was proved effective for stimulating the healing of joint defects and preventing joint stiffness. The authors then extended CPM for clinical application on humans for immediate postoperative treatment [117]. Nine case studies showed that CPM can be safe to use, reduce postoperative pain and help recover joint range of motion.

Since the invention of CPM, it has been exploited for rehabilitation following joint surgery. For example, rehabilitation for ankle joint [118] to reduce joint stiffness, wrist [119] to decrease spasticity, elbow [120] to tackle flexion contractures. CPM is also popular among shoulder joint rehabilitation [121-123] and finger/hand rehabilitation [124-126]. It is used for pain relief, ROM recovery [122, 123], muscle strength and function [123] in the shoulder, and for flex tendon repair [125, 126].

Though CPM is popular among joint rehabilitation, it can also be applied to patents following stroke [127] or spinal cord injury [128, 129]. For stroke patients, CPM has been tested for improving shoulder joint integrity. For spinal cord injury, CPM can be used for reducing hypertonia and revering adapted spinal circuit.

Current exoskeleton devices usually have the passive model which can provide CPM-based rehabilitation. However, such exoskeletons are aims to provide more complicated rehabilitation programs, they turn out to be bulky and complicated. As CPM scheme is much compact compared with other protocols such as: interactive or assist-as-needed. A device based on CPM can be more portable and lightweight. Therefore, this thesis investigates the combination of a linkage-based design and CPM for a compact and portable leg exoskeleton.

One-DOF linkage design has a parallel structure, which can provide highly repetitive and stable rehabilitation exercise. This makes such devices well-suited for CPM based

rehabilitation. However current devices are mostly developed for finger or hand rehabilitation. No 1-DOF linkage-based leg exoskeleton has been developed.

2.4 Energy Saving in Leg Exoskeletons

2.4.1 Energy Saving Attempts in Leg Exoskeletons

Current rehabilitation exoskeletons usually utilize a fixed frame or movable platform, which requires a significant amount of power supply. Some portable devices, like ReWalk and Ekso use portable power supplies to make the device standalone. However, working hours of such devices are limited to several hours owing to the size of the batteries [130]. Realizing a long operation duration with limited battery size requires improving the energy efficiency of the devices.

A good source of energy saving techniques can be from human walking itself, as humans tend to walk with minimal energy cost [131-135]. Leg exoskeletons mimic human walking gait by the means of a mechanical musculoskeletal system. Therefore, understanding the human locomotion energetics would inspire techniques to improve the energy efficiency of the human-exoskeleton system as a whole. Techniques applied to humans for locomotion energy saving would also benefit the human-exoskeleton system.

High efficiency of human walking is mainly achieved through two major means: passive dynamics and elastic energy utilization [136]. Passive dynamics walking interprets human

walking as an inverted pendulum; Energetic exchange happens between kinetic and potential energy in walking. Elastic energy utilization stores gravitational potential and kinetic energy as elastic energy in compliant tissue and tendons and release the energy to assist movements.

Drawing from the insights of human walking, especially elastic energy utilization, a number of studies attempted to make walking even more energy efficient [130, 137-139]. In [137], the author proposed 4 conceptual exotendon designs to save joint energy for walking. The exotendon demonstrated great potential for offloading joint moment and reducing joint work. The conceptual design was later evaluated by another study [130]. However, the experimental study disapproves the underlining assumptions and end up not saving metabolic cost. Another study [140] employed springs and dampers, with controlled timings, in a load carrying exoskeleton. When the passive elements are involved in walking, the study demonstrated energy saving compared with walking without the passive elements. Collins [138] further exploited the capability of passive elements using a clutched-spring mechanism at the ankle joint. The study ends up with 7.2% metabolic cost saving walking with the exoskeleton, convincing the effectiveness of a fully passive exoskeleton.

The clutched-spring mechanisms utilize the negative and positive energy pattern at the ankle joint to store and realize energy to assist human locomotion. The spring is turned on when heel strike happens, as the human propels, the spring stretches and store elastic

energy. In the following push-off, the stored energy is released, assisting push-off. Then the spring is deactivated before the next heel strike. The study also investigated the optimal spring stiffness on energy-saving performance. Highest energy saving was observed at a medium stiffness. Higher or lower spring stiffness both increase the metabolic cost. The study underscores the importance of proper spring stiffness and on/off timings of the spring for saving human locomotion energy.

The negative/positive energy pattern also exists at hip and the knee joints [139]. Though ankle joint has the highest potential for energy saving, as ankle joint account for the largest portion of negative/positive energy during walking, applying the CSMs at the hip and knee joint may also save metabolic cost due to the same energetic pattern.

CSMs may also improve the energy efficiency of leg exoskeleton devices. Leg exoskeletons mimic the motion patterns of the human leg. The techniques benefit human motion energetics may also reduce mechanical work by the leg exoskeleton motors. Limited working hours remaining a major obstacle for practical application of portable leg exoskeleton. Implementing CSMs in an active exoskeleton may help reduce the energy cost of the devices. This may extend the battery life for longer working hours.

2.4.2 Energy Saving with Human Motion Simulation

The CSM parameters in [138] were obtain based on energetic data from subject's locomotion and a great number of experiments. This method becomes impractical when designing clutched-spring mechanisms for a given individual. On the contrary, virtual modelling has advantages in device prototyping, especially in reducing design time and cost. Some simulation methods may obtain optimal CSM design via studies on a human-exoskeleton model.

2.4.2.1 Data-Driven Human Motion Simulation

Data-driven method for simulating human walking utilize captured motion and optimization to reveal the muscle forces [141-144]. In the optimization problem, muscle forces are the design variables; metabolic cost per unit distance usually serves as the objective; forward dynamics were carried out by integrating the equations of motions. The captured motions are used as constraints to ensure the model accurately reproduce the captured motion. Solving the optimization problem return the muscles forces that lead to the captured motion.

A number of programs, that support comprehensive musculoskeletal models [145-148], are developed based on data-driven simulation methods. These programs are able to measure and compute key biomechanical quantities ranging from limb position and tendon extension to joint torque and power. Some of the programs also support the

addition of external structures, which allow researchers and engineers efficiently to test their devices in virtual simulation rather than constructing a physical prototype.

The desired software package should meet the following requirements to study metabolic cost: a close musculoskeletal simulation of human walking, modelling of an exoskeleton and metabolic consumption calculation. OpenSim [147] provides readily human gait models built on accurate experimental observation and features tools for metabolic cost calculation. Therefore, OpenSim is suitable for investigating the energetic effects of clutched-spring mechanisms at the hip or knee joint.

2.4.2.2 Predictive Dynamics

An optimization-based human motion simulation method was proposed by Xiang [149] in 2010. The author named the method predictive dynamics. PD [149] is an alternative method to simulate human motion while considering the physics of the human body and the environments. It is an optimization-based approach, in which performance measures were minimized. Several constraints such as joint torque limits, joint ranges of motion, constraints for specific tasks, etc. are included. The method does not require captured motion of the human model and the forces that cause the motion. The method itself can generate natural motion and reveal the forces required to achieve the motion.

The human body itself is a complicated system consisting of many segments. The mathematic model for human motion involves highly nonlinear coupled differential equations. In addition, several constraints need to be considered according to the complexity of the motion of consideration. Integrating the equations to reproduce the human motion is almost impossible. While in the PD formulation the equations of motion are used for inverse dynamics (ID) or serve as constraints. Therefore, the integration of the equations of motion is avoided in PD. This method makes the prediction of human motion possible for highly complicated dynamics system of the human body.

As the PD method uses performance measures to guide the motion of the human model instead of tracking captured motions, it is able to predict the human when the model parameters are changed. This feature makes predictive dynamics suitable for cause and effect study.

The method has been successfully applied to reproduce/predict motion humans for walking, running, lifting climbing, etc. As the method enables cause and effect study on the human motion, for example, predicting the human gait with increasing loads, it has the potential to be extended to conduct simulation on a human-exoskeleton model. It may have the ability to assist in the development of leg exoskeleton devices.

2.5 Conclusions

Robotic rehabilitation has been proved effective to assist patients to regain locomotion skills. Portable exoskeletons provide a solution for walking training robots beyond clinical settings. Moreover, single-DOF linkages have the potential for compact and portable devices, which can be used for CPM based rehabilitation.

Improving the energy efficiency of leg exoskeletons is of significance considering the limited operating hours of current devices. Insights in human walking energetics and techniques to improve walking energy efficiency provide potential solutions for higher energy efficiency in exoskeletons. Human motion simulation platforms may be used to study clutched-spring mechanisms for locomotion energy saving at hip and knee joint. PD may introduce clutched-spring mechanisms into leg exoskeletons, while obtaining optimal clutched-spring mechanism design.

Part II Leg Exoskeleton Development – Linkage Design Focused

Chapter 3 A Planar 1-DOF Linkage Design Methodology for Exoskeletons

Abstract

Recent compact exoskeleton designs employ 1-DOF planar linkages with only revolute joints to drive multiple joint angular outputs. This has introduced a challenge in mechanism design: generating multiple successive function generation outputs using planar 1-DOF linkages. A systematic design methodology involving problem definition, type synthesis, and dimensional synthesis was proposed in this chapter to solve the problem. Problem definition identifies the requirements on 1-DOF linkage-based exoskeletons. Type synthesis proposes candidate linkages for multiple successive angular outputs, while dimensional synthesis optimizes them for reproducing a reference motion.

3.1 Introduction

This thesis attempts to use planar 1-DOF linkages for a leg exoskeleton design. The aimed linkage is required to reproduce a human-like gait pattern at hip and knee joint. This creates a linkage design problem that has not been addressed in the literature: generating multiple successive function generation outputs using planar 1-DOF linkages with only revolute joints.

A systematic solution to the problem requires three major components in mechanism design: problem definition, type synthesis, and dimensional synthesis. Type synthesis should thoroughly discuss the issues of 1-DOF linkages for exoskeleton applications and propose proper requirements. Type synthesis needs to generate a sufficient number of candidate linkages for selection. Dimensional synthesis should be able to obtain the linkage parameters to track a reference motion.

3.2 Linkage Design

3.2.1 Problem Definition

Developing a single DOF linkage-based rehabilitation exoskeleton demands a number of requirements to make the desired device functional.

1) The linkage should be a planar single-DOF linkage with only revolute joints.
2) Compactness should be ensured wherever possible. This can be done by restricting the number of links and link dimensions.
3) The exoskeleton should have a human morphology to make the device easy to wear. This requires that the counterparts of the human leg components in the exoskeleton share the same lengths with the human's, and the overall shape of the exoskeleton should resemble the human body.
4) The exoskeleton should be able to mimic human motions closely to provide rehabilitative movements. This can be achieved by generating multiple successive function generation outputs that replicate the human joint angular profiles.

5) Safety issues should be tackled carefully. Joint ROMs and singularities need to be considered in this regard.

3.2.2 Type Synthesis

In this thesis, we adopted a similar Assur Group based method from [91]. The type synthesis for linkages with 2 or 3 outputs is given in Fig. 3.1. At first, an RRR dyad is added onto the base AB and the rotating link AD to form a four-bar linkage ABCD. The first angular output is generated between the base and side BE. For the second angular output, dyad EFG is connected to the four-bar linkage. As joint E is attached to BE, the number of linkage types equals the number of connecting options for joint G. Three options (base, link AD, CD) are available for joint G. In such a way, the 3 linkage types for 2 angular outputs can be proposed. Similarly, 5 options (base, link AD, CD, BCE, FG) are available for joint J. Therefore, totally 15 types can be enumerated for 3 angular outputs.

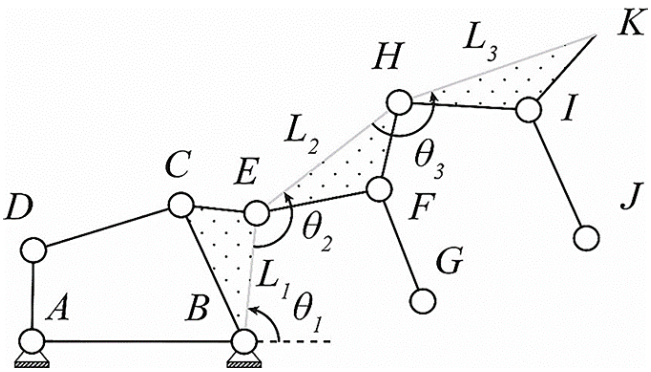

Fig. 3.1 Type synthesis

We can use this method to propose linkages with 2 or 3 angular outputs as in Fig. 3.2 and Fig. 3.3. The output links are in grey. Note that the linkages types in Fig. 3.3 are developed upon type a_0, b_0, and c_0 from Fig. 3.2

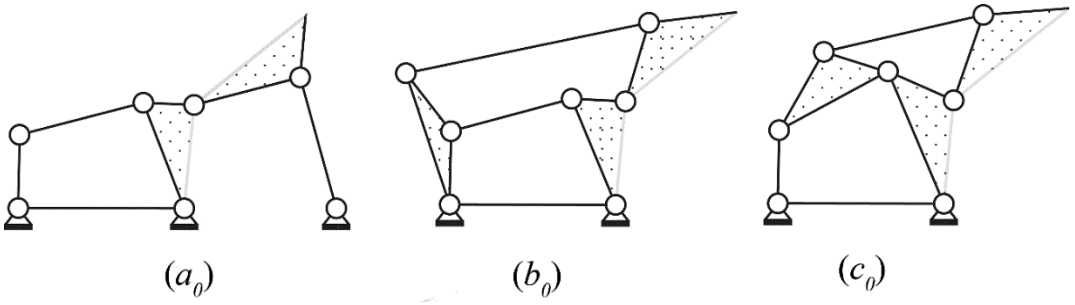

Fig. 3.2 Linkage types for 2 angular outputs

All the proposed linkages consist of a number of loops. In each loop, the added dyad accounts for the two output links. Therefore, each loop has two different configurations. This leads to multiple configurations for a given type. For example, type (a_0), which consists of 2 loops, has 4 configurations. As these configurations return different angular outputs, they are regarded as different designs. Thus, for the 2-output linkages from Fig. 3.2 there are 12 different designs. For 3-output linkages from Fig. 3.3 there are 120 designs. Notations to represent the design are introduced in Fig. 3.4 for convenience. The letter with subscript indicates the linkage types from Fig. 2 and Fig. 3.3. The following 1s and 2s give information about loop configurations. They are given according to the kinematic analysis on the linkages.

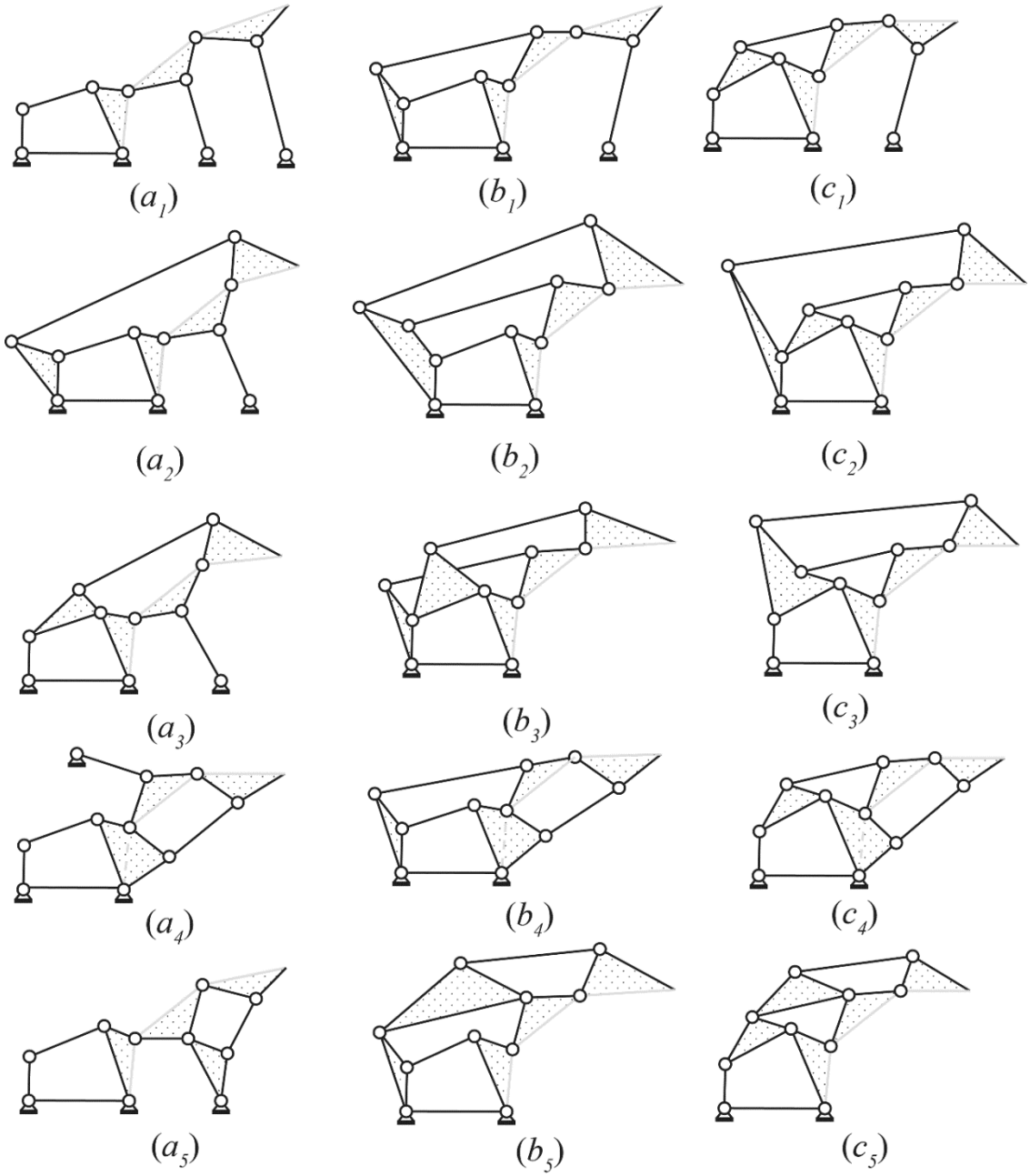

Fig. 3.3 Linkage types for 3 angular outputs

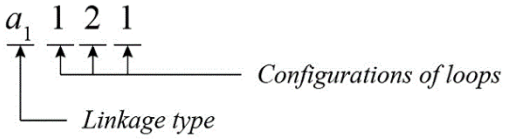

Fig. 3.4 Linkage notations

3.2.3 Dimensional Synthesis

Dimensional synthesis is realized by solving a constraint optimization problem. Design variables are first determined according to the linkage type and task requirements. Then the objective is established to evaluate the performance of the linkage, followed by constraints and bounds. Solving the optimization problem via evolutionary algorithms returns the optimal values for the design variables. This study concerns the angular output of the linkages, therefore, kinematic analysis is needed for angular outputs.

3.2.3.1 Kinematic Analysis

Kinematic analysis models the angular outputs as a function of the linkage parameters and the active DOF. A vector loop equation on each loop can be established as:

$$\sum_{i=1}^{N} l_i e^{i\varphi_i} = 0 \tag{3.1}$$

where, N is the total number of links in the loop, l_i the length of the i^{th} link; φ_i the angular displacement of the i^{th} link.

Let l_{n-1} and l_n and be the output links in that loop. Solving equation (3.1) for angular displacements of l_{n-1} and l_{n-1} yields:

$$\begin{aligned} \varphi_{n-1} &= 2\tan^{-1}\frac{F_{N-1} \pm \sqrt{E_{N-1}{}^2 + F_{N-1}{}^2 - G_{N-1}{}^2}}{E_{N-1} - G_{N-1}} \\ \varphi_n &= 2\tan^{-1}\frac{F_N \pm \sqrt{E_N{}^2 + F_N{}^2 - G_N{}^2}}{E_N - G_N} \end{aligned} \tag{3.2}$$

where

$$E_{N-1} = 2l_{N-1}\sum_{i=1}^{N-2} l_i \cos\varphi_i \ , \ E_N = 2l_N \sum_{i=1}^{N-2} l_i \cos\varphi_i \ ;$$

$$F_{N-1} = 2l_{N-1}\sum_{i=1}^{N-2} l_i \sin\varphi_i \ , \ F_N = 2l_N \sum_{i=1}^{N-2} l_i \sin\varphi_i \ ;$$

$$G_{N-1} = (\sum_{i=1}^{N-2} l_i \sin\varphi_i)^2 + (\sum_{i=1}^{N-2} l_i \cos\varphi_i)^2 + {l_{N-1}}^2 - {l_N}^2 ,$$

$$G_N = (\sum_{i=1}^{N-2} l_i \sin\varphi_i)^2 + (\sum_{i=1}^{N-2} l_i \cos\varphi_i)^2 + {l_N}^2 - {l_{N-1}}^2 .$$

Apply equations (3.2) on the linkage loops in sequence can solve for the angular displacement for each link. Note that the square roots in φ_{n-1} and φ_n should have opposite signs for a coupled solution. The classification of linkages configurations is based on the solution of φ_{n-1} from equation (3.2), a configuration is given 1 if the positive square root is adopted. Otherwise a 2 is given.

Then the angular outputs θ_i, as illustrated in Fig. 3.1, can be given as:

$$\theta_i = \Phi_i - \Phi_{i-1} \tag{3.3}$$

where Φ_i is the angular displacement of L_i in Fig. 3.1; Φ_0 denotes the base.

3.2.3.2 Optimization Problem Construction

The input parameters are lengths from the leg. These values are obtained by measuring the lengths of the subject. Design variables consist of linkage parameters and parameters for the active DOF. The overall design variable vector can be given as follows:

$$X = [l_1, l_2, \cdots, l_m, \alpha_1, \alpha_2, \cdots, \alpha_n, \beta_0, \beta_T] \tag{3.4}$$

where l_1 to l_m are the linkage lengths, α_1 to α_m angles for ternary and quaternary links. β_0 and β_T initial and final position of the input link. If the input link rotates for 360 degrees, only the initial position is needed.

The objective is defined as the weighted sum of the structural error between the human and exoskeleton joint profiles, given as:

$$J = \sum_{1}^{M} [\frac{r_j}{\sum_{1}^{M} r_j} \sum_{i=1}^{N} ({}^{H}\theta_j^i - {}^{E}\theta_j^i)^2] \tag{3.5}$$

where J is the objective, N the number of the reference points from human joint profile at each joint, ${}^{H}\theta_j^i$ the i^{th} reference point from the j^{th} human joint, ${}^{E}\theta_j^i$ the i^{th} corresponding point to ${}^{H}\theta_j^i$ from the exoskeleton joint, M the number of output joints, r_j difference between the maximum and minimum angle in the reference motion at j^{th} joint. For the j^{th} joint, $\sum_{i=1}^{N} ({}^{H}\theta_j^i - {}^{E}\theta_j^i)^2$ denotes the structural error, $\frac{r_j}{\sum_{1}^{M} r_j}$ weights this error.

Constraints serve two purposes. On one hand, as optimization algorithms operate upon real values, proper constraints can ensure the algorithm search the solution space effectively; On the other hand, design requirements can be formulated into constraints. In this study, the constraints include loop closure constraints, type constraints for the driving 4-bar linkages, functionality constraints, singularity constraints, and joints ROM constraints.

Loop closure constraints ensure that the links form closed loops. This is guaranteed by making the length of any link less than the sum of the rest.

$$2l_i - \sum_{1}^{N} l_j < 0 \tag{3.6}$$

where l_i is the length of the i^{th} link of consideration, N the number of the links, l_j the length of the j^{th} link.

In the type synthesis process, each exoskeleton is derived from a specified driving four-bar linkage. The choice of this linkage is according to [150] and based on the requirements of the exoskeleton. A constraint is established to specify the type of the driving 4-bar linkage.

To make the linkage functional with randomly generated input link displacement, each loop should be able to generate movements for the entire range. This is satisfied by returning real solutions for all angular displacements in each loop. For each loop, one such

constraint is established based on equation (3.2). It is easy to prove that $E_{N-1}{}^2 + F_{N-1}{}^2 - G_{N-1}{}^2 = E_N{}^2 + F_N{}^2 - G_N{}^2$. Therefore, this constraint can be written as:

$$E_{N-1}{}^2 + F_{N-1}{}^2 - G_{N-1}{}^2 > 0 \tag{3.7}$$

In each loop singularities occur when the two output links align, which may potentially change the configuration of the linkage. This can damage the human joints. The following constraint prevent such situations:

$$| l_{n-1} - l_n | + \xi < d < l_{n-1} + l_n - \xi \tag{3.8}$$

where l_{n-1} and l_n are the lengths of the two output links, d the distance between the two connecting joints of the added dyads, ζ a small positive value.

It is necessary to ensure the exoskeleton to operate in a safe range, to avoid over flexion/extension. This can be achieved by constraining the exoskeleton's maximal and minimal angular displacements at each joint, which can be expressed as follows:

$$\begin{aligned} \max({}^H\theta_j) &> \max({}^E\theta_j) \\ \min({}^H\theta_j) &< \min({}^E\theta_j) \end{aligned} \tag{3.9}$$

where ${}^H\theta_j$ is the human joint profile at the j^{th} joint, ${}^E\theta_j$ the exoskeleton joint profile at the j^{th} joint. The maxima and minima of the joint angles are obtained from the ROM of the subject.

Bounds constrain the size of the links for compactness and functionality. For link length bounds, lower bounds are set to values to allocate revolute joints. Upper bounds are set to values that confine the overall dimensions of the linkage. For angle bounds, lower bounds are set as 0 and upper bounds are set as 2π. For active DOF bounds, the bounds are given according to the actuation type and actuator requirements. These bounds may vary from case to case based on their specific design requirements.

Therefore, the optimization problem can be established as:

$$\textit{Objective}:\ \min.\ J = \sum_{1}^{M}\left[\frac{r_j}{\sum_{1}^{M} r_j}\sum_{i=1}^{N}\left({}^{H}\theta_j^i - {}^{E}\theta_j^i\right)^2\right]$$

$$\textit{Design variable}:\ X = [l_1, l_2, \cdots, l_m, \alpha_1, \alpha_2, \cdots, \alpha_n, \beta_0, \beta_T]$$

Subject to

Constraints: from (3.6), (3.7), (3.8), and (3.9).

Bounds are set accordingly.

Then the optimization problem is solved using genetic algorithm from the Global Optimization Toolbox in MATLAB.

3.2.4 Design Procedure

Based on the linkage types form Fig. 3.2 there are 12 candidates for 2 angular outputs. The total number of candidates increases dramatically to 120 for 3 angular outputs (Fig.

3.3). Applying dimensional synthesis on all these candidates can be tedious and time-consuming. Therefore, we propose a procedure that can reduce the candidates that need to be optimized, as in Fig. 3.5. This procedure can both be applied to design linkages for 2 and 3 outputs.

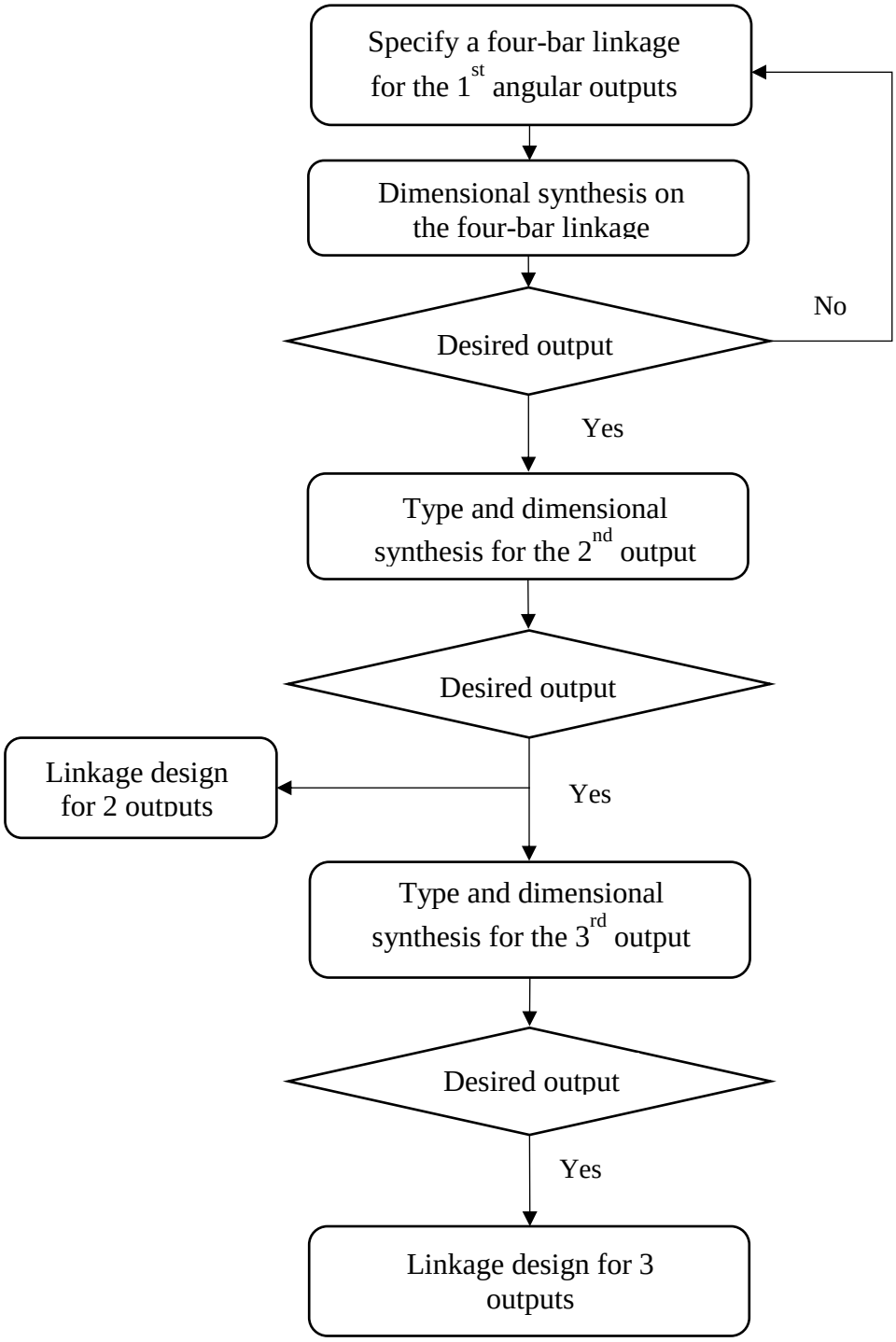

Fig. 3.5 Design procedure

A four-bar linkage is first specified based on the design requirements, including the type of the four-bar linkage, motor location, link size, etc. Then the linkage is optimized for

the 1st angular output. This process requires some trials and errors to arrive at an appropriate design. Then designs for the 2nd output can be proposed base on the four-bar linkage. If only 2-angular-output linkages are required, the synthesis process explores the design in sequence until a feasible one is found. If 3-angular-output linkages are considered, all the proposed linkages for 2 outputs are synthesized. The survivals are then used to propose linkages for 3 outputs. Then we can explore these linkages in sequence until one feasible design is found.

3.5 Discussion

Designing 1-DOF linkages for rehabilitation exoskeleton requires quite a number of requirements. The method we proposed can satisfy these requirements and achieve feasible designs. It is validated by an index finger exoskeleton and a leg exoskeleton in our study [151]. Both devices can produce a close match to the reference motion.

This method only exploits four-bar linkages for the first angular outputs. Designs for following angular outputs are proposed based on the four-bar linkage and only one or two RRR dyads are added. For more complicated cases, where using a four-bar link is not capable for the first angular output, a more complicated linkage can be tested. For following angular outputs, adding more RRR dyads is also possible.

The proposed method mainly focuses on compact linkages that well satisfy our requirements. It does not enumerate all the designs of a given number of DOFs. This

method can be efficient as only a limited number of designs are optimized. By contrast, it would be overly time-consuming and computationally expensive to enumerate all the designs with a given number of links and implement them for multiple successive angular outputs.

This method proposes several compact linkages types for 2 and 3 successive angular outputs. This approach can be extended to design linkages with more than 3 angular outputs and serve other purposes beyond the exoskeleton domain, where multiple successive angular outputs are required. Dimensional synthesis method proposed in this study discusses converting necessary kinematic requirements into optimization components. This can also help with other linkage-based exoskeleton designs.

3.6 Conclusions

This study proposed an integrated type and dimensional synthesis method for designing compact 1-DOF planar linkages with only revolute joints for rehabilitation exoskeletons. Design requirements on 1-DOF linkages for exoskeleton applications are thoroughly discussed. Type synthesis proposes candidate linkages, while dimensional synthesis optimizes them to reproduce a reference motion. The method can also be employed to design compact linkages for other purposes where 2 and 3 successive angular outputs are required. This method is also possible for more complicated outputs by adding more RRR dyads.

Chapter 4 Development of a Planar 1-DOF Linkage-Based Leg Exoskeleton

Abstract

A great number of exoskeleton devices have been created in the past decades to serve various purposes. In rehabilitation, exoskeletons are used to assist the patients to accomplish training motions in order to increase the patients' motor skills. However, current devices are mostly heavy and bulky devices which limits their applications in hospitals and clinical centres. On the contrary, 1-DOF linkage-based exoskeletons which use only one motor to drive multiple joint outputs turn out to be compact and portable. However, the similar concept has not been exploited in leg exoskeletons. This chapter investigated 1-DOF planar linkages for leg exoskeleton design using the method proposed in Chapter 3. First, dimensional synthesis was conducted on the linkage for optimal linkage parameters. Then dynamic simulation estimated the input torque on a 3D model in ADAMS for actuation design. An open-loop control system followed to control the device. In the end, a leg exoskeleton that could generate a human-like gait pattern simultaneously at hip and knee joints was achieved. The device is able to deliver CPM-based rehabilitation. In addition, the device is stand-alone and portable, which makes it possible for applications beyond clinical settings.

4.1 Introduction

The aimed leg exoskeleton is used to deliver CPM to the human lower limb to assist recovery after spinal cord injury or stroke. For the leg exoskeleton in this thesis, we choose human walking gait in the sagittal plane as the target motion. This is because walking is an essential motion in daily life, and the majority of the current rehabilitation leg exoskeletons are also developed focusing on human walking. Another benefit of using walking as a reference motion is that human walking has been studied intensively in the literature. A great number of clinical gait studies [152-155] are available to provide reference gait patterns, considering infeasibility of obtaining the patients walking gait after injuries.

In this study, we use the reference gait from [153] to design a leg exoskeleton for a subject with the same height. A standing still configuration is used to develop the device, as it is the natural gesture for walking. In practice, the patient can be held standing still on the level ground and the leg exoskeleton assist the human leg to generate a human-like gait pattern for the hip and knee joints.

Human walking is a cyclic motion. A stride is usually used to represent a walking gait, as in Fig.4.1. A stride starts with a heel strike and end with the same strike, interconnected by several events in between. It can be separated into two main phases: double support phase with both feet contacting ground and single support phase with only one foot contacting the ground.

Joint kinematics are usually used to quantify a walking gait. In this study hip and knee joint angular displacements are of consideration. Figure *b* and *c* demonstrate the angular hip and knee angular displacements from subjects with an average height of 1.71 m, weight of 68.5 kg [153]. Nine of the subjects are male and eleven are female. The joint angular displacement data are provided in Table 4.1. Joint angles are given with respect to the percentage of a stride.

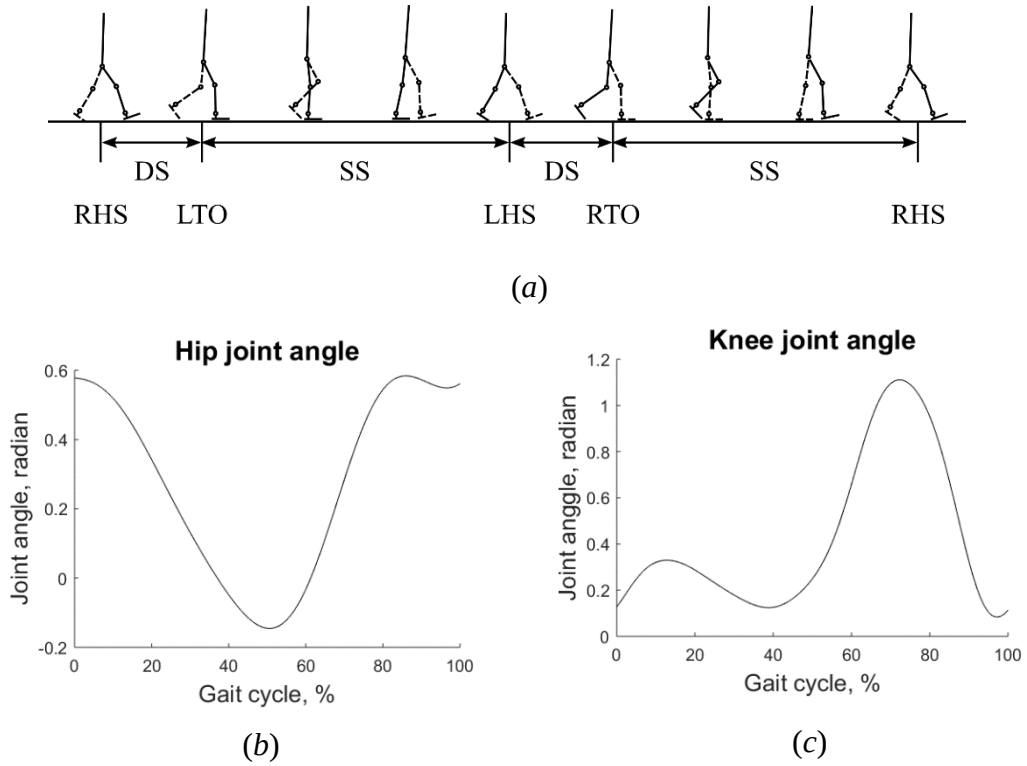

Fig. 4.1 A stride and joint angular displacements. (a), a typical stride; (b) and (c), hip and knee joint angular displacements throughout a stride. RHS, right heel strike; LTO, left toe off; LHS, left heel strike; RTO, right toe off; DS, double support phase; SS, single support phase

The joint angular displacements are used as a reference motion in this study. Reference points are evenly distributed along the gait cycle, posing same weight on different section

of a walking gait. As the leg exoskeleton focuses on reproducing the joint profile rather than on control the events, heel strike, toe-off, etc., such a scheme would not affect the functionality of the device.

Table 4.1 Gait reference points

Gait cycle (%)	Hip joint angle (10^{-2} radian)	Knee joint angle (10^{-2} radian)
0	57.79	12.71
5	56.32	24.78
10	51.89	32.04
15	44.18	32.51
20	34.21	28.73
25	23.50	23.20
30	13.14	17.89
35	3.60	13.69
40	-4.86	12.54
45	-11.45	16.35
50	-14.52	24.88
55	-12.14	40.34
60	-3.24	65.83
65	11.31	93.66
70	28.47	109.49
75	44.05	109.08
80	54.44	95.26
85	58.31	67.42
90	57.26	32.52
95	55.08	10.44
100	56.12	11.27

4.2 Design Requirements and Development Procedure

4.2.1 Design Requirements

In order to deliver human walking gait to the injured leg, a number of issues should be addressed carefully. Above all, the safety of the patient should be guaranteed. Safety hazards should be identified and ruled out during the design process. Proper functionality of the device is also essential. The devices should be able to mimic the natural walking gait. Such issues can be broken down into design requirements to make sure they are addressed properly. The design requirements and corresponding solutions are listed as follows:

1) The desired linkage should have only 1-DOF, this can be guaranteed by applying the type synthesis method we proposed in Chapter 3. The method can ensure 1-DOF while proposing candidate linkages.
2) The linkage should be able to generate human-like gait at hip and knee joints. This can be achieved by using the proposed dimensional synthesis method. The method optimizes the linkage to closely mimic a natural gait.
3) The motion generated by the leg exoskeleton should not cause injuries to the human joints. The joint motion provided by the leg exoskeleton should stay within the ROM of the human joints.
4) Singularity conditions should be ruled out carefully. The configuration of the linkage may change when singularities occur during operation. This would end up damaging the human joints. The singularities are tackled by constraints in the dimensional synthesis process.

5) As the leg exoskeleton is used to assist the motion of the lower limb, the actuation component should be sufficient to drive the leg exoskeleton together with the human leg. We adopted a simulation-based method to estimate the output torque and choose proper motor and gearhead based on the estimated torque.
6) Harnesses are used to fasten the leg exoskeleton to the human leg. It is important to make the device easy to don and doff and avoid discomfort caused by the harnesses. This can be accomplished by customizing the harness based on the dimension of the human leg.
7) The device should be easy to operate. An open-loop control system has been developed for this purpose.

4.2.2 Development Procedure

To satisfy the design requirements raised above, a general design procedure has been proposed for the customized leg exoskeleton, as in Fig. 4.2. The leg exoskeleton design mainly consists of three major steps: linkage, actuation, and control system design. Linkage design aims to accomplish a planar 1-DOF linkage to generate human-like motions at hip and knee joints. Actuation design focuses on choosing a proper motor and a gearhead to drive the device. Control system design develops a control system for easy operation.

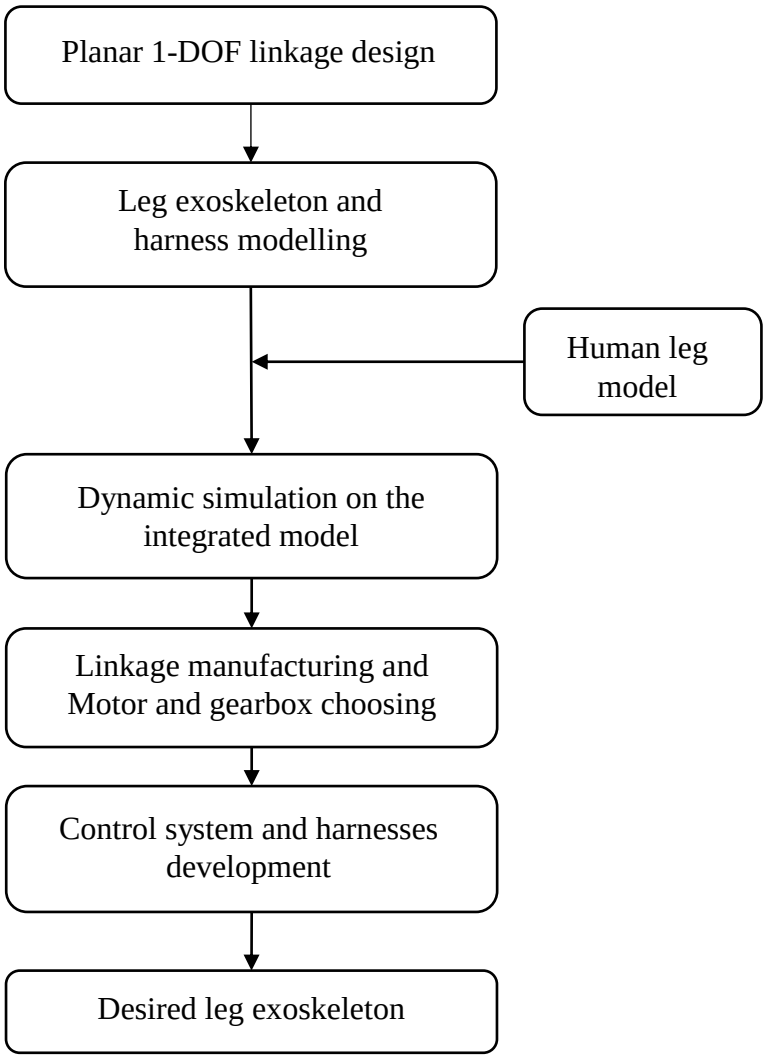

Fig. 4.2 Leg exoskeleton design procedure

In the first step, a planar 1 DOF linkage is accomplished to mimic the reference human gait. We adopted the method proposed in Chapter 3 to achieve a linkage for successive angular outputs at hip and knee joints.

After obtaining the linkage dimensions from the first step, a 3D of the leg exoskeleton is built in SolidWorks for further simulation and manufacturing. Harnesses are also

modelled in this step. They are customized based on the dimensions of the wearer's leg. In the physical prototype, mattresses and straps are used to make the device comfortable to wear. The mechanical components of the harnesses are all 3D printed. This makes the device easy to customize for different patients.

It is important to choose a proper motor and gearhead to drive the device after achieving the mechanism design. To obtain information about the driving torque, we adopt dynamic simulation to estimate the input torque. This is accomplished in ADAMS. As the leg exoskeleton is responsible for driving the leg and itself. A model of the user's leg is also built and attached to the leg exoskeleton. Then simulation is conducted on the integrated model. Considering the walking speed is too fast for patients after surgery, we use ¼ of normal walking speed to conduct the simulation. Estimation of the input torque can then be obtained from the simulation results. Motor and gearhead are then chosen based on the estimation.

One notable benefit of 1-DOF linkage-based exoskeleton is that corresponding control system can be light. This is because the motion provided by the linkage is constrained, therefore, safe to the user. In this study, an open-loop control system is enough to control the device. A user can simply operate the device using a joy stick.

The entire device is powered by portable batteries, this makes the device stand-alone and portable. It is possible to use the device outside clinical settings, while current devices are only available in hospitals and therapy centres.

4.3 Linkage Design

The leg exoskeleton should be capable of generating similar angular displacement at hip and knee joints. The angles at the hip and knee joints are illustrated in Fig. 4.3. The gait data is from [153] for individuals of height 1.71 m. A subject of the same height is chosen in this study.

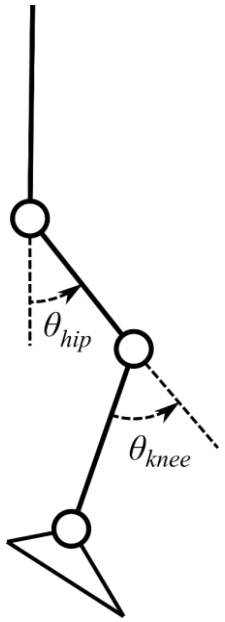

Fig. 4.3 Leg joint angles

The linkage design process started with iteration on four-bar linkages to achieve the angular displacements at the hip joint. As walking is a cyclic motion, and the thigh oscillates during walking, a crank-rocker type is preferred for such a task. Proper location of the motor is also an issue to be considered. Ideally, it should be placed behind the torso.

Dimensional synthesis was conducted on such four-bar linkages to evaluate their capability for generating the gait pattern at the hip joint. In the end, a four-bar linkage was found effective for such a task, as given in Fig. 4.4. Its parameters are given in Table 4.2.

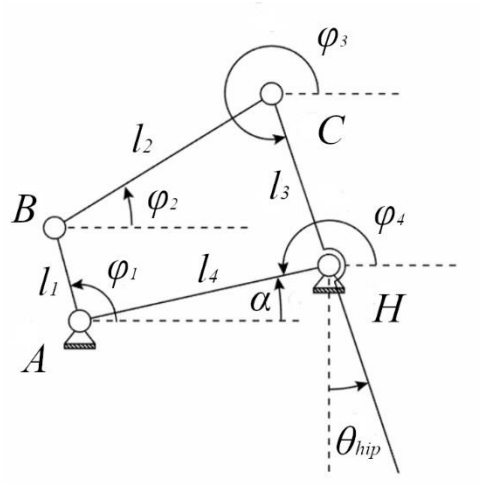

Fig. 4.4 Leg exoskeleton driving linkage schematic

Table 4. 2 Four-bar linkage parameters

Name	Value
l_1[mm]	37.39
l_2[mm]	170.79
l_3[mm]	115.96
l_4[mm]	150.78
α[radian]	0.06

The design has five parameters, four for link lengths and one for an angle to locate the crank. Link *CH* is responsible for the angular displacements at the hip joint and the motor is located behind the torso. Performance of the proposed four-bar linkage is evaluated in Fig. 4.5. A close match with the human walking gait is guaranteed. It is notable that only the current configuration of the linkage is able to produce such a pattern.

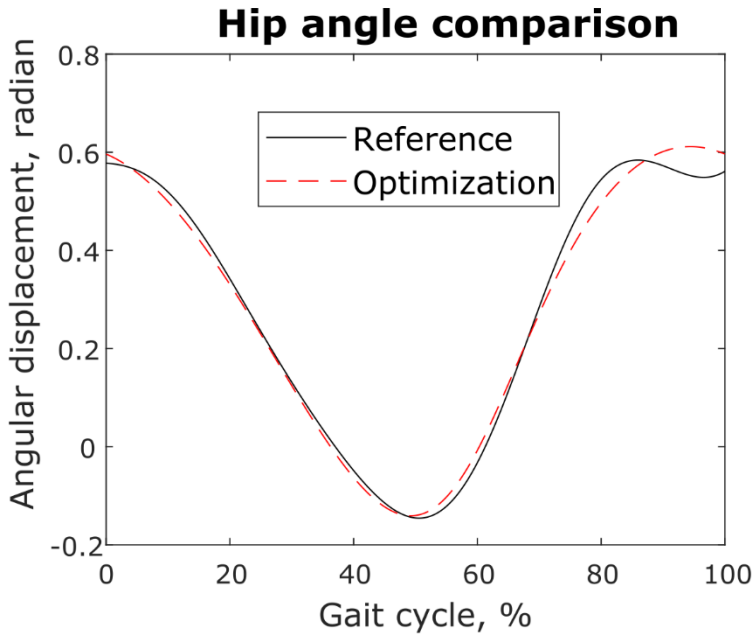

Fig. 4.5 Driving linkage output evaluation

Five linkage types were proposed for the knee angular output as in Fig. 4.6. As the driving four-bar linkage has only one configuration, the linkage types only provide 14 designs. In the end, a 1-DOF-8-bar-10-joint linkage (D112) was found effective to mimic the human gait.

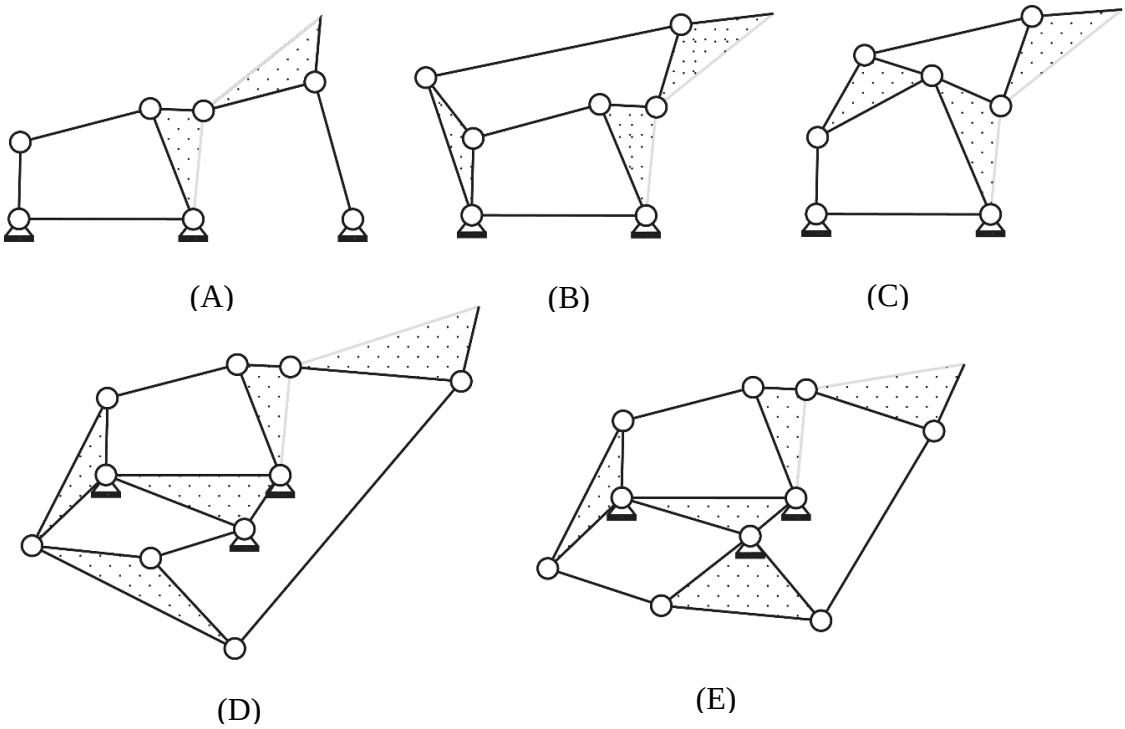

Fig. 4.6 Leg exoskeleton candidate linkage types

A schematic of the leg exoskeleton is illustrated in Fig. 4.7. The angular output at hip and knee joints are illustrated as θ_{hip} and θ_{knee} according to the definition [154]. AHG is the base link, which is connected to the human body. HK and KF are counterparts of the human thigh and shank respectively. The hip angular output is generated between HK and the human torso; knee angular output is generated between HK and FK. The entire linkage is driven by the input crank AB, which puts the motor behind the torso. Overall, the

linkage has a human morphology. This reduces the overall size of the device and makes it easy to wear.

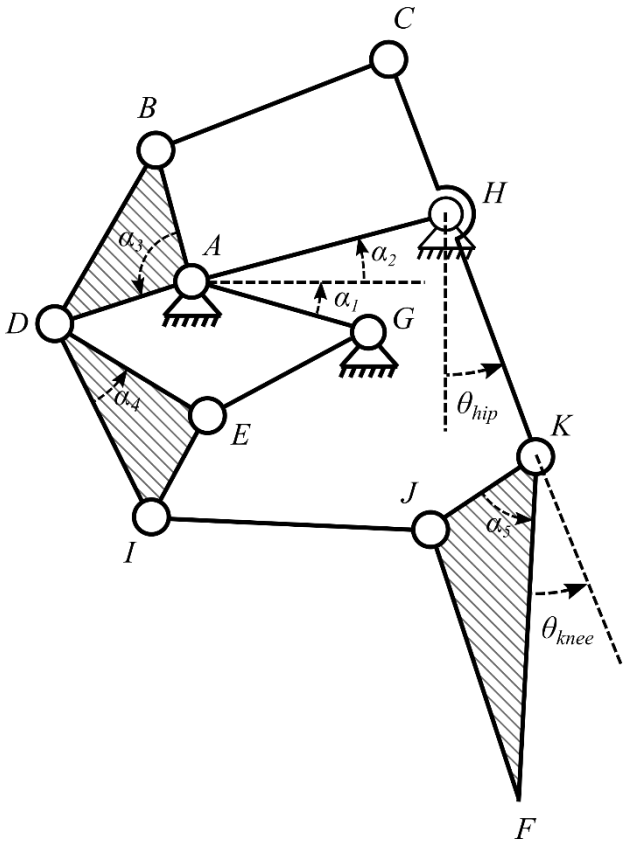

Fig. 4.7 Leg exoskeleton schematic

The optimal design of the linkage is obtained by conducting dimensional synthesis on the linkage. This is achieved by constructing an optimization problem. Solving the optimization problem will return the optimal dimensions. To construct the optimization problem, kinematic analysis is first conducted on the linkage for the hip and knee angular outputs.

4.3.1 Kinematic Analysis

The linkage can be separated into three loops: ABCH, ADEG and ADIJKH corresponding vector loops are illustrated in Fig. 4.8. By solving the vector equations for each loop, angular displacements for each link can be derived. Thus, the angular outputs at hip and knee joints can then be formulated for establishing the optimization problem.

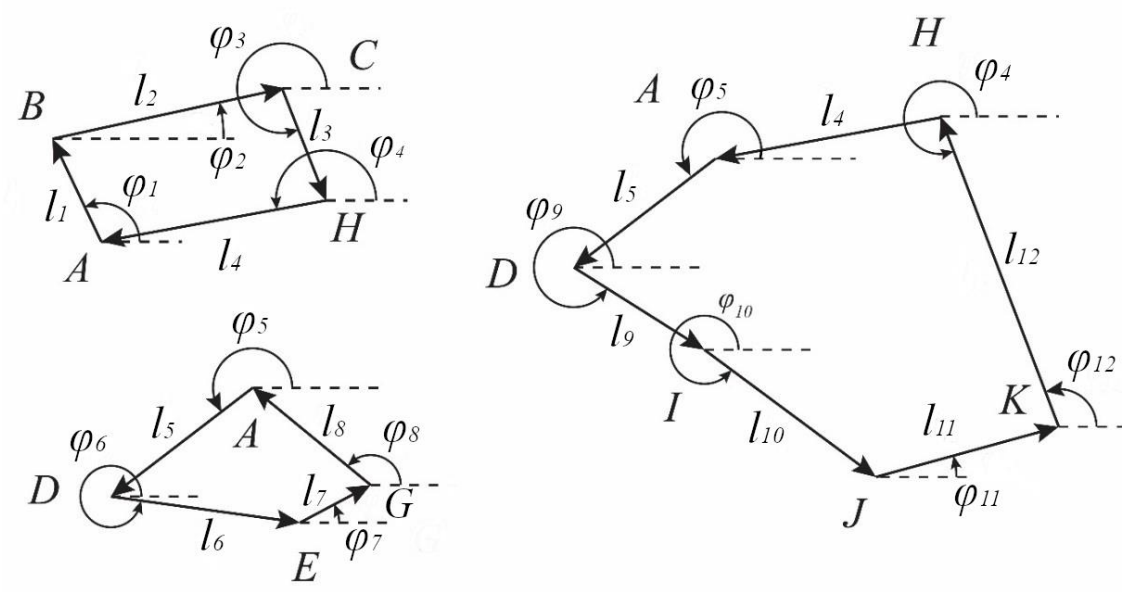

Fig. 4.8 Leg exoskeleton vector loops

The hip and knee joint angular displacement can be expressed as:

$$\theta_{hip} = \varphi_3 + \frac{\pi}{2} \tag{4.1}$$

$$\theta_{knee} = \varphi_{12} - \varphi_{11} - \alpha_5 \tag{4.2}$$

The vector loop equations for loop ABCH, ADEG and ADIJKH can be expressed as:

$$l_1 e^{i\varphi_1} + l_2 e^{i\varphi_2} + l_3 e^{i\varphi_3} + l_4 e^{i\varphi_4} = 0 \tag{4.3}$$

$$l_5 e^{i\varphi 5} + l_6 e^{i\varphi_6} + l_7 e^{i\varphi_7} + l_8 e^{i\varphi_8} = 0 \tag{4.4}$$

$$l_4 e^{i\varphi 4} + l_5 e^{i\varphi_5} + l_9 e^{i\varphi_9} + l_{10} e^{i\varphi_{10}} + l_{11} e^{i\varphi_{11}} + l_{12} e^{i\varphi_{12}} = 0 \tag{4.5}$$

In the ABCH loop we have

$$\varphi_4 = \pi + \alpha_1 \tag{4.6}$$

Substitute (4.6) into (4.3) solve for φ_3 yields:

$$\varphi_3 = 2\tan^{-1}\frac{F_3 + \sqrt{E_3^{\,2} + F_3^{\,2} - G_3^{\,2}}}{E_3 - G_3} \tag{4.7}$$

where

$E_3 = 2l_3(l_1\cos\varphi_1 + l_4\cos\varphi_4)$,

$F_3 = 2l_3(l_1\sin\varphi_1 + l_4\sin\varphi_4)$,

$G_3 = (l_1\cos\varphi_1 + l_4\cos\varphi_4)^2 + (l_1\sin\varphi_1 + l_4\sin\varphi_4)^2 + l_3^{\,2} - l_2^{\,2}$.

Substitute (4.7) into (4.1) gives the angular output at hip joint:

$$\theta_{hip} = 2\tan^{-1}\frac{F_3 + \sqrt{E_3^{\,2} + F_3^{\,2} - G_3^{\,2}}}{E_3 - G_3} + \frac{\pi}{2} \tag{4.8}$$

The angular displacement of l_{12} can be expressed as:

$$\varphi_{12} = 2\tan^{-1}\frac{F_3 + \sqrt{E_3^{\,2} + F_3^{\,2} - G_3^{\,2}}}{E_3 - G_3} + \pi \tag{4.9}$$

In the ADEG loop we have:

$$\varphi_5 = \varphi_1 + \alpha_3 \tag{4.10}$$

$$\varphi_8 = \pi + \alpha_2 \tag{4.11}$$

Substitute (4.10) and (4.11) into (4.4) solve for φ_6 yields:

$$\varphi_6 = 2\tan^{-1}\frac{F_6 + \sqrt{E_6^{\,2} + F_6^{\,2} - G_6^{\,2}}}{E_6 - G_6} \tag{4.12}$$

where

$E_6 = 2l_6(l_5\cos\varphi_5 + l_8\cos\varphi_8)$,

$F_6 = 2l_6(l_5\sin\varphi_5 + l_8\sin\varphi_8)$,

$G_6 = (l_5\sin\varphi_5 + l_8\sin\varphi_8)^2 + (l_5\cos\varphi_5 + l_8\cos\varphi_8)^2 + l_6^2 - l_7^2$.

Thus,

$$\varphi_9 = \varphi_6 + \alpha_4 \tag{4.13}$$

Substitute (4.6), (4.9), (4.10) and (4.13) into (4.5) solve for φ_{11} gives:

$$\varphi_{11} = 2\tan^{-1}\frac{F_{11} - \sqrt{E_{11}^{\,2} + F_{11}^{\,2} - G_{11}^{\,2}}}{E_{11} - G_{11}} \tag{4.14}$$

where

$E_{11} = 2l_{11}(l_4\cos\varphi_4 + l_5\cos\varphi_5 + l_9\cos\varphi_9 + l_{12}\cos\varphi_{12})$,

$F_{11} = 2l_{11}(l_4\sin\varphi_4 + l_5\sin\varphi_5 + l_9\sin\varphi_9 + l_{12}\sin\varphi_{12})$,

$$G_6 = (l_4\cos\varphi_4 + l_5\cos\varphi_5 + l_9\cos\varphi_9 + l_{12}\cos\varphi_{12})^2 + (l_4\cos\varphi_4 + l_5\cos\varphi_5 + l_9\cos\varphi_9 + l_{12}\cos\varphi_{12})^2 + l_{10}^2 - l_{11}^2$$

Substitute (4.9) and (4.14) in (4.2) gives the knee joint angular displacement:

$$\theta_{knee} = 2\tan^{-1}\frac{F_3 + \sqrt{E_3^{\,2} + F_3^{\,2} - G_3^{\,2}}}{E_3 - G_3} - 2\tan^{-1}\frac{F_{11} - \sqrt{E_{11}^{\,2} + F_{11}^{\,2} - G_{11}^{\,2}}}{E_{11} - G_{11}} + \pi - \alpha_5 \tag{4.15}$$

It is notable that equation (4.8) and (4.15) only represent one configuration of the linkage. Each loop has 2 configurations based on the solution for φ_3, φ_6 and φ_{11}. The negative and positive roots of the square root result in 2 different configurations. As the linkage has 3 loops and each loop has 2 different configurations, there are totally 8 different configurations for the linkage. Such linkages have all been evaluated. The configuration represented by equation (4.8) and (4.15) returns the closest match to the human gait.

4.3.2 Dimensional Synthesis

Dimensional synthesis concerns finding the optimal parameters for the linkage. This is achieved by constructing an optimization problem and solve the problem using genetic algorithms. The optimization problem should be well constructed such that the algorithms can successfully converge. This can be separated into the establishment of design variables, objective, constraints as well as bounds for design variables.

Input parameters are used to formulate the optimization problem. These values are known and remain constant during the optimization. In this study, only one input parameter is needed, i.e. the length of the human thigh (l_{12}). The parameter is obtained by measuring the thigh length of the user.

Design variable for the leg exoskeleton includes lengths for binary links, lengths, and angles for ternary links. In addition, variables to represent the initial displacement of the input crank is also needed. The overall design variable vector can be given as follows:

$$X = [l_1, l_2, l_3, l_4, l_5, l_6, l_7, l_8, l_9, l_{10}, l_{11}, \alpha_1, \alpha_2, \alpha_3, \alpha_4, \alpha_5, \beta] \tag{4.16}$$

where l_i represents the link lengths, α_i angles for ternary links, β the initial angular displacement of the input crank AB in Fig 4.7, i.e. the initial value of φ_1 in Fig 4.8.

In this study, the leg exoskeleton is used to mimic the human walking pattern at hip and knee joints. Therefore, we adopted the structural error between the exoskeleton and human joint angles as the objective function. The joint angular outputs for the exoskeletons were obtained from kinematic analysis on the exoskeleton. The human joint angular profiles were obtained from literature, in which the subject share the same height with the target user. The errors for the hip and joints were weighted by the ranges of motion at the corresponding joints. Therefore, the overall objective function can be expressed as:

$$J = \frac{r_{hip}}{r_{hip} + r_{knee}} \sum_{i=1}^{N} ({}^{H}\theta_{hip}^{i} - {}^{E}\theta_{hip}^{i})^2 + \frac{r_{hip}}{r_{hip} + r_{knee}} \sum_{i=1}^{N} ({}^{H}\theta_{knee}^{i} - {}^{E}\theta_{knee}^{i})^2 \tag{4.17}$$

where J is the objective, N the number of the reference points from human gait, r_{hip} and r_{knee} the ranges of motion of the walking gait for hip and knee joints, ${}^{H}\theta_{hip}^{i}$ and ${}^{E}\theta_{hip}^{i}$ human and exoskeleton hip angular displacement at the i^{th} point.

Design requirements were converted into constraints. In such a way, the optimal solution could guarantee the leg exoskeleton meets the requirements. Such constraints included loop closure constraints, linkage type constraint for the driving 4-bar linkages, functionality constraints, singularity avoidance constraints, and joints ROM constraints.

The leg exoskeleton has 3 loops. Both loop ABCH and ADEF are 4-bar crank-rocker linkages. Grashof condition should be satisfied in such loops. Moreover, the input crank should be the shortest and the floating link should be the longest in that loop. Applying Grashof conditions on the loops ensured the generated populations can always form functional 4-bar linkages. Such constraints were expressed in a matrix form as:

$$\begin{bmatrix} 1 & 1 & -1 & -1 \\ 1 & -1 & 0 & 0 \\ 1 & 0 & -1 & 0 \\ 1 & 0 & 0 & -1 \\ 0 & -1 & 1 & 0 \\ 0 & -1 & 0 & 1 \end{bmatrix} \begin{bmatrix} l_1 \\ l_2 \\ l_3 \\ l_4 \end{bmatrix} < \vec{0} \tag{4.18}$$

$$\begin{bmatrix} 1 & 1 & -1 & -1 \\ 1 & -1 & 0 & 0 \\ 1 & 0 & -1 & 0 \\ 1 & 0 & 0 & -1 \\ 0 & -1 & 1 & 0 \\ 0 & -1 & 0 & 1 \end{bmatrix} \begin{bmatrix} l_5 \\ l_6 \\ l_7 \\ l_8 \end{bmatrix} < \vec{0} \tag{4.19}$$

In order to make the links in loop ADIJKH to form a loop, a loop closure constraint should also be satisfied. That is any link length should be less than the sum of the rest link lengths, which was ensured by the following equation.

$$\begin{bmatrix} 1 & -1 & -1 & -1 & -1 & -1 \\ -1 & 1 & -1 & -1 & -1 & -1 \\ -1 & -1 & 1 & -1 & -1 & -1 \\ -1 & -1 & -1 & 1 & -1 & -1 \\ -1 & -1 & -1 & -1 & 1 & -1 \\ -1 & -1 & -1 & -1 & -1 & 1 \end{bmatrix} \begin{bmatrix} l_4 \\ l_5 \\ l_9 \\ l_{10} \\ l_{11} \\ l_{12} \end{bmatrix} < \vec{0} \tag{4.20}$$

During the optimization process, the linkage was provided with arbitrary lengths and the input crank rotates for 360 degrees to mimic a gait cycle. To ensure the linkage functional for the entire gait cycle, in addition to the loop closure constraint, another constraint should also be satisfied, given as:

$$E_{11}^{\ 2} + F_{11}^{\ 2} - G_{11}^{\ 2} > 0 \tag{4.21}$$

This constraint ensured the optimization always returns real solutions for all the link angular displacements. Therefore, the linkage could be functional for an entire cycle.

To ensure safety to the wear, the joint angle outputs at hip and knee joints should not exceed that of the human joints. Such constraints were given as:

$$\begin{aligned} 0.52 < \theta_{hip} < 1.92 \\ 0.09 < \theta_{knee} < 2.53 \end{aligned} \tag{4.22}$$

Singularities occur when the output links in each loop align. To avoid such situations, constraints were imposed on the output links in each loop. Such constraints can be given as follows:

$$\begin{aligned} |l_2 - l_3| + \xi < \left|\overrightarrow{BH}\right| < l_2 + l_3 - \xi \\ |l_6 - l_7| + \xi < \left|\overrightarrow{DF}\right| < l_6 + l_7 - \xi \\ |l_{10} - l_{11}| + \xi < \left|\overrightarrow{IK}\right| < l_{10} + l_{11} - \xi \end{aligned} \tag{4.23}$$

where ξ is positive real value to avoid the alignment of the output links.

Bounds were used to specify the overall configuration and limit the size of the device. Lower bounds for link lengths were set as 10 mm for allocating revolute joints, and upper bounds for link lengths were set as 600 mm. Lower bounds for the link angles and initial displacement of the input crank were set as 0 and upper bounds as 2π in general. In this design to ensure the actuation components to locate behind the torso, lower bounds for α_2 and α_3 were set as $-\pi/2$ and $\pi/2$ respectively. The lower and upper bounds are given in the following vectors:

$$\begin{aligned} LB &= [10,10,10,10,10,10,10,10,10,10,10,0,-\frac{\pi}{2},-\frac{\pi}{2},0,0] \\ UB &= [600,600,600,600,600,600,600,600,600,600,600,2\pi,\frac{\pi}{2},\frac{\pi}{2},2\pi,2\pi] \end{aligned} \tag{4.24}$$

With all components for constructing the optimization problem discussed, the optimization problem can be defined as follows:

$$\textit{Objective: } J = \frac{r_{hip}}{r_{hip}+r_{knee}}\sum_{i=1}^{N}({}^{H}\theta_{hip}^{i} - {}^{E}\theta_{hip}^{i})^2 + \frac{r_{hip}}{r_{hip}+r_{knee}}\sum_{i=1}^{N}({}^{H}\theta_{knee}^{i} - {}^{E}\theta_{knee}^{i})^2$$

$$\textit{Design variable: } X = [l_1, l_2, l_3, l_4, l_5, l_6, l_7, l_8, l_9, l_{10}, l_{11}, \alpha_1, \alpha_2, \alpha_3, \alpha_4, \alpha_5, \beta];$$

Subject to

Constraints: equation (4.18) to (4.23),

Bounds: equation (4.24).

Solving the optimization problem returns the optimal dimensions for the linkage.

The same process can also be applied on other candidate linkages. We compare the results from several candidate linkages. Schematics and their parameters are illustrated in Fig. 4.9, and optimization results are given in Table 4.3. From each type, one has been selected for the comparison study, and their performance is compared in Fig. 4.10. It is clear that the design from type D (Fig. 4.7) gives the best results. Note that type (*E*) has not been investigated as a feasible design has been achieved from type (*D*).

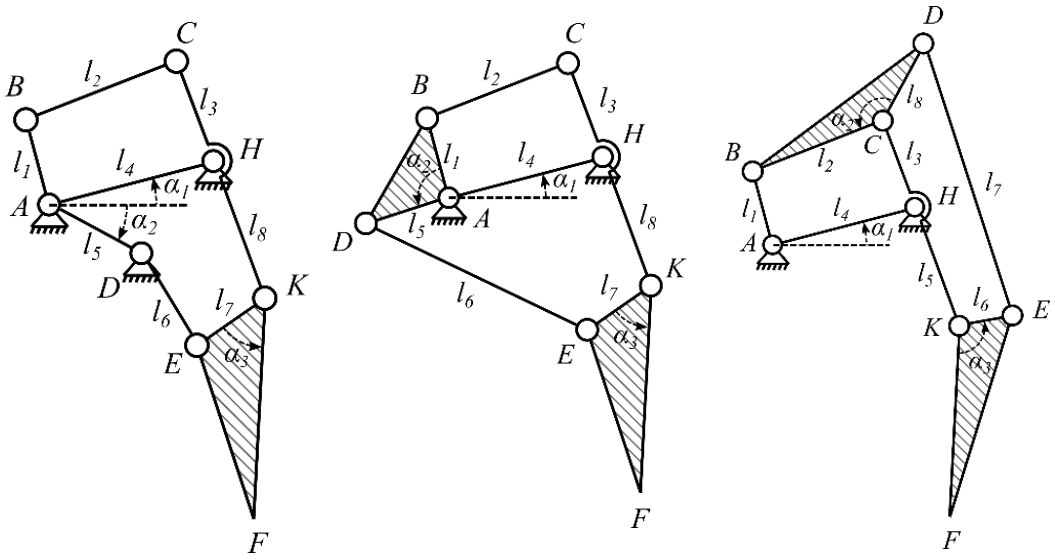

Type (A) Type (B) Type (C)

Fig. 4.9 Investigated linkages

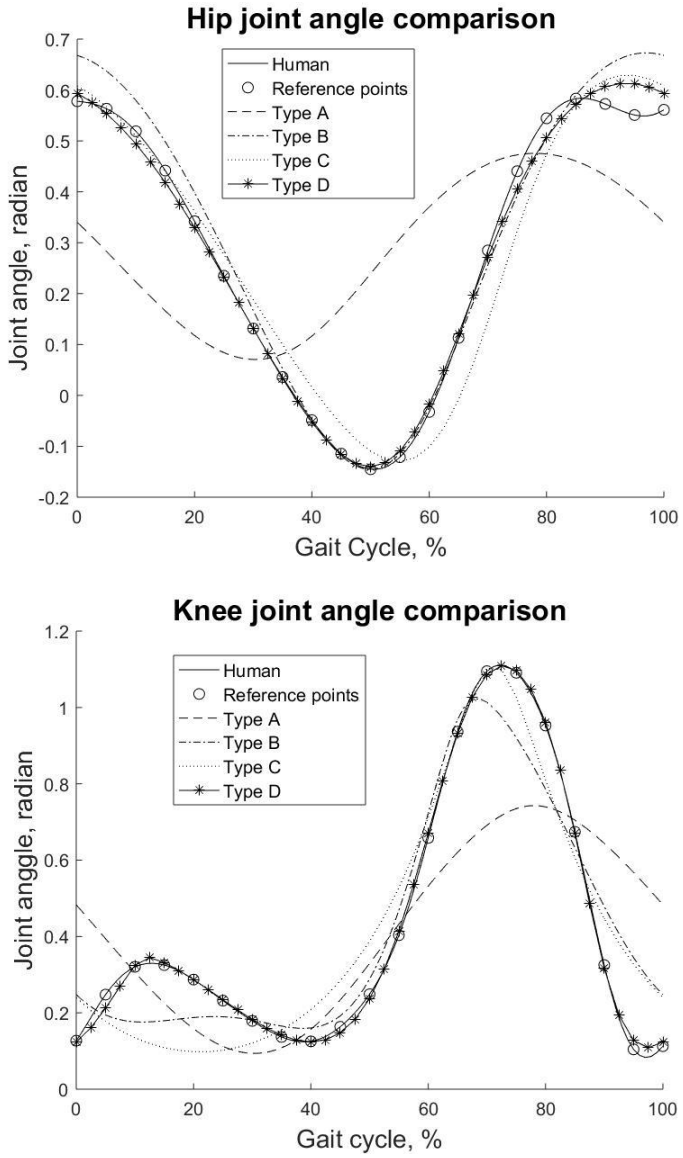

Fig. 4.10 Linkage performance comparison

Table 4.3 Optimization results from various candidate linkages

Type A		Type B		Type C		Type D	
l_1[mm]	81.42	l_1[mm]	76.49	l_1[mm]	38.56	l_1[mm]	26.48
l_2[mm]	550.65	l_2[mm]	356.24	l_2[mm]	252.46	l_2[mm]	171.86
l_3[mm]	450.36	l_3[mm]	208.79	l_3[mm]	252.46	l_3[mm]	87.72
l_4[mm]	534.84	l_4[mm]	332.83	l_4[mm]	106.11	l_4[mm]	148.82
l_5[mm]	67.71	l_5[mm]	140.98	l_5[mm]	370	l_5[mm]	66.73
l_6[mm]	440.93	l_6[mm]	391.30	l_6[mm]	403.79	l_6[mm]	184.93
l_7[mm]	382.73	l_7[mm]	223.09	l_7[mm]	581.13	l_7[mm]	167.46
l_8[mm]	370	l_8[mm]	370	l_8[mm]	600.00	l_8[mm]	152.51
α_1[rad]	-0.12	α_1[rad]	0.09	α_1[rad]	0.05	l_9[mm]	127.80
α_2[rad]	1.26	α_2[rad]	1.98	α_2[rad]	0.03	l_{10}[mm]	396.35
α_3[rad]	1.78	α_3[rad]	1.44	α_3[rad]	2.74	l_{11}[mm]	90.82
β [rad]	2.57	β [rad]	3.72	β [rad]	4.52	l_{12}[mm]	370
						α_1[rad]	0.25
						α_2[rad]	-0.05
						α_3[rad]	2.96
						α_4[rad]	1.61
						α_5[rad]	1.20
						β[rad]	3.70

4.4 Prototype Development

4.4.1 Actuation Design

It is necessary to choose a proper motor to drive the linkage. In previous studies, as a motor is directly applied to each joint, the motors and gearbox are designed according to the human gait analysis data. However, in our case, we only use one motor to actuate the hip and knee joints. In addition, the linkage only mimics the gait pattern, it does not assist the patient walk on the ground. It becomes infeasible to directly choose a motor based on the human joint torque profiles in a walking cycle. It is necessary to obtain information about the input torque for the leg exoskeleton. We employed a simulation-based method to estimate the input torque. ADAMS was used to conduct the simulation.

First, a model of the leg exoskeleton was built in SolidWorks based on the achieved dimensions from the dimensional synthesis, as in Fig. 4.11. As the leg exoskeleton is also responsible to drive the human leg, a model for the wearer's right leg was built. The leg model approximates the human leg by using the dimensions of the user's leg. The right leg is modelled as a 2-bar link connected by a revolute joint at the knee joint. The hip is connected to the leg exoskeleton through a revolute joint that aligns with the leg exoskeleton hip joint. The weight of the leg is estimated based on the weight of the user and human anatomy studies [156]. The links' weights are obtained from the leg exoskeleton's 3D model. Mass properties of the model are given in Table 4.4.

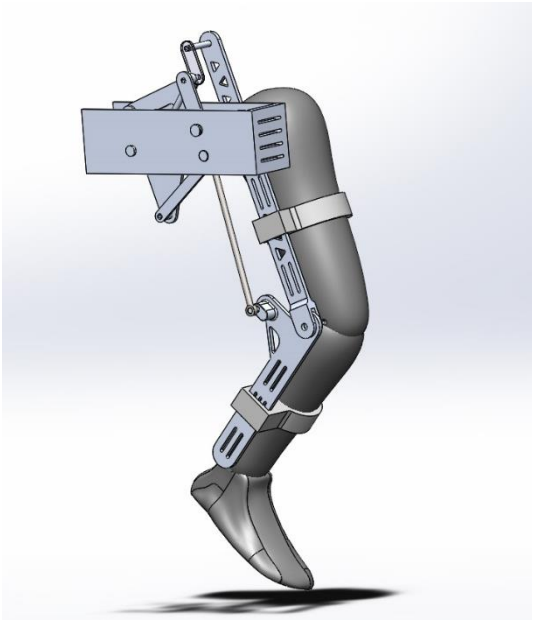

Fig. 4.11 Leg exoskeleton and human leg simulation model

Table 4.4 Linkage and leg masses

Link name	Mass (kg)
Link 1	0.0926
Link 2	0.0443
Link 3	0.527
Link 4	0.272
Link 5	0.0472
Link 6	0.0918
Link 7	0.434
Thigh	8.682
Shank	3.540

A standing still gesture was chosen to conduct the simulation as it is the natural gesture for walking. The subject stands still on the level ground and the leg exoskeleton moves the human leg in the air. In practical application, the patient can be supported by therapists or a weight support frame to remain standing.

A few assumptions were made to conduct dynamic simulation. 1) The motor of the exoskeleton runs at a constant speed. 2) The leg and the leg exoskeleton remain in the sagittal plane during a cycle. 3) The leg joints always align with the leg exoskeleton joints during the cycle. 4) The mass of the human leg is evenly distributed. 5) As the patient is asked to stand still during training, the upper body motion is not considered. 6) There are no relative motions between the foot and shank. Then a simulation model integrating the leg exoskeleton and the human leg was built to estimate the input torque.

The model simulated the motion of human walking for the entire gait cycle starting with the heel strike. Considering natural walking speed can be too fast for a patient after surgery, which may cause injury to the patient, we adopted 1/4 of the natural walking speed as the constant speed to conduct the simulation. Friction coefficients were selected according to the materials in the joints. The input torque was then generated for choosing of the motor. According to the simulation results, the maximum torque during the gait cycle is about 4.88 Nm. A Maxon motor and gearhead combination was selected with a maximum output torque of 5.6 Nm. The output speed of the combination is 13.97 RPM, which is close to ¼ of the normal walking speed.

4.4.2 Control System and Harnesses Development

The motion of the linkage is restricted by its parallel nature. The motions are also safe due to the constraints we applied in the dimensional synthesis process. No additional requirements are needed for the control system to guarantee the safety of the user. In addition, CPM does not require complicated operation and interaction between the human and leg exoskeleton. Therefore, an open-loop control system is sufficient for the device. The Maxon motor is controlled by a Maxon position controller, and a Raspberry Pi is used to program the control system for the device. A joystick is used to activate the exoskeleton.

After the development of the linkage, motor and gearbox choosing and the development of the control system. The leg exoskeleton and harnesses were then manufactured and assembled.

4.5 Results and Discussion

The prototype of the leg exoskeleton is illustrated in Fig. 4.12. The frame is attached to the human torso using harnesses and straps. The counterparts of the thigh and shank are also attached to the leg via customized harnesses. The motor is located behind the wearer's torso.

Fig. 4.12 Leg exoskeleton prototype

A gait cycle of the device is given in Fig. 4.13. To evaluate the device's capability of reproducing the human walking gait at hip and knee joint, the angular displacement of the leg exoskeleton at hip and knee joints are compared with the reference gait data and the optimization results, as in Fig. 4.14.

Fig. 4.13 Gait cycle of the leg exoskeleton

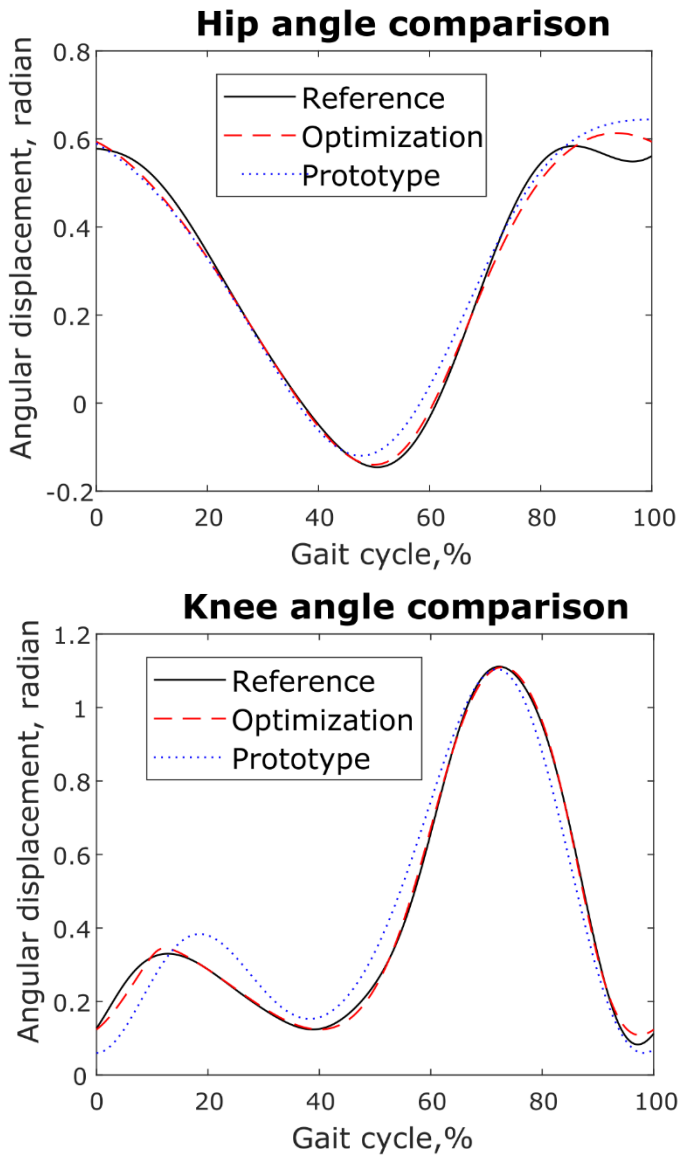

Fig. 4.14 Evaluation of the leg-exoskeleton joint angles

Generally, the optimization results show a close match to the human walking gait. Maximal differences occur at the 97% of the cycle at the hip joint (0.09 radians) and at 20% of the cycle at knee angle (0.12 radians). Differences are expected due to the manufacturing errors and the flexibility of the materials. As the device is only used to move the human lower limb in the air, level ground walking is not considered. Such differences would not affect the rehabilitation effects.

Both the ranges of motion at hip and knee joints stay within that of the human joints. Singularities are also tested by running the device repetitively. No singularities occurred during the operation. The device is able to run forward and backward safely.

This leg exoskeleton proves that a planar linkage is able to be developed into a leg exoskeleton for CPM rehabilitation. The dimensional synthesis method tailored for the leg exoskeleton design is able to achieve a customized leg exoskeleton.

The simulation method to estimate the input torque is also evaluated by comparing the simulated torque with the actual input torque obtained from experiments. A healthy subject wore the leg exoskeleton and stood still on the level ground to conduct the experiments. The subject was asked to relax his leg to follow the device passively. Such practice keeps for several minutes until the subject adapted to the leg exoskeleton. The collected motor current data was processed using a Butterworth low pass filter. Motor torque was then calculated from the current data. The comparison is given in Fig. 4.15.

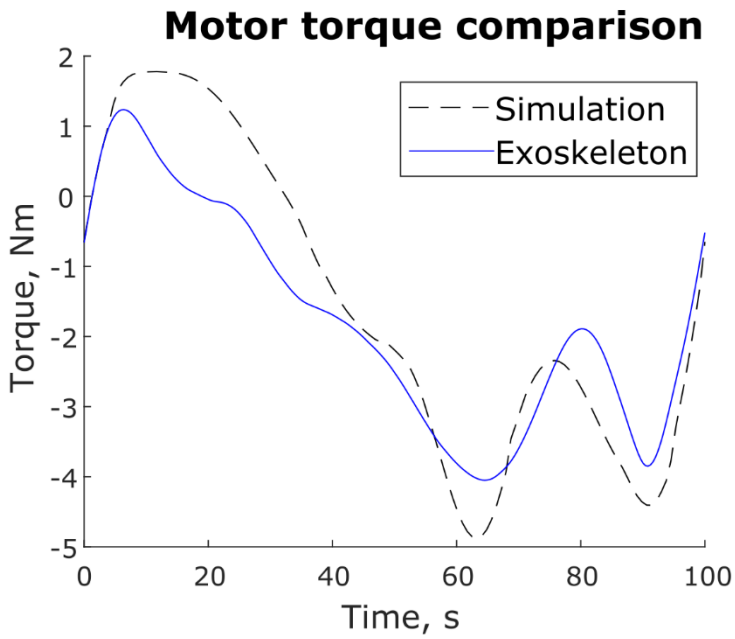

Fig. 4.15 Motor torque validation

The simulated and experimental torque share the same pattern. Differences between the torques are expected as a number of simplifications have been made on the model. Such differences can come from a number of sources, such as the modelling of the frictions, simplicity of the human model, angular displacement differences between the actual device and the optimization results, etc. The simulated maximum torque is slightly greater than the actual maximum input torque. Therefore, simulated torque information can help select the motor and gearhead.

Overall the device is stand-alone, portable and easy to operate compared with the current rehabilitation devices. It can be used outside clinical settings. Future development would concern making the linkage lengths changeable to suit patients with different lower limb dimensions.

In this study, a walking gait is used as a reference motion and a stand still gesture is chosen. Training for other gestures (sitting or lying down) or motions (sit-to-stand transition, stand-to-stand transition, and stair-climbing) are not supported by the current device. However, the 1-DOF-linkage-design methodology can develop exoskeletons for a specific motion in a certain gesture. Simply supplying the design method another reference motion, e.g. sit-to-stand transition, may end up with an exoskeleton for the given motion.

The 1-DOF linkage-based design brings about two major limitations. The leg exoskeleton only provides an embedded motion pattern; A different reference motion requires a re-design of the linkage. Lack of versatility in training modes can affect rehabilitation outcomes. Morphology and gait variations across patients imposes another challenge in developing 1-DOF leg exoskeleton. A customized linkage for a patient with a specific thigh length and gait pattern would not work on another patient. This hinders its application across patients.

4.6 Conclusion

This chapter exploited planar 1-DOF linkages to design a leg exoskeleton for CPM-based rehabilitation. A design procedure was proposed to develop a customizable leg exoskeleton. In the end, a customized 1-DOF linkage-based leg exoskeleton was achieved. The gait pattern provided by the leg exoskeleton is similar to the reference gait. Safety issues have also been addressed effectively. The device is able to provide motions for

CPM based rehabilitation at hip and knee joints. The simulation method for estimating the input torque results in similar pattern and values with the actual input torque for motor and gearbox choosing. The open-loop control system is able to control the device. The 1-DOF leg exoskeleton turns out to be compact and portable, which may be used beyond hospitals or therapy centres.

Part III Clutched-Spring Mechanisms for Energy Efficiency

Chapter 5 Simulation-Based Study on Clutched-Spring Mechanisms for Reducing Walking Metabolic Cost

Abstract

Reducing the metabolic cost of walking has long been a challenge for exoskeleton researchers. A recent breakthrough reported a passive exoskeleton that yielded 7.2% energy saving with a CSM working in parallel with calf muscles. This chapter investigated whether the same biomechanics exists in the hip and knee joints. The study employed OpenSim, an open source platform, and the MATLAB Optimization Toolbox to obtain the optimal on/off timings and the stiffness of the CSMs for walking energetic efficiency. When applied to the ankle joint, the proposed approach yielded results that agree with the reported study. We then extended this method to the hip and knee joints, respectively. The simulations show that the springs could save up to 6.38%, 4.85% and 7.63% for the ankle, knee and hip joints at the optimal stiffness of 8.20 kN/m, 7.35 kN/m and 4.15 kN/m, respectively.

5.1 Introduction

The proposed leg exoskeleton in this thesis provides assistance at hip and knee joints. Our aim is to use CSMs at hip and knee joints in the leg exoskeleton to reduce energy consumption. However, the previous study only used CSMs at the ankle joint. The mechanism's performance at hip and knee joints is unknown. Therefore, this chapter

extended the mechanism to hip and knee joints. Though the 1-DOF leg exoskeleton does not assist level ground walking. The motion between the leg exoskeleton and human level ground walking still share some similarities, especially during the swing phase of ground walking. Therefore, studies on the CSMs at hip and knee joints in walking energetics may also benefit the 1-DOF leg exoskeleton design.

5.2 Clutched-Spring Mechanism in Simulation

5.2.1 Simulation Environment and human model

OpenSim is a piece of software capable of accurate musculoskeletal locomotion simulation, featuring powerful tools such as residual reduction algorithm, computed muscle control (CMC) and metabolic probe [147]. This study employs the COM tool and the metabolic probe. The CMC tool reveals the muscle forces based on the gait kinematics and ground reaction forces; the metabolic probe can calculate the energy consumption the whole body.

The CMC tool plays a key role in achieving an optimal CSM. It is a static optimization process to minimize a cost function, which is a sum of squared muscle controls plus a weighted sum of squared acceleration errors, it is given as follows:

$$J = \sum_{i=1}^{n_x} x_i^2 + \sum_{j=1}^{n_q} w_j (\ddot{q}_{tj} - \ddot{q}_{mj})^2 \tag{5.1}$$

where n_x is the number of muscles; x_i is the i^{th} muscle force, $0 \leq x_i \leq 1$; n_q the number of coordinates to be tracked; w_j the weight assigned to each acceleration error; $\ddot{q}_{tj}$ the tracked acceleration of the j^{th} coordinate; $\ddot{q}_{mj}$ the acceleration of the j^{th} coordinate generated by muscles. The first term $\sum_{i=1}^{n_x} x_i^2$ ensures minimal muscle efforts; the second term $\sum_{j=1}^{n_q} w_j (\ddot{q}_{tj} - \ddot{q}_{mj})^2$ guarantees the muscle driven model reproduce a given motion. Overall, the optimization problem reveals the muscle forces for a provided motion.

An accurate human musculoskeletal walking simulation for level ground locomotion is essential to this study. The OpenSim community has developed a number of walking models [157] readily for research purposes. In this study, we used the "gait10dof18musc" model which focuses on the lower limbs. The model is from a male subject, 75 kg in weight and 1.8 m in height, walking at 1.2 m/s on a horizontal treadmill. It is notable that a number of simplifications have been made in the model: 1) The upper body is concentrated at the torso. 2) Only movements in sagittal plane are considered. 3) Muscles are modelled into key flexor/extensor muscle groups.

5.2.2 Clutched Spring Mechanism Investigation

To mount the springs in parallel with human muscle groups, a wearable exoskeleton was built in SolidWorks based on the morphology of the subject. The exoskeleton model and

its schematic are given in Fig. 5.1. Then the 3D model was imported and attached to the human model. The exoskeleton is made massless to avoid the influence of adding masses to the walking model. A walking cycle for the human-exoskeleton model were then generated in OpenSim, as given in Fig. 5.2.

In a CSM, the extension spring generates a tension force/torque during a walking gait. A clutch (Fig. 5.1 (*b*)) is coupled with the spring to manage the tension force/torque. For example, at the ankle joint after the spring is turned on at ankle joint, if |BC| increases the spring is stretched and exerts a tension force. If the force assists the leg movement, the clutch remains on; whereas the clutch is turned off if it resists the leg movement.

At the ankle joint, the spring assists plantarflexion, therefore, it can be considered as planar flexor. At the hip and knee joint, the springs assists flexion, and they represent flexor muscles. The configuration was chosen based on walking energetics [158]. Another study [138] has shown that a CSM at ankle joint with proper spring stiffness and on/off timings can reduce locomotion energy. We hypothesis that the mechanism can also be applied to hip and knee joint.

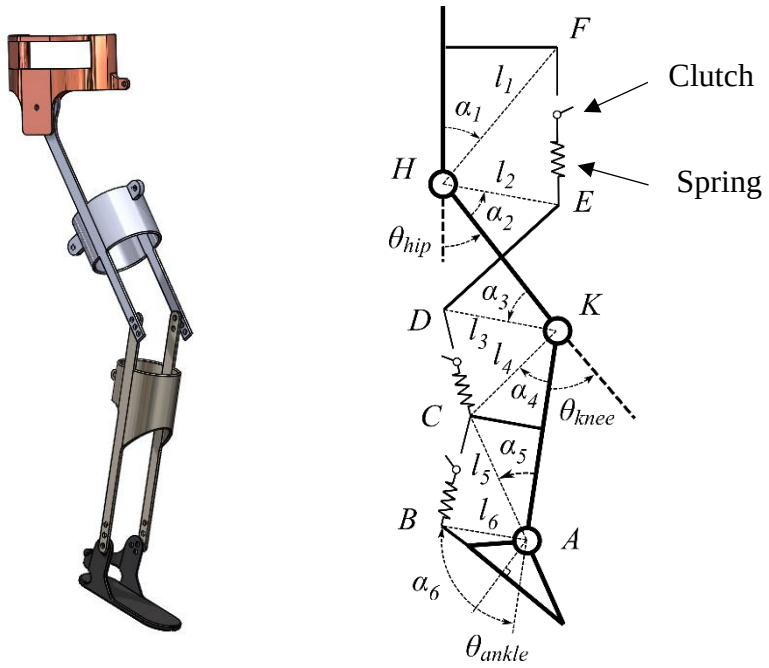

(*a*) (*b*)

Fig. 5.1 CSM leg exoskeleton 3D model and schematics

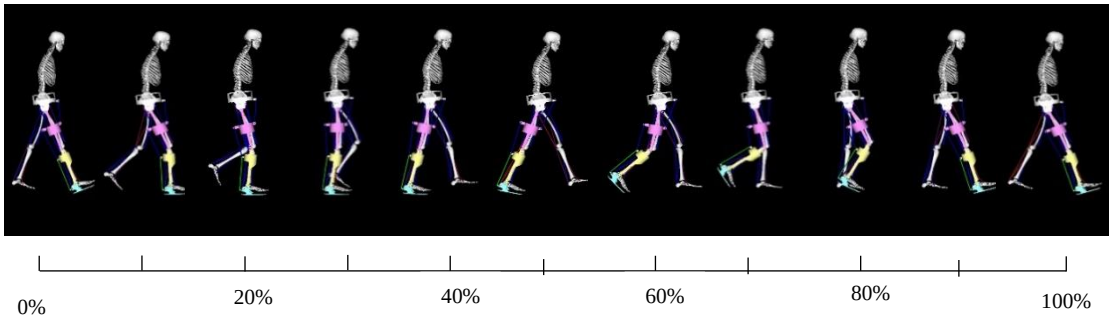

Fig. 5.2 Gait cycle of the human-exoskeleton model

OpenSim does not support direct optimization of a CSM in a human walking model. We proposed a two-step method to obtain a CSM design for maximal energy saving as in Fig 5.2. First, we introduce a tension force to replace the CSM at a leg joint, e.g. BC at ankle

joint. The force functions like a muscle and its profile can also be optimized in the CMC process. We use the term “virtual muscle” to distinguish it from the muscles in the human model. Conducting CMC on the human walking model with the virtual force returns the force profile of the virtual muscle, from which the CSM’s optimal on/off timings can be identified.

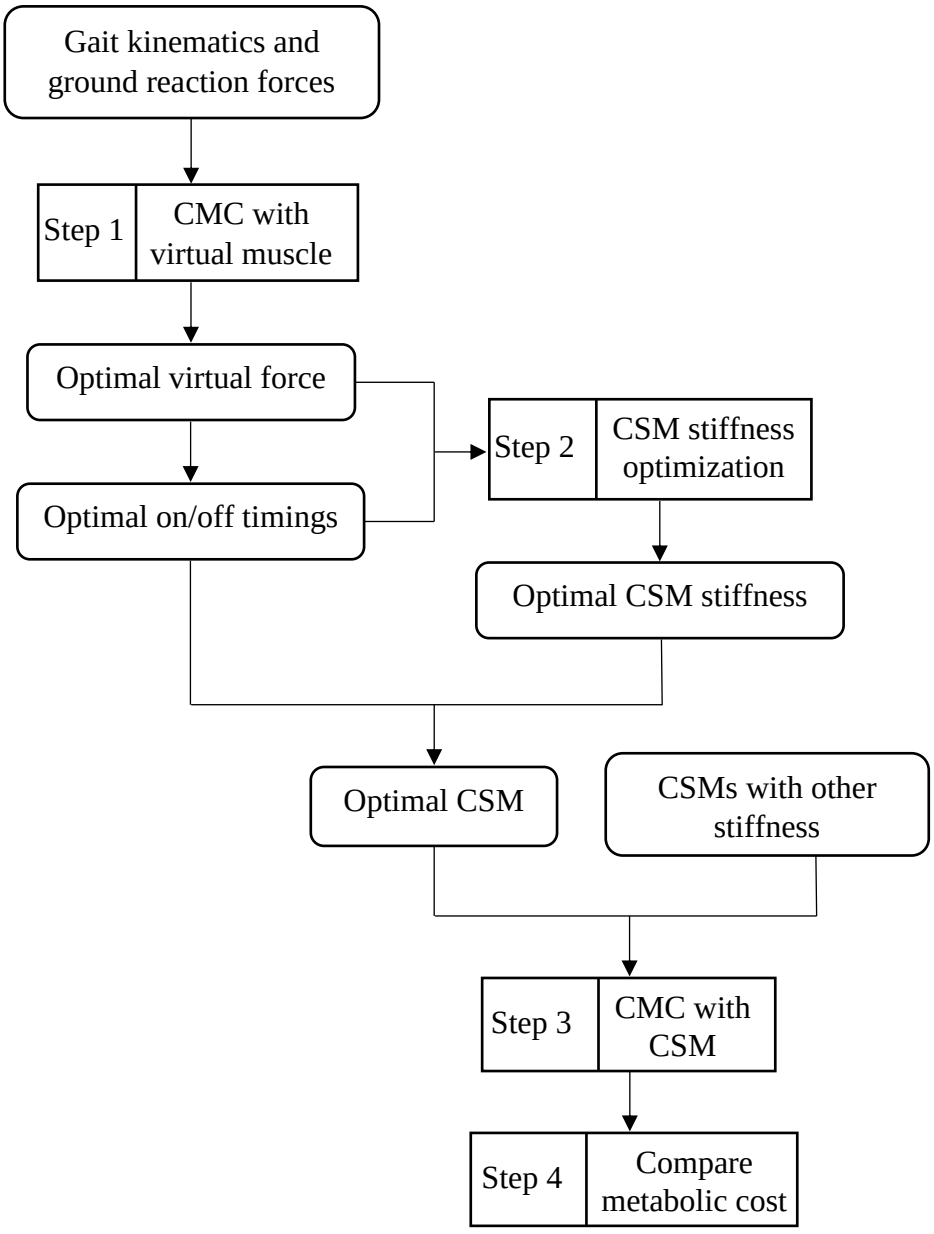

Fig. 5.3 CSM study flowchart

In the second step, we take the force profile between the on and off timings as reference and optimize the CSM's stiffness to reproduce the reference force. Thus, the optimal CSM design can be obtained via Step 1 and 2. The optimal CSM is then put into the walking model e.g. CSM BC at ankle joint in Fig. 5.1, to calculate the metabolic cost following

Step 3 and Step 4. Its metabolic cost is also compared with other CSMs with same on/off timings but different stiffness for validating the optimal CSM stiffness.

In Step 2, the cost function for the optimization of each spring stiffness is defined as the sum of squared error between actuator force and spring generated force in the reference points.

$$J = \sum_{t=t_{on}}^{t_{off}} (F_{ref}(t) - k\Delta l(t))^2 \tag{5.2}$$

where k is the spring stiffness; t_{off} is the off timing of a spring; t_{on} is the off timing of a spring; $F_{ref}(t)$ is the virtual muscle force at time t; $\Delta l(t)$ is the spring stretch after the engaging timing. The spring disengages when $\Delta l(t) = 0$.

The parameters of the exoskeleton are given in Table 5.1.

Table 5.1 CSM leg exoskeleton parameters

Angle	Value (radian)	Length	Value (mm)
α_1	1.40	l_1	172.62
α_2	0.36	l_2	244.00
α_3	0.51	l_3	242.00
α_4	0.58	l_4	150.91
α_5	0.27	l_5	309.82
α_6	1.01	l_6	94.34

The spring stretches $\Delta l(t)$ are given by the following equations:

$$\Delta l_{ankle}(t) = d_{BC}(t) - d_{BC}(t_{on}) \tag{5.3}$$

where

$d_{BC}(t) = l_5^2 + l_6^2 - 2l_5 l_6 \cos[\pi + \theta_{ankle}(t) - \alpha_5 - \alpha_6]$;

$$\Delta l_{knee}(t) = d_{CD}(t) - d_{CD}(t_{on}) \tag{5.4}$$

where

$d_{CD}(t) = l_3^2 + l_4^2 - 2l_3 l_4 \cos[\pi + \theta_{knee}(t) - \alpha_3 - \alpha_4]$;

$$\Delta l_{hip}(t) = d_{EF}(t) - d_{EF}(t_{on}) \tag{5.5}$$

where

$d_{EF}(t) = l_1^2 + l_2^2 - 2l_1 l_2 \cos[\pi - \theta_{hip}(t) - \alpha_1 - \alpha_2]$.

d_{BC}, d_{CD} and d_{EF} are the distance between the spring connecting points at time t for ankle, knee and hip joints; $\Delta_{ankle}(t)$, $\Delta_{knee}(t)$ and $\Delta_{hip}(t)$ are the spring stretches after engagement at time t for ankle, knee and hip joints; $\theta_{ankle}(t)$, $\theta_{knee}(t)$ and $\theta_{hip}(t)$ are the angular displacements for ankle, knee and hip joints respectively at time t.

Using function "fmincon" in the MATLAB Optimization Toolbox, we obtained the optimal stiffness for each spring. To evaluate the effectiveness of the optimization results, the metabolic cost of walking with optimal stiffness and other spring stiffness values were compared.

5.3 Results and Discussion

The on/off timings of the springs are given in Fig. 5.4. The on timings were obtained from the virtual muscle profiles in Fig. 5.5. The off timings were obtained when the joint angle return to the value at spring-on timings, when the springs return to their lengths at spring-on timings. The on/off timings of the springs show that the both hip and knee springs can assist the swing phase (1.38s – 1.9s).

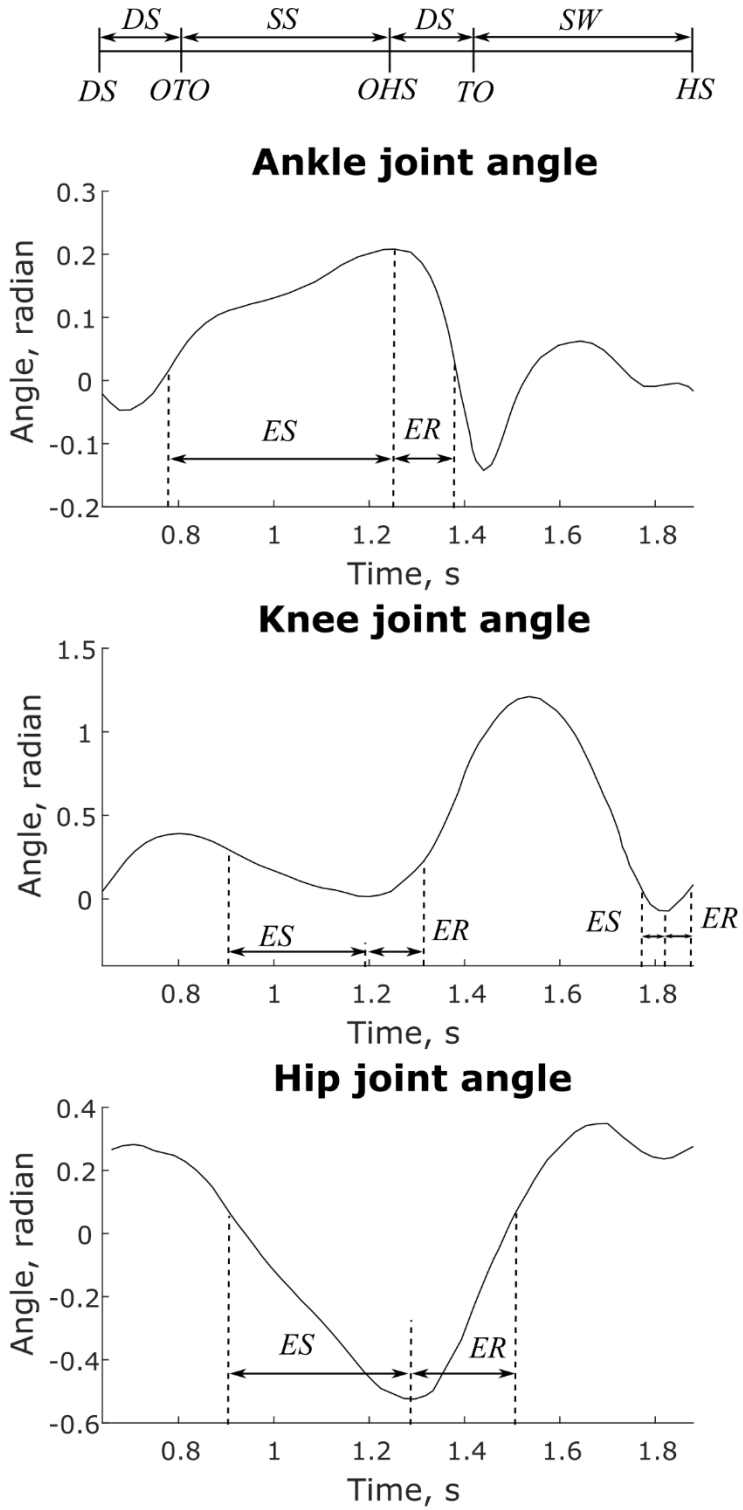

Fig. 5.4 Angular displacements comparison. Gait events and phases are indicated at the top of the plots: HS = Heel strike, OTO = Opposite toe off, OHS = Opposite heel strike, TO = Toe off, DS = Double support phase, SS = Single support phase, SW = Swing phase. Energy storage and return phases are marked in the plots: ES = Energy storage, ER = Energy release.

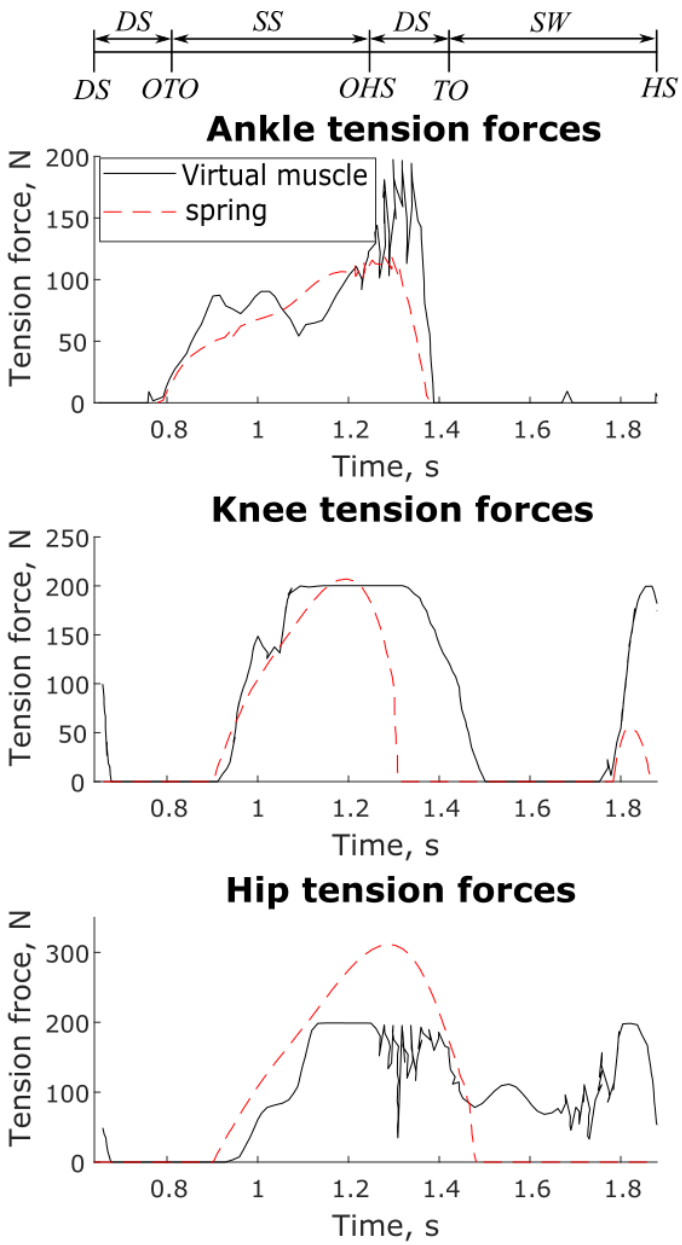

Fig. 5.5 Tension force comparison

The optimal virtual muscle force for each joint is given in Fig. 5.5. The ankle virtual force is engaged at 0.78s, slightly after the ankle angle reaches the first minimum. This slightly differs from the unpowered exoskeleton in [138] whose engaging timing is at the minimum. According to [159, 160] human seeks a similar torque pattern when walking

with assistive devices at the ankle joint. A typical ankle torque profile indicates that at the first minimal ankle angle the torque is provided for dorsiflexion [153]. If the actuator is engaged during 0.71s-0.78 it works opposite to the gross muscle torque. Inferentially, this would result in more energy consumption. Therefore, a slightly late engagement would save more energy. The actuator disengages at 1.38s after toe-off, which is due to no torque is needed at the ankle joint in the swing phase. This is in line with the disengaging time in [138]. Between the engaging and disengaging time, the actuator exerts forces with similar patterns with human ankle joint torque. This indicates its capability for reducing the muscle work. In summary, the optimal force provides a good match with the previous study [138], which verifies the proposed method.

The knee virtual muscle is engaged in two periods. The first period starts at 0.90s and ends at 1.33s, occupying single stance phase, push off phase and early swing phase. The second period happens at 1.77s and ends with the heel strike, to aid deceleration and flexion in the late swing. The hip virtual muscle is engaged around 0.9s. And it is disengaged after heel strike. It assists the single stance, push off, and the entire swing phase.

Overall, the virtual muscles are engaged mainly for single stance phase, push-off phase and early swing phase, where pushing-off and leg swing cost most of the energy during a walking cycle. The curves indicate that hip and knee joint are also potential of comparable energy saving, which can be estimated by the areas under the curves. However, in the previous study, the knee and hip joint have not been fully explored.

The optimization results of spring stiffness are also illustrated in Fig. 5.5, in comparison with the optimal virtual muscle forces. The springs are restricted by the geometry of the exoskeleton and angular displacement of each joint. When the springs return to their rest length after the engagement, they can no longer provide tension force. Differences between optimal virtual forces and spring provided forces are expected. Overall, the ankle spring has the best match. Engaging and disengaging timing coincides with the optimal force. Both hip and knee joints have early a disengaging timing, which reduces the effect for energy saving.

The energy storage and return phases of each spring are illustrated in Fig. 5.4. The springs store energy until a joint angular extremum occurs, when the springs reach their maximum length, and return energy assisting the following phases. It is obvious that all the springs store energy during single support phase and return energy to assist push off. Additionally, hip spring also assists early swing.

The metabolic for 3 conditions: free walking, walking with virtual muscle assistance and walking with spring assistance, are compared in Fig. 5.6. The optimal actuator forces end up with maximal energy saving of 17.48%, 22.33% and 12.07% for hip knee and ankle joint respectively. This hints powered assistance for knee joint in exoskeletons, while the previous exoskeleton mostly concern hip and ankle joint.

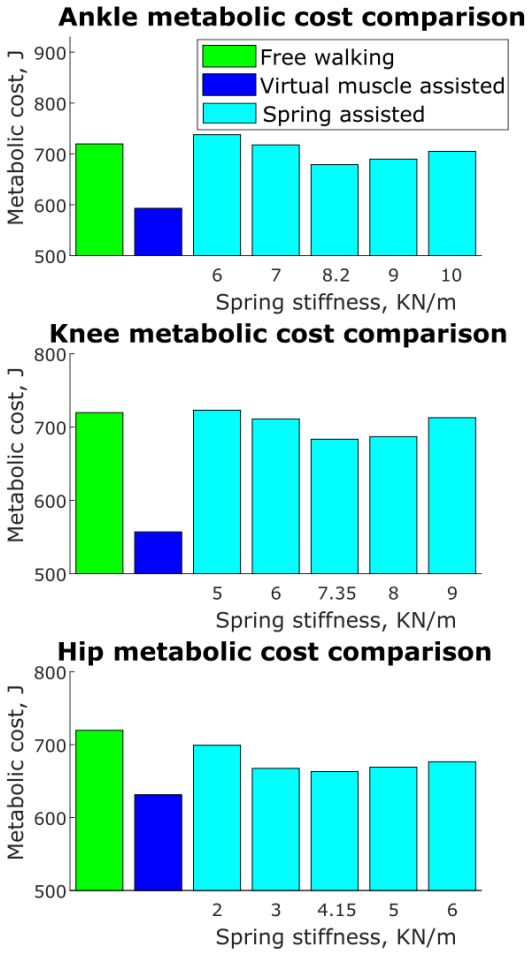

Fig. 5.6 Optimal stiffness evaluation

Springs are not equivalent to active tension forces at energy saving due to the restricted stretching of the springs. The optimal stiffness values bring about the highest energy efficiency in three joints. These values are found to be 8.20 kN/m, 7.35 kN/m and 4.15 kN/m for ankle, knee, and hip joint respectively, with metabolic savings of 6.38%, 4.85% and 7.63%. The metabolic cost vs spring stiffness pattern in ankle joint agrees with study in [138]. Compliant springs save less energy due to their inability to generate sufficient forces. Stiff springs are likely to cause the muscle to balance the over-generated spring force, resulting in increases of metabolic cost. This validates the simulation-based method

for investigating the clutched-spring mechanism in energy saving. Similar patterns are also found in hip and knee joints, which suggests the same bio-mechanism in hip and knee joints.

5.4 Conclusions

We extended the concept of a CSM-based exoskeleton for ankle assistance into the hip and knee joints by using a spring-loaded exoskeleton. The simulation results of ankle joint matched those in the previous studies in terms of on/off timings and stiffness pattern. This validated the effectiveness of our simulation-based method. The CSMs were also found energetically beneficial for the hip and knee joints. Both the hip and knee CSMs can assist the swing phase, which indicates their applications in the 1-DOF leg exoskeleton as the motion of the 1-DOF exoskeleton can be considered as an extended swing phase.

Chapter 6 Predictive Dynamics on a Single Pendulum Leg

Abstract

Recent studies on human motion simulation employ an optimization-based method, called predictive dynamics (PD), to generate human-like motions such as walking, running, lifting, stair climbing, etc. Performance measures, rather than collected motion data, are used to guide the motion of the human model. As a result, the PD method can perform cause and effect study on human motion. However, current studies mainly focus on reproducing human motions using PD; its application for designing exoskeleton devices has not be exploited. This chapter investigated the application of the PD on obtaining the optimal design of a CPM. A pendulum leg model was used to test the method and obtain insights into the functionality of the CSMs. The study compares the performance of unclutched-spring mechanisms (UCSMs) and CSMs at various speeds. Both unclutched ones and clutched ones can reduce the motor work, whereas more energy is saved with clutched ones at slow speeds. We conclude that PD is effective for finding the optimal designs of CSM in the pendulum leg. The results also suggest the use of CSMs to save energy cost of a human or a human-exoskeleton system.

6.1 Introduction

Predictive dynamics is a powerful method for simulating complex multibody dynamic systems, e.g. human motions. In this study, we extend its application to leg exoskeleton

development. PD avoids the integration of equations of motion which makes solving the dynamic equations more convenient. PD also enables cause-effect study, which allows adding springs into leg exoskeleton and investigate their performance.

This chapter tested the effectiveness of PD method on designing a clutched torsional spring for a single pendulum leg. Preliminaries of PD is first introduced and followed by description and formulation of a pendulum leg model. The PD method is then applied on the leg model for 2 cases: with an UCSM and with a CSM.

In this study, the leg (Fig. 6.1) is driven by a motor which is assisted by a clutched torsional spring at the hip joint. The spring spans the base and the pendulum leg. When the spring is turned on and twisted it exerts a torque which can be used to assist the movement of the leg. Three parameters are used to represent the mechanism: spring stiffness, on and off timings of the clutch. We hypothesize that a proper combination of such parameters would reduce the mechanical energy to drive the pendulum.

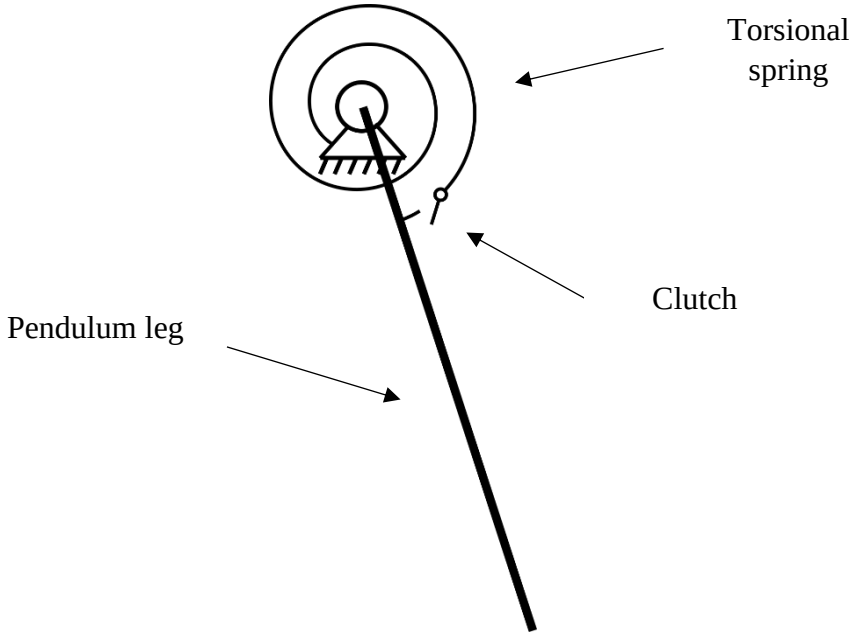

Fig. 6.1 Pendulum leg model

In the OpenSim study, we used linear springs mounted on an exoskeleton. This is for the easy realization of a physical prototype in future study. In the pendulum study, we use a torsional spring instead. The torsional spring CSM removes the parameters arisen from the exoskeleton (as in Fig 5.1 (*b*)) and makes the study focus on the effect of the springs. This can lead to insights into the functionality of a CSM through the motion.

6.2 Predictive Dynamics Preliminaries

PD is defined as a general optimization approach for human motion prediction with unknown forces and state variables. This model converts the problem of predicting human

motion into an optimization problem. Resolving the optimization problem returns the joint torques and model states. The general formulation of the PD method can be given as:

$$\begin{aligned} &\min \quad J(\boldsymbol{q},\boldsymbol{\tau},t) \\ &\boldsymbol{s.t.}: \ \boldsymbol{g} \le 0 \\ &\quad \boldsymbol{q}^L \le \boldsymbol{q} \le \boldsymbol{q}^U \\ &\quad \boldsymbol{\tau}^L \le \boldsymbol{\tau} \le \boldsymbol{\tau}^L \end{aligned} \tag{6.1}$$

where,

$\boldsymbol{q} = f_1(\boldsymbol{Q},T)$,

$\boldsymbol{\tau} = f_2^{-1}(\boldsymbol{q})$.

The objective J is usually a function of joints states ($\boldsymbol{q}$), motor torques ($\boldsymbol{\tau}$), and time t. $\boldsymbol{g}$ includes the constraints for a specific motion. $\boldsymbol{q}^L \le \boldsymbol{q} \le \boldsymbol{q}^U$ sets up the constraints for joint states, while $\boldsymbol{\tau}^L \le \boldsymbol{\tau} \le \boldsymbol{\tau}^L$ restricts the joint torques. Joint states $\boldsymbol{q}$ are represented by B-splines, which are defined by control points $\boldsymbol{Q}$ and total motion time T. Joint torque are then calculated using ID: $f_2^{-1}(\boldsymbol{q})$. Therefore, the design variables of the optimization are the control points of the B-splines for defining the joint profiles.

Joint states are represented by B-splines curves. Splines are widely used for representing curves and surfaces. B-splines is a linear combination of basis functions (Basic-splines). Using a B-spline to define the joint displacement bring about benefits such as continuity, differentiability, endpoint interpolation and local control [161].

A B-spline curve can be constructed using the following recursive form:

$$C(u) = \sum_{k=0}^{n} N_{k,p}(u) P_k \tag{6.2}$$

where

$$N_{k,p}(u) = \frac{u - u_k}{u_{k+p} - u_k} N_{k,p-1}(u) + \frac{u_{k+p+1} - u}{u_{k+p+1} - u_{k+1}} N_{k+1,p-1}(u), \tag{6.3}$$

when $p = 0$,

$$N_{k,0} = \begin{cases} 1 & \text{if } u_k \le u \le u_{k+1} \\ 0 & \text{otherwise} \end{cases} \tag{6.4}$$

A B-spline curve is defined by n+1 control points P_0 to P_n, a knot vector $U = [u_0, ..., u_m]$, and its degree p. The number of control points (n+1), the number of knots (m+1) and B-spline degree should satisfy the following relationship:

$$m = n + p + 1 \tag{6.5}$$

The joint velocity and acceleration can be obtained by taking derivatives of the joint displacement B-spline curve. Derivatives of a B-spline curve can be calculated using the following equation:

$$C^i(u) = \sum_{k=0}^{n} N_{k,p}^i(u) P_k \tag{6.6}$$

where

$$N_{k,p}^i(u) = \frac{p!}{(p-k)!} \sum_{j=0}^{i} a_{i,j} N_{k+j}^{p-i} \tag{6.7}$$

with

$$a_{0,0} = 1,$$

$$a_{i,0} = \frac{a_{i-1,0}}{u_{k+p-i+1} - u_k},$$

$$a_{i,j} = \frac{a_{i-1,j} - a_{i-1,j-1}}{u_{k+p+j-i+1} - u_{k+j}},$$

$$a_{i,i} = \frac{-a_{i-1,i-1}}{u_{k+p+1} - u_{k+i}}.$$

In order to calculate the acceleration, the degree of the B-spline should be greater than 3. In this study, we used 4th degree B-spline to achieve smooth acceleration profile.

The objective can take multiple forms such as dynamic effort, mechanical energy, metabolic energy, etc., or a combination of these [162]. In this study, we focused on the energy consumption of the motor. Therefore, the mechanical energy.is selected as the objective. This can lead to minimal motor energy cost.

In literature [162], the problem is solved via sequence quadratic programming algorithms, which is gradient based. SNOPT was used in previous studies. PD aims to solve complex optimization problems, in which hundreds of design variables are involved. This makes sequential quadratic programming an effective and efficient way to find local optimum. Therefore, in the study, the SQP algorithm was used to solve the optimization problem. “fmincon” in MATLAB was used. To obtained global optimum, Global Search is used with randomly generated initial populations.

6.3 Pendulum Leg Study

Before applying PD on the leg exoskeleton, it is first tested on a pendulum leg. This serves 2 purposes. On one hand, a simple model can test the effectiveness of the PD method. On the other hand, the study can provide insights into the functionality of CSMs, which is important for successful implementation on the leg exoskeleton.

Our leg exoskeleton aims to provide passive motion for the right leg, while the left leg keeps standing straight. In this configuration, the leg can be simply considered as a pendulum. Therefore, we use a pendulum model to represent the human leg. To make the model resemble the leg motion, the pendulum is required to reproduce the joint angle profile at the hip joint. The revolute joint can be considered as the hip joint, which is driven by an actuator. To further simplify the problem, we use a torsional spring instead of a linear spring to assist the joint. The torsional spring can be turned on/off for once during the cycle. In this study, the aim is to obtain the optimal on/off timings and spring stiffness that reduces the actuator torque. The pendulum model is given in Fig. 6.1.

6.3.1 Dynamic Analysis

The mathematical model of the pendulum can be given as follows:

$$\tau = I\ddot{q} + mg\frac{l}{2}\cos q + k\Delta q_{spring} \tag{6.8}$$

where m is the mass of the leg; I the moment inertia; l the length; k the stiffness of the torsional spring. Δq_{spring} the change of spring turning angle since turned on.

The parameters of the pendulum leg are given in Table 6.1. The mass of the leg was estimated from a subject of 60 kg and human morphological studies [156]. Leg lengths were obtained from the subject. Moment inertia was approximated using a cylinder model.

Table 6.1 Pendulum leg parameters

Name	Value
Mass	11.916 kg
Moment of inertia	0.6677 kg·m^2
Length	0.82 m

6.3.2 Construction of the Optimization Problem.

Design variables consist of a number of control points, and parameters for the torsional spring if the spring is considered in the model. The following vectors give the design parameters:

$$X = [Q_1, Q_2, ...Q_n, t_{on}, t_{off}, k] \tag{6.9}$$

where, Q_1 to Q_n are the B-spline controls points that defines the angular displacement of the pendulum; t_{on} and t_{off} the on and off timings of the spring. k the stiffness of the torsional spring.

The design variables vary according to the cases to set up the optimization problem. This study considers three cases: without spring, with UCSMs, and with CSMs. It first evaluated the PD method without the spring, then explored the effects of spring with UCSMs, and further investigated the influence of introducing clutches with CSMs.

The hip joint displacement q is represented using a B-spline of degree 4. Twenty-one control points have been used to define the curve. Then the joint angle acceleration can be obtained by taking the second derivative of joint displacement B-spline.

We attempt to reduce the energy cost by the hip joint motor, therefore, we employed the mechanical energy by the joint torque as the objective. The objective can be given as the following equation.

$$J = \int_0^T | \tau \dot{q} | dt \tag{6.10}$$

The pendulum is required to precisely reproduce the motion of the exoskeleton hip joint for a walking cycle. A number of equality constraints have been set on the joint angles for this purpose.

$$q^i_{pendulum} - q^i_{exoskeleton} = 0 \tag{6.11}$$

where $q^i_{pendulum}$ is the i^{th} point in the pendulum angular profile, while q^i_{human} is the corresponding angular displacement from the leg exoskeleton hip joint.

An inequality constraint is also needed when the clutches are included in the optimization problem.

$$t_{on} - t_{off} < 0 \tag{6.12}$$

Bounds have been applied on the control points and spring parameters. Bounds on control points cover the ROM of the pendulum. Bounds on spring parameters make the optimization problem returns a feasible solution. We use the following bounds to constraint the design variables.

$$\begin{aligned} LB &= [-\pi, ..., -\pi, 0, 0, 0], \\ UB &= [0, ..., 0, 4T, 4T, 100] \end{aligned} \tag{6.13}$$

Lower bounds for joint angle have been set as $-\pi$, and for on/off timings and spring stiffness as 0; Upper bounds for joint angle have been set as 0, for on/off timings as $4T$, and for spring stiffness as 100.

If the spring is clutched, turning off the spring during the motion may cause a sudden motor torque change, which leads to discontinuity in the optimization problem. This can lead to failures in finding optimal solutions. To avoid the problem, we use an approximation of a step function to turn the spring off. This modification does not alter

the nature of the study, while removes the discontinuity in the problem. The step function approximation used in the study is given as follows:

$$f = \frac{1}{1+e^{300(t-t_{off})}} \tag{6.14}$$

Thus, the spring stiffness curve can be expressed as:

$$k_{modified} = \begin{cases} 0, & if\ \ t < t_{on} \\ \dfrac{k}{1+e^{300(t-t_{off})}}, & if\ \ t \geq t_{on} \end{cases} \tag{6.15}$$

where *k* is the spring stiffness, $k_{modified}$ is the modified spring stiffness curve.

Therefore, the optimization problem can be established as:

Objective: $\min. J = \int_0^T |\tau \dot{q}| dt$

Design variable: $X = [Q_1, Q_2, ...Q_n, t_{on}, t_{off}, k]$, where the spring parameters are added accordingly.

Constraints: from equations (6.11), and (6.12).

Bounds: from equation (6.13).

6.4 Inverse Dynamics Analysis for Validation

The spring assisted results are compared with ID based study. As the pendulum follows the motion of the leg exoskeleton. Therefore, the angular states of the pendulum take the following form:

$$\begin{aligned} q &= \varphi_3, \\ \ddot{q} &= \ddot{\varphi}_3. \end{aligned} \tag{6.16}$$

According equation (4.7) in Chapter 4,

$$\varphi_3 = 2\tan^{-1}\frac{F_3 + \sqrt{E_3^{\,2} + F_3^{\,2} - G_3^{\,2}}}{E_3 - G_3} \tag{6.17}$$

Take the second derivative of the loop equation (4.3) and solve for $\ddot{\varphi}_3$ equal

$$\ddot{\varphi}_3 = -\frac{l_1\ddot{\varphi}_1\sin(\varphi_1-\varphi_2) + l_1\dot{\varphi}_1^{\,2}\cos(\varphi_1-\varphi_2) + l_2\dot{\varphi}_2^{\,2} + l_3\dot{\varphi}_3^{\,2}\cos(\varphi_3-\varphi_2)}{l_3\sin(\varphi_3-\varphi_2)} \tag{6.18}$$

Substitute (6.17) and (6.18) through (6.16), then into (6.8), where $k = 0$, returns the motor torque. The mechanical energy can further be calculated using equation (6.10). The results serve as reference to evaluate the effectiveness of the PD method.

6.5 Results and Discussion

Three cases were considered: without spring, without UCSMs, and with CSMs. In the without-spring case, we investigate if the PD method is able to reproduce the exoskeleton hip joint angle with the proper joint torque. Its results are compared with ID analysis. The

comparison is given in Fig. 6.2. Both the joint angle and the joint torque are identical with the inverse dynamic analysis. Errors between the curves are small. A mechanical energy cost of 16.67 J is observed in both studies. Therefore, the PD based method is able to reproduce the motion of the exoskeleton-driven leg and reveal the joint torque required to achieve the motion. The PD method does obtain the joint profile and torque without conducting integrations on the equations of motion.

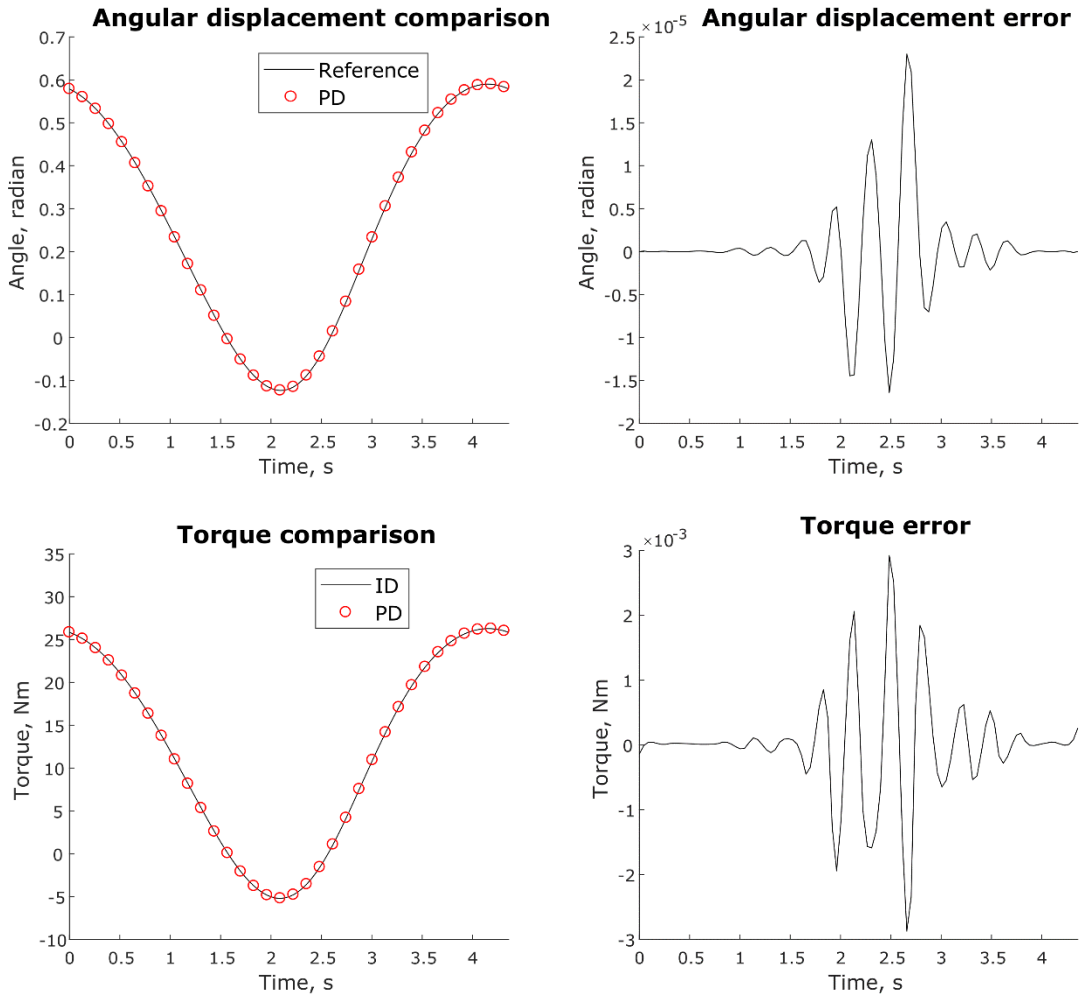

Fig. 6.2 Pendulum study results – without spring

A torsional spring was then added in the pendulum leg. The spring is turned on during the entire cycle of the motion. The study investigates if adding the spring can reduce the motor energy cost. As the proposed 1-DOF leg exoskeleton aims to provide slow motion for CPM rehabilitation, the study examines the springs at various motion speeds: ¼ of, ½ of, ¾ of, and the normal walking speed.

The torques are compared in Fig. 6.3 and the optimal spring stiffness at various speeds are given in Table 6.2. In Fig. 6.3, adding the spring does not affect the hip joint angle. In addition, the net torque to drive the motion remains unchanged. This is because the dynamic model and state profiles are the same with or without a spring.

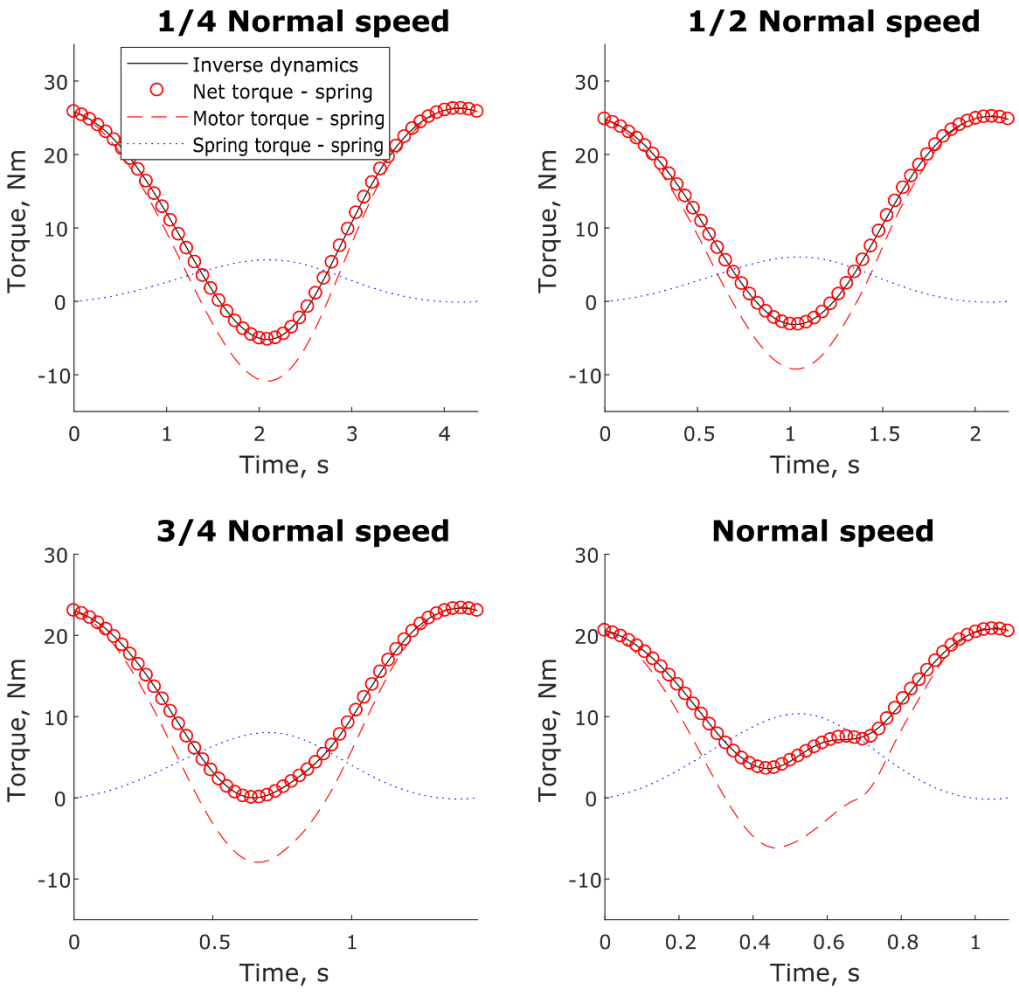

Fig. 6.3 Pendulum study results – with UCSMs at various speeds

Table 6.2 Spring stiffness from PD

Speeds (of normal walking speed)	Spring stiffness (Nm/radian)
¼	8.08
½	8.63
¾	11.45
1	14.75

We took the absolute values of the torques to better understand the effects of the springs, which gives Fig 6.4. In the cases of with or without spring, the motion remain the same. Therefore, $\dot{q}$ remains the same. According to equation (6.10), the mechanical energy is directly affected by the absolute value of motor torque. A spring provides assistance effect when the absolute value of the motor torque is reduced, whereas generate resistance effect when the absolute value of the motor torque is increased. Figure 6.4 shows that springs work along with motor at the beginning and end of the motion, whereas against motor in the middle part. At the beginning and end of the motion, stiffer springs tend to provide more assistance, whereas the middle part prefers softer springs for less spring resistance. The optimization process eccentrically finds the optimal spring stiffness that balances the assistance and the resistance effect.

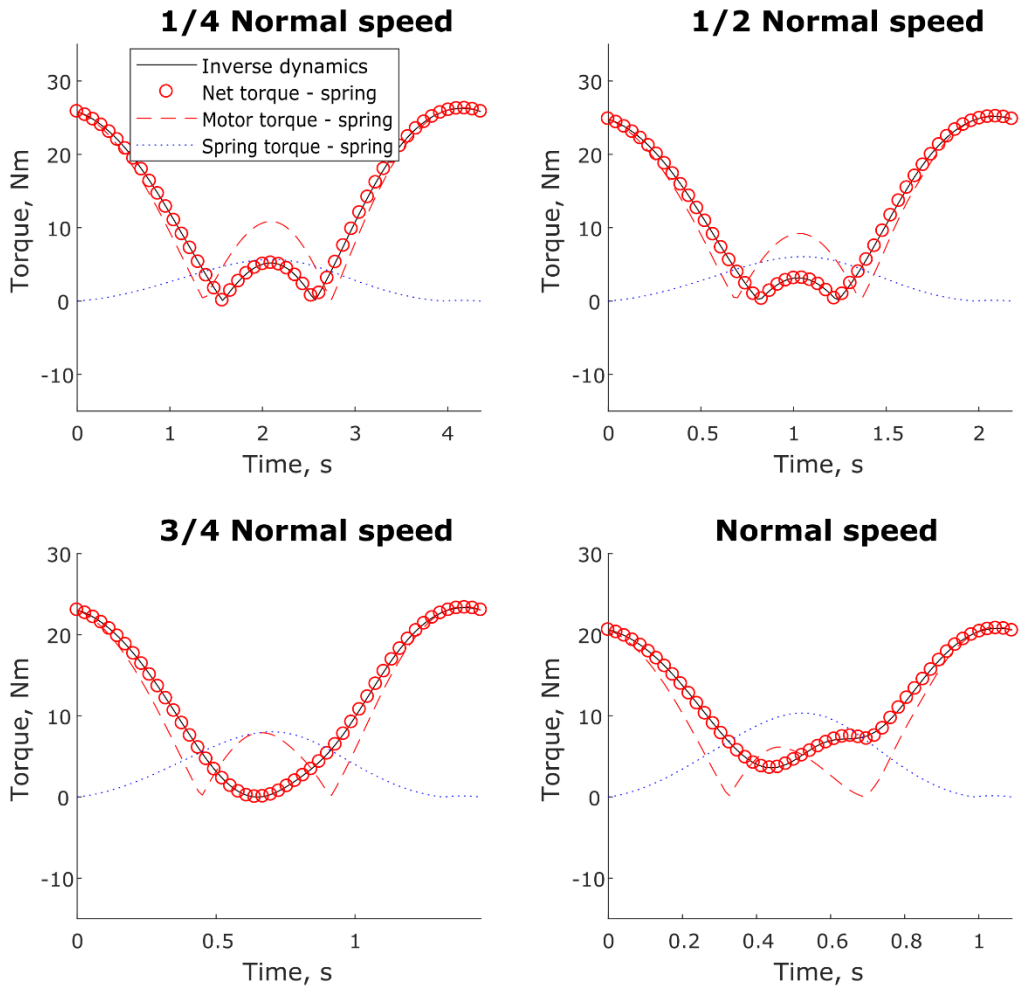

Fig. 6.4 Absolute values of the torques

At slower speeds, the resistance effect is more sensitive due to the high increase of the absolute value of the motor torque in the middle part. As speed increases, this increase of in the middle part decreases, the model becomes more sensitive to the assistance effect. Therefore, the pendulum prefers softer springs at slow speeds, but stiffer springs in high speeds. This is convinced by the spring stiffness from Table 6.2.

From the assistance/resistance pattern of the springs, we can also hypothesise that removing the resistance effect of the springs may further improve the energy efficiency of the pendulum leg. This practice might be realized by introducing clutches into the springs.

Clutches were then added to the springs. The study also investigates the performance of the clutched spring at different motion speeds. The torques are compared in Fig 6.5, and the energy saving performance at various speeds is given in Fig. 6.6 in comparison with the results from ID and PD with UCSMs. The optimal parameters are given in Table 6.3.

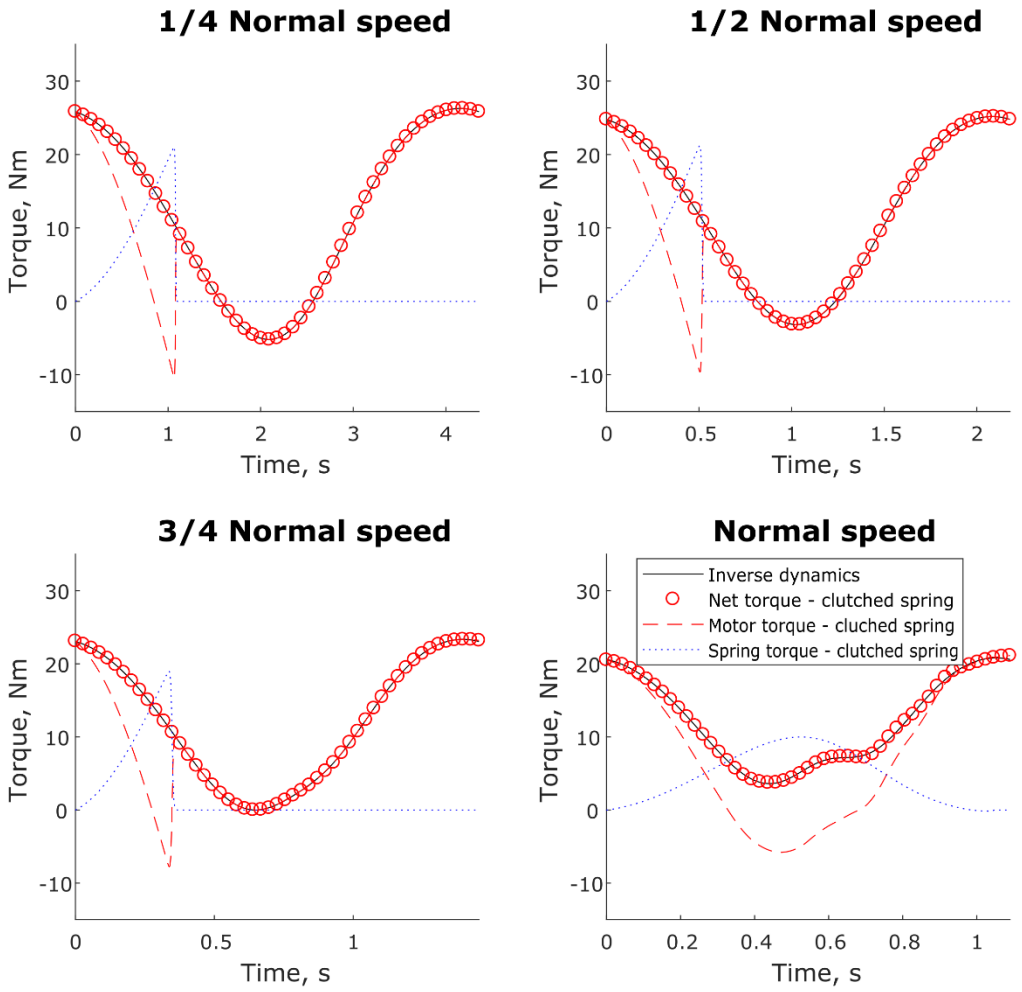

Fig. 6.5 Pendulum results – with CSM in various speeds

Table 6.3 CSM parameters from PD

Speeds of normal walking speed)	On time (% of gait cycle)	Off time (% of gait cycle)	Spring stiffness (N*m/radian)
¼	0	24.79	59.47
½	0	23.70	65.22
¾	0	23.95	58.41
1	0	95.74	14.24

The first three graphs in Fig. 6.3 indicate that the clutches indeed remove the resistance effect of the springs. Higher torque reductions are obtained via much stiffer springs, as in Table 6.3. Though turning off the springs early fails to assist the later part of the motion, the overall energy consumption still decreases, as in Fig. 6.5. This further underscores the spring resistance effect at slow speeds. At the normal walking speed, the spring tends to work throughout the entire cycle, highlighting the assistance effect at later part and undermining the resistance effect in the middle part. The results align well with the assistance/resistance analysis.

The energy consumptions are compared with the without-spring case in Fig. 6.6. In comparison of ID and UCSMs, the total mechanical energy costs have dropped at all speeds. As speed increases, springs save more energy; a maximum energy saving of 30.38% is observed at normal walking speed. This is in line with assistance/resistance effect analysis, where resistance effect contributes less as speed increase. The results together with the analysis support the effectiveness of the PD method for finding optimal spring stiffness for minimal energy consumption. In addition, the results illustrate the energy saving effect of purely adding a spring in a dynamic system.

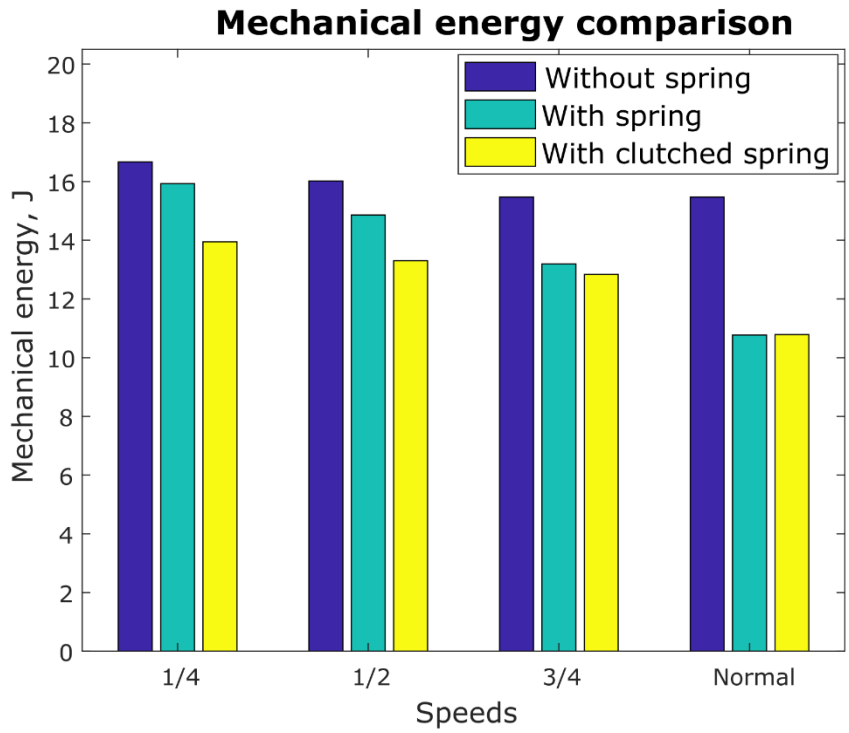

Fig. 6.6 Mechanical energy comparison

More energy can be saved if the springs are clutched, especially at slow speeds. The results encourage the introduction of clutched-spring mechanisms and support the use of PD to obtain optimal clutched-spring mechanism parameters for maximum energy saving.

The focus of the study is on the effectiveness of spring and clutched springs for energy saving. A predefined trajectory makes the motions in three cases the same, which requires the same net torque. The motor/spring toque differences between three cases can be easily visualized. This makes the comparison the torques straight-forward and explicit, facilitating insights into the functionality of the springs.

The PD method is used for its capability of cause-effect study. A slight change in the equations of motion can take a spring or a clutched spring into consideration. Running the optimization problem can automatically return the optimal parameters for a spring or a clutched spring.

6.6 Conclusions

In this chapter, we employed PD to obtain optimal CSM parameters for minimal energy consumption of a pendulum leg. Studies applying PD on UCSMs and CSMs were carried out to obtain insights into the functionality of CSMs.

The PD method is effective to track the required motion while considering the dynamics of the model. This is validated by comparing the results of ID and the results from PD. The PD method can also simultaneously return the optimal parameters of a UCSM/CSM for maximum energy saving.

The pendulum leg study also demonstrates the energetic benefits of purely assisting motion with springs. Moreover, better energy performance can be achieved when these springs are turned on/off at proper timings. The studies encourage the use of CSMs for saving motor energy in a dynamic system.

Chapter 7 Clutched-Spring Mechanisms on Improving Leg Exoskeleton Energy Efficiency

Abstract

This chapter investigated the energy-saving performance of CSMs in the 1-DOF leg exoskeleton. Kinematic and dynamic analysis were first carried out to establish the PD optimization problem. CSMs were then added at the hip and knee joints to save the motor work. Four cases were studied: without CSMs, with a hip CSM, with a knee CSM, and with hip and knee CSMs. Adding a CSM at either hip or knee joint can improve the energy efficiency of the exoskeleton. An energy saving of 30.85% was achieved with both hip and knee CSMs included. Therefore, we conclude that CSMs can be used in the leg exoskeleton for saving motor work. The mechanicals may also benefit other portable leg exoskeletons for longer working hours.

7.1 Introduction

The pendulum study has proved the effectiveness of CSMs for better energy performance. In this chapter, CSMs were added into the 1-DOF leg exoskeleton at hip and knee joints to save mechanical energy, as in Fig. 7.1. At the hip joint a torsional spring spans the base link (AH) and the thigh link (CHK), and a clutched (as the switch in Fig. 7.1) turns the spring on/off during a movement. The spring generates a torque when twisted. Similarly,

the knee CSM spans the thigh link (CHK) and the shank link (JKF), and it can also provide a torque when turned on.

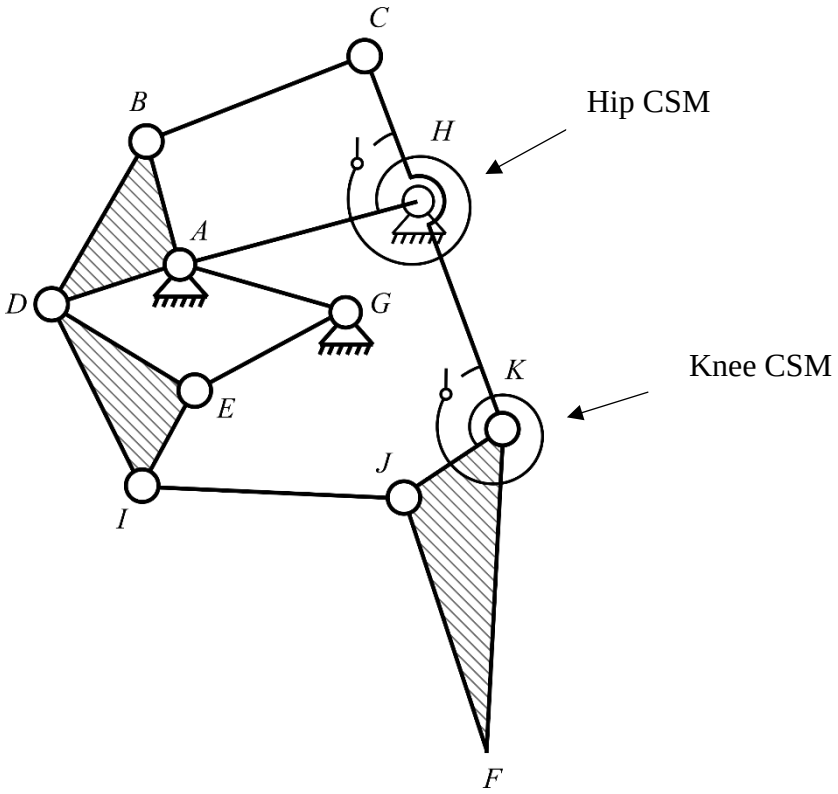

Fig. 7.1 Schematic of leg exoskeleton with CSMs

In order to carry out PD on the leg exoskeleton, kinematic and dynamic analysis on the leg exoskeleton are necessary to calculate the motor torque. The kinematic analysis calculated the angular velocities and accelerations, centre of mass linear velocities and accelerations; dynamic analysis then returned the motor torque. With the results from the dynamic analysis, the optimization problem was established. In the optimizations, the exoskeleton operates at ¼ of normal walking speed as we presented in Chapter 4.

Four cases were considered in the study. The motion-only case compared the results with ID results to validate the PD method on the leg exoskeleton. The hip-CSM case investigated the effect of the mechanism at hip joint, whereas knee-CSM case focused on the knee joint. In the end, both joints were assisted with a CSM. The torques and energy consumptions were then compared.

7.2 Kinematic Analysis

The PD method requires the equations of motion on the leg exoskeleton. Kinematic analysis needs to be carried out first in order to conduct dynamic analysis for the equations of motion. The kinematic analysis includes derivations for link angular states (displacement, velocity, and acceleration) and link COM states (linear displacement, velocity, and acceleration).

7.2.1 Link Angular States

Taking the first and second derivatives of (4.3), (4.4), and (4.5), and solving the equations give the angular velocities and accelerations of the links. Details of the derivations are provided in Appendix A.1.

The angular velocities of the links are given as:

$$\dot{\varphi}_2 = -\frac{l_1\dot{\varphi}_1 \sin(\varphi_1 - \varphi_3)}{l_2 \sin(\varphi_2 - \varphi_3)}$$

$$\dot{\varphi}_3 = -\frac{l_1\dot{\varphi}_1 \sin(\varphi_1 - \varphi_2)}{l_3 \sin(\varphi_3 - \varphi_2)}$$

$$\dot{\varphi}_4 = 0$$

$$\dot{\varphi}_5 = 0$$

$$\dot{\varphi}_6 = -\frac{l_5\dot{\varphi}_5 \sin(\varphi_5 - \varphi_7)}{l_6 \sin(\varphi_6 - \varphi_7)}$$

$$\dot{\varphi}_7 = -\frac{l_5\dot{\varphi}_5 \sin(\varphi_5 - \varphi_6)}{l_7 \sin(\varphi_7 - \varphi_6)}$$

$$\dot{\varphi}_8 = 0$$

$$\dot{\varphi}_9 = \dot{\varphi}_6$$

$$\dot{\varphi}_{10} = -\frac{l_5\dot{\varphi}_5 \sin(\varphi_5 - \varphi_{11}) + l_9\dot{\varphi}_9 \sin(\varphi_9 - \varphi_{11}) + l_{12}\dot{\varphi}_{12} \sin(\varphi_{12} - \varphi_{11})}{l_{10} \sin(\varphi_{10} - \varphi_{11})}$$

$$\dot{\varphi}_{11} = -\frac{l_5\dot{\varphi}_5 \sin(\varphi_5 - \varphi_{10}) + l_9\dot{\varphi}_9 \sin(\varphi_9 - \varphi_{10}) + l_{12}\dot{\varphi}_{12} \sin(\varphi_{12} - \varphi_{10})}{l_{11} \sin(\varphi_{11} - \varphi_{10})} \qquad (7.1)$$

$$\dot{\varphi}_{12} = \dot{\varphi}_3$$

The angular accelerations of the links can be given as:

$$\ddot{\varphi}_2 = -\frac{l_1\ddot{\varphi}_1 \sin(\varphi_1-\varphi_3)+l_1\dot{\varphi}_1{}^2\cos(\varphi_1-\varphi_3)+l_3\dot{\varphi}_3{}^2+l_2\dot{\varphi}_2{}^2\cos(\varphi_2-\varphi_3)}{l_2\sin(\varphi_2-\varphi_3)}$$

$$\ddot{\varphi}_3 = -\frac{l_1\ddot{\varphi}_1 \sin(\varphi_1-\varphi_2)+l_1\dot{\varphi}_1{}^2\cos(\varphi_1-\varphi_2)+l_2\dot{\varphi}_2{}^2+l_3\dot{\varphi}_3{}^2\cos(\varphi_3-\varphi_2)}{l_3\sin(\varphi_3-\varphi_2)}$$

$$\ddot{\varphi}_4 = 0$$

$$\ddot{\varphi}_5 = \ddot{\varphi}_1$$

$$\ddot{\varphi}_6 = -\frac{l_5\ddot{\varphi}_5 \sin(\varphi_5-\varphi_7)+l_5\dot{\varphi}_5{}^2\cos(\varphi_5-\varphi_7)+l_6\dot{\varphi}_6{}^2\cos(\varphi_6-\varphi_7)+l_7\dot{\varphi}_7{}^2}{l_6\sin(\varphi_6-\varphi_7)}$$

$$\ddot{\varphi}_7 = -\frac{l_5\ddot{\varphi}_5 \sin(\varphi_5-\varphi_6)+l_5\dot{\varphi}_5{}^2\cos(\varphi_5-\varphi_6)+l_7\dot{\varphi}_7{}^2\cos(\varphi_7-\varphi_6)+l_6\dot{\varphi}_6{}^2}{l_7\sin(\varphi_7-\varphi_6)}$$

$$\ddot{\varphi}_8 = 0$$

$$\ddot{\varphi}_9 = \ddot{\varphi}_6$$

$$\ddot{\varphi}_{10} = -\frac{l_5\ddot{\varphi}_5 \sin(\varphi_5-\varphi_{11})+l_5\dot{\varphi}_5{}^2\cos(\varphi_5-\varphi_{11})}{l_{10}\sin(\varphi_{10}-\varphi_{11})} - \frac{l_9\ddot{\varphi}_9 \sin(\varphi_9-\varphi_{11})+l_9\dot{\varphi}_9{}^2\cos(\varphi_9-\varphi_{11})}{l_{10}\sin(\varphi_{10}-\varphi_{11})}$$
$$- \frac{l_{10}\dot{\varphi}_{10}{}^2\cos(\varphi_{10}-\varphi_{11})+l_{11}\dot{\varphi}_{11}{}^2}{l_{10}\sin(\varphi_{10}-\varphi_{11})} - \frac{l_{12}\ddot{\varphi}_{12}\sin(\varphi_{12}-\varphi_{11})+l_{12}\dot{\varphi}_{12}{}^2\cos(\varphi_{12}-\varphi_{11})}{l_{10}\sin(\varphi_{10}-\varphi_{11})}$$

$$\ddot{\varphi}_{11} = -\frac{l_5\ddot{\varphi}_5 \sin(\varphi_5-\varphi_{10})+l_5\dot{\varphi}_5{}^2\cos(\varphi_5-\varphi_{10})}{l_{11}\sin(\varphi_{11}-\varphi_{10})} - \frac{l_9\ddot{\varphi}_9 \sin(\varphi_9-\varphi_{10})+l_9\dot{\varphi}_9{}^2\cos(\varphi_9-\varphi_{10})}{l_{11}\sin(\varphi_{11}-\varphi_{10})}$$
$$- \frac{l_{10}\dot{\varphi}_{10}{}^2+l_{11}\dot{\varphi}_{11}{}^2\cos(\varphi_{11}-\varphi_{10})}{l_{11}\sin(\varphi_{11}-\varphi_{10})} - \frac{l_{12}\ddot{\varphi}_{12}\sin(\varphi_{12}-\varphi_{10})+l_{12}\dot{\varphi}_{12}{}^2\cos(\varphi_{12}-\varphi_{10})}{l_{11}\sin(\varphi_{11}-\varphi_{10})}$$

$$\ddot{\varphi}_{12} = \ddot{\varphi}_3 \tag{7.2}$$

7.2.2 Link Centre of Mass States

The links in the leg exoskeleton are numbered in Table 7.1 based on the schematics of the leg exoskeleton in Fig. 7.1. Let R_i be the arm of the COM in its link and γ_i be the angle of the arm with respect to a side. For binary links $\gamma_i = 0$. The displacements, velocity and acceleration of the link COMs can then be formulated. Details of the derivations are provided in Appendix A.2.

Table 7.1 Link numbering

Number	Link name
1	ABD
2	BC
3	CHK
4	DEI
5	EG
6	IJ
7	JKF

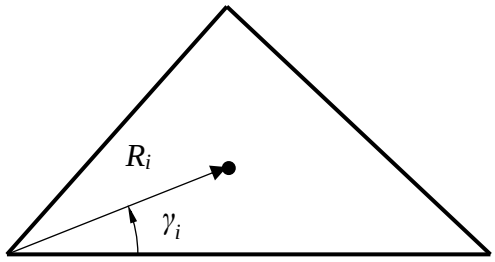

Fig. 7.2 COM location in link *i*

The displacements of the link COMs can be expressed as:

$$
\begin{aligned}
\mathrm{p}_{1,x} &= R_1 \cos(\varphi_1 + \gamma_1) \\
\mathrm{p}_{1,y} &= R_1 \sin(\varphi_1 + \gamma_1) \\
\mathrm{p}_{2,x} &= l_1 \cos\varphi_1 + R_2 \cos(\varphi_2 + \gamma_2) \\
\mathrm{p}_{2,y} &= l_1 \sin\varphi_1 + R_2 \sin(\varphi_2 + \gamma_2) \\
\mathrm{p}_{3,x} &= l_1 \cos\varphi_1 + l_2 \cos\varphi_2 + R_3 \cos(\varphi_3 + \gamma_3) \\
\mathrm{p}_{3,y} &= l_1 \sin\varphi_1 + l_2 \sin\varphi_2 + R_3 \sin(\varphi_3 + \gamma_3) \\
\mathrm{p}_{4,x} &= l_5 \cos\varphi_5 + R_4 \cos(\varphi_6 + \gamma_4) \\
\mathrm{p}_{4,y} &= l_5 \sin\varphi_5 + R_4 \sin(\varphi_6 + \gamma_4) \\
\mathrm{p}_{5,x} &= l_5 \cos\varphi_5 + l_6 \cos\varphi_6 + R_5 \cos(\varphi_7 + \gamma_5) \\
\mathrm{p}_{5,y} &= l_5 \sin\varphi_5 + l_6 \sin\varphi_6 + R_5 \sin(\varphi_7 + \gamma_5) \\
\mathrm{p}_{6,x} &= l_5 \cos\varphi_5 + l_9 \cos\varphi_9 + R_6 \cos(\varphi_{10} + \gamma_6) \\
\mathrm{p}_{6,y} &= l_5 \sin\varphi_5 + l_9 \sin\varphi_9 + R_6 \sin(\varphi_{10} + \gamma_6) \\
\mathrm{p}_{7,x} &= l_5 \cos\varphi_5 + l_9 \cos\varphi_9 + l_{10} \cos\varphi_{10} + R_7 \cos(\varphi_{11} + \gamma_7) \\
\mathrm{p}_{7,y} &= l_5 \sin\varphi_5 + l_9 \sin\varphi_9 + l_{10} \sin\varphi_{10} + R_7 \sin(\varphi_{11} + \gamma_7)
\end{aligned} \tag{7.3}
$$

where $p_{i,x}$ is the i^{th} link's COM linear displacement along *x*-axis, whereas $p_{i,y}$ along the *y*-axis.

The velocities of link COMs can be expressed as:

$$\dot{\mathrm{p}}_{1,x} = R_1\dot{\varphi}_1 \cos(\varphi_1 + \gamma_1 + \frac{\pi}{2})$$

$$\dot{\mathrm{p}}_{1,y} = R_1\dot{\varphi}_1 \sin(\varphi_1 + \gamma_1 + \frac{\pi}{2})$$

$$\dot{\mathrm{p}}_{2,x} = l_1\dot{\varphi}_1 \cos(\varphi_1 + \frac{\pi}{2}) + R_2\dot{\varphi}_2 \cos(\varphi_2 + \gamma_2 + \frac{\pi}{2})$$

$$\dot{\mathrm{p}}_{2,y} = l_1\dot{\varphi}_1 \cos(\varphi_1 + \frac{\pi}{2}) + R_2\dot{\varphi}_2 \cos(\varphi_2 + \gamma_2 + \frac{\pi}{2})$$

$$\dot{\mathrm{p}}_{3,x} = l_1\dot{\varphi}_1 \cos(\varphi_1 + \frac{\pi}{2}) + l_2\dot{\varphi}_2 \cos(\varphi_2 + \frac{\pi}{2}) + R_3\dot{\varphi}_3 \cos(\varphi_3 + \gamma_3 + \frac{\pi}{2})$$

$$\dot{\mathrm{p}}_{3,y} = l_1\dot{\varphi}_1 \sin(\varphi_1 + \frac{\pi}{2}) + l_2\dot{\varphi}_2 \sin(\varphi_2 + \frac{\pi}{2}) + R_3\dot{\varphi}_3 \sin(\varphi_3 + \gamma_3 + \frac{\pi}{2})$$

$$\dot{\mathrm{p}}_{4,x} = l_5\dot{\varphi}_5 \cos(\varphi_5 + \frac{\pi}{2}) + R_4\dot{\varphi}_6 \cos(\varphi_6 + \gamma_4 + \frac{\pi}{2})$$

$$\dot{\mathrm{p}}_{4,y} = l_5\dot{\varphi}_5 \sin(\varphi_5 + \frac{\pi}{2}) + R_4\dot{\varphi}_6 \sin(\varphi_6 + \gamma_4 + \frac{\pi}{2})$$

$$\dot{\mathrm{p}}_{5,x} = l_5\dot{\varphi}_5 \cos(\varphi_5 + \frac{\pi}{2}) + l_6\dot{\varphi}_6 \cos(\varphi_6 + \frac{\pi}{2}) + R_5\dot{\varphi}_7 \cos(\varphi_7 + \gamma_5 + \frac{\pi}{2})$$

$$\dot{\mathrm{p}}_{5,y} = l_5\dot{\varphi}_5 \sin(\varphi_5 + \frac{\pi}{2}) + l_6\dot{\varphi}_6 \sin(\varphi_6 + \frac{\pi}{2}) + R_5\dot{\varphi}_7 \sin(\varphi_7 + \gamma_5 + \frac{\pi}{2})$$

$$\dot{\mathrm{p}}_{6,x} = l_5\dot{\varphi}_5 \cos(\varphi_5 + \frac{\pi}{2}) + l_9\dot{\varphi}_9 \cos(\varphi_9 + \frac{\pi}{2}) + R_6\dot{\varphi}_{10} \cos(\varphi_{10} + \gamma_6 + \frac{\pi}{2})$$

$$\dot{\mathrm{p}}_{6,y} = l_5\dot{\varphi}_5 \sin(\varphi_5 + \frac{\pi}{2}) + l_9\dot{\varphi}_9 \sin(\varphi_9 + \frac{\pi}{2}) + R_6\dot{\varphi}_{10} \sin(\varphi_{10} + \gamma_6 + \frac{\pi}{2})$$

$$\dot{\mathrm{p}}_{7,x} = l_5\dot{\varphi}_5 \cos(\varphi_5 + \frac{\pi}{2}) + l_9\dot{\varphi}_9 \cos(\varphi_9 + \frac{\pi}{2}) + l_{10}\dot{\varphi}_{10} \cos(\varphi_{10} + \frac{\pi}{2}) + R_7\dot{\varphi}_{11} \cos(\varphi_{11} + \gamma_7 + \frac{\pi}{2})$$

$$\dot{\mathrm{p}}_{7,y} = l_5\dot{\varphi}_5 \sin(\varphi_5 + \frac{\pi}{2}) + l_9\dot{\varphi}_9 \sin(\varphi_9 + \frac{\pi}{2}) + l_{10}\dot{\varphi}_{10} \sin(\varphi_{10} + \frac{\pi}{2}) + R_7\dot{\varphi}_{11} \sin(\varphi_{11} + \gamma_7 + \frac{\pi}{2})$$

(7.4)

where $\dot{p}_{i,x}$ represents the i^{th} link's COM linear velocity along the *x*-axis, whereas $\dot{p}_{i,y}$ along the *y*-axis.

The accelerations of the link COMs can be expressed as:

$$\ddot{p}_{1,x} = R_1\ddot{\varphi}_1 \cos(\varphi_i + \gamma_1 + \frac{\pi}{2}) + R_1\dot{\varphi}_1^{\,2} \cos(\varphi_i + \gamma_1 + \pi)$$

$$\ddot{p}_{1,y} = R_1\ddot{\varphi}_1 \sin(\varphi_i + \gamma_1 + \frac{\pi}{2}) + R_1\dot{\varphi}_1^{\,2} \sin(\varphi_i + \gamma_1 + \pi)$$

$$\ddot{p}_{2,x} = l_1\ddot{\varphi}_1 \cos(\varphi_2 + \frac{\pi}{2}) + l_1\dot{\varphi}_1^{\,2} \cos(\varphi_2 + \pi) + R_2\ddot{\varphi}_2 \cos(\varphi_2 + \gamma_2 + \frac{\pi}{2})$$
$$+ R_2\dot{\varphi}_2^{\,2} \cos(\varphi_2 + \gamma_2 + \pi)$$

$$\ddot{p}_{2,y} = l_1\ddot{\varphi}_1 \sin(\varphi_2 + \frac{\pi}{2}) + l_1\dot{\varphi}_1^{\,2} \sin(\varphi_2 + \pi) + R_2\ddot{\varphi}_2 \sin(\varphi_2 + \gamma_2 + \frac{\pi}{2})$$
$$+ R_2\dot{\varphi}_2^{\,2} \sin(\varphi_2 + \gamma_2 + \pi)$$

$$\ddot{p}_{3,x} = l_1\ddot{\varphi}_1 \cos(\varphi_1 + \frac{\pi}{2}) + l_1\dot{\varphi}_1^{\,2} \cos(\varphi_1 + \pi) + l_2\ddot{\varphi}_2 \cos(\varphi_2 + \frac{\pi}{2}) + l_2\dot{\varphi}_2^{\,2} \cos(\varphi_2 + \pi)$$
$$+ R_3\ddot{\varphi}_3 \cos(\varphi_3 + \gamma_3 + \frac{\pi}{2}) + R_3\dot{\varphi}_3^{\,2} \cos(\varphi_3 + \gamma_3 + \pi)$$

$$\ddot{p}_{3,y} = l_1\ddot{\varphi}_1 \sin(\varphi_1 + \frac{\pi}{2}) + l_1\dot{\varphi}_1^{\,2} \sin(\varphi_1 + \pi) + l_2\ddot{\varphi}_2 \sin(\varphi_2 + \frac{\pi}{2}) + l_2\dot{\varphi}_2^{\,2} \sin(\varphi_2 + \pi)$$
$$+ R_3\ddot{\varphi}_3 \sin(\varphi_3 + \gamma_3 + \frac{\pi}{2}) + R_3\dot{\varphi}_3^{\,2} \sin(\varphi_3 + \gamma_3 + \pi)$$

$$\ddot{p}_{4,x} = l_5\ddot{\varphi}_5 \cos(\varphi_5 + \frac{\pi}{2}) + l_5\dot{\varphi}_5^{\,2} \cos(\varphi_5 + \pi) + R_4\ddot{\varphi}_6 \cos(\varphi_6 + \gamma_4 + \frac{\pi}{2})$$
$$+ R_4\dot{\varphi}_6^{\,2} \cos(\varphi_6 + \gamma_4 + \pi)$$

$$\ddot{p}_{4,y} = l_5\ddot{\varphi}_5 \sin(\varphi_5 + \frac{\pi}{2}) + l_5\dot{\varphi}_5^{\,2} \sin(\varphi_5 + \pi) + R_4\ddot{\varphi}_6 \sin(\varphi_6 + \gamma_4 + \frac{\pi}{2})$$
$$+ R_4\dot{\varphi}_6^{\,2} \sin(\varphi_6 + \gamma_4 + \pi)$$

$$\ddot{p}_{5,x} = l_5\ddot{\varphi}_5 \cos(\varphi_5 + \frac{\pi}{2}) + l_5\dot{\varphi}_5^{\,2} \cos(\varphi_5 + \pi) + l_6\ddot{\varphi}_6 \cos(\varphi_6 + \frac{\pi}{2}) + l_6\dot{\varphi}_6^{\,2} \cos(\varphi_6 + \pi)$$
$$+ R_5\ddot{\varphi}_7 \cos(\varphi_7 + \gamma_5 + \frac{\pi}{2}) + R_5\dot{\varphi}_7^{\,2} \cos(\varphi_7 + \gamma_5 + \pi)$$

$$\ddot{p}_{5,y} = l_5\ddot{\varphi}_5 \sin(\varphi_5 + \frac{\pi}{2}) + l_5\dot{\varphi}_5^{\,2} \sin(\varphi_5 + \pi) + l_6\ddot{\varphi}_6 \sin(\varphi_6 + \frac{\pi}{2}) + l_6\dot{\varphi}_6^{\,2} \sin(\varphi_6 + \pi)$$
$$+ R_5\ddot{\varphi}_7 \sin(\varphi_7 + \gamma_5 + \frac{\pi}{2}) + R_5\dot{\varphi}_7^{\,2} \sin(\varphi_7 + \gamma_5 + \pi)$$

$$\ddot{p}_{6,x} = l_5\ddot{\varphi}_5 \cos(\varphi_5 + \frac{\pi}{2}) + l_5\dot{\varphi}_5^{\,2} \cos(\varphi_5 + \pi) + l_9\ddot{\varphi}_9 \cos(\varphi_9 + \frac{\pi}{2}) + l_9\dot{\varphi}_9^{\,2} \cos(\varphi_9 + \pi)$$
$$+ R_6\ddot{\varphi}_{10} \cos(\varphi_{10} + \gamma_6 + \frac{\pi}{2}) + R_6\dot{\varphi}_{10}^{\,2} \cos(\varphi_{10} + \gamma_6 + \pi)$$

$$\ddot{p}_{6,y} = l_5\ddot{\varphi}_5 \sin(\varphi_5 + \frac{\pi}{2}) + l_5\dot{\varphi}_5^{\,2} \sin(\varphi_5 + \pi) + l_9\ddot{\varphi}_9 \sin(\varphi_9 + \frac{\pi}{2}) + l_9\dot{\varphi}_9^{\,2} \sin(\varphi_9 + \pi)$$
$$+ R_6\ddot{\varphi}_{10} \sin(\varphi_{10} + \gamma_6 + \frac{\pi}{2}) + R_6\dot{\varphi}_{10}^{\,2} \sin(\varphi_{10} + \gamma_6 + \pi)$$

$$
\begin{aligned}
\ddot{\mathrm{p}}_{7,x} &= l_5\ddot{\varphi}_5\cos(\varphi_5+\frac{\pi}{2}) + l_5\dot{\varphi}_5{}^2\cos(\varphi_5+\pi) + l_9\ddot{\varphi}_9\cos(\varphi_9+\frac{\pi}{2}) + l_9\dot{\varphi}_9{}^2\cos(\varphi_9+\pi) \\
&\quad + l_{10}\ddot{\varphi}_{10}\cos(\varphi_{10}+\frac{\pi}{2}) + l_{10}\dot{\varphi}_{10}{}^2\cos(\varphi_{10}+\pi) + R_7\ddot{\varphi}_{11}\cos(\varphi_{11}+\gamma_7+\frac{\pi}{2}) \\
&\quad + R_7\dot{\varphi}_{11}{}^2\cos(\varphi_{11}+\gamma_7+\pi) \\
\ddot{\mathrm{p}}_{7,y} &= l_5\ddot{\varphi}_5\cos(\varphi_5+\frac{\pi}{2}) + l_5\dot{\varphi}_5{}^2\cos(\varphi_5+\pi) + l_9\ddot{\varphi}_9\cos(\varphi_9+\frac{\pi}{2}) + l_9\dot{\varphi}_9{}^2\cos(\varphi_9+\pi) \\
&\quad + l_{10}\ddot{\varphi}_{10}\cos(\varphi_{10}+\frac{\pi}{2}) + l_{10}\dot{\varphi}_{10}{}^2\cos(\varphi_{10}+\pi) + R_7\ddot{\varphi}_{11}\cos(\varphi_{11}+\gamma_7+\frac{\pi}{2}) \\
&\quad + R_7\dot{\varphi}_{11}{}^2\cos(\varphi_{11}+\gamma_7+\pi)
\end{aligned}
\tag{7.5}
$$

where $\ddot{p}_{i,x}$ represents the i^{th} link's COM linear acceleration along the *x*-axis, whereas $\ddot{p}_{i,y}$ along the *y*-axis.

7.3 Force Analysis

Force analysis derives the equations of motion on the leg exoskeleton, which is used to construct the PD optimization problem. The Newton-Euler formation was used to carry out the force analysis. This method not only returns the motor torque but also returns the interaction forces between the links, which can assist the exoskeleton's future development.

Free-body diagrams of the links are given in Fig. 7.2. Equations of motion can then be derived as follows. Detailed derivations are provided in Appendix B.

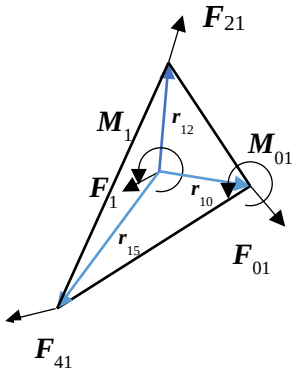

Link 1

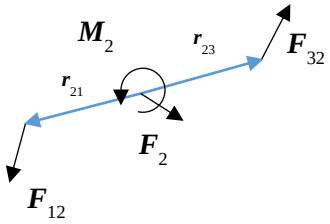

Link 2

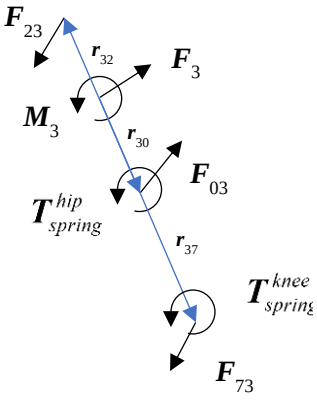

Link 3

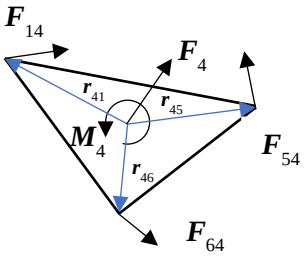

Link 4

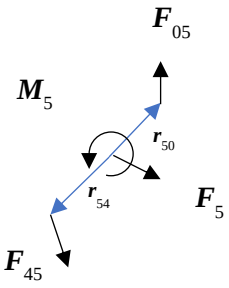

Link 5

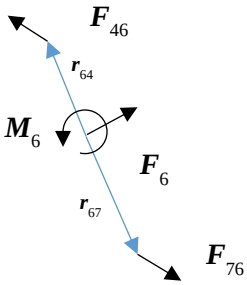

Link 6

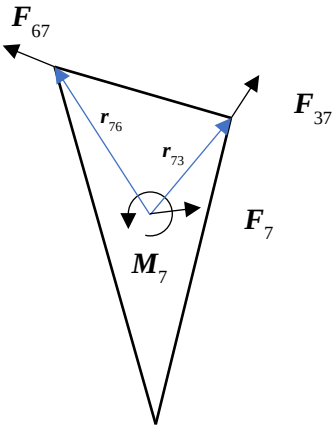

Link 7

Fig. 7.3 Free body diagrams

$$
\begin{aligned}
&F_{01,x} - F_{12,x} - F_{14,x} + F_{1,x} = 0 \\
&F_{01,y} - F_{12,y} - F_{14,y} + F_{1,y} + G_{1,y} = 0 \\
&r_{10,x}F_{01,y} - r_{10,y}F_{01,x} - r_{12,x}F_{12,y} + r_{12,y}F_{12,x} - r_{14,x}F_{14,y} + r_{14,y}F_{14,x} + M_{01,z} + M_{1,z} = 0 \\
&F_{12,x} - F_{23,x} + F_{2,x} = 0 \\
&F_{12,y} - F_{23,y} + F_{2,y} + G_{2,y} = 0 \\
&r_{21,x}F_{12,y} - r_{21,y}F_{12,x} - r_{23,x}F_{23,y} + r_{23,y}F_{23,x} + M_{2,z} = 0 \\
&F_{23,x} + F_{03,x} - F_{37,x} + F_{3,x} = 0 \\
&F_{23,y} + F_{03,y} - F_{37,y} + F_{3,y} + G_{3,y} = 0 \\
&r_{32,x}F_{23,y} - r_{32,y}F_{23,x} + r_{30,x}F_{03,y} - r_{30,y}F_{03,x} - r_{37,x}F_{37,y} + r_{37,y}F_{37,x} + M_{3,z} + T_{spring}^{Hip} - T_{spring}^{Knee} = 0 \\
&F_{14,x} - F_{45,x} - F_{46,x} + F_{4,x} = 0 \\
&F_{14,y} - F_{45,y} - F_{46,y} + F_{4,y} + G_{4,y} = 0 \\
&r_{41,x}F_{14,y} - r_{41,y}F_{14,x} - r_{45,x}F_{45,y} + r_{45,y}F_{45,x} - r_{46,x}F_{46,y} + r_{46,y}F_{46,x} + M_{4,z} = 0 \\
&F_{05,x} + F_{45,x} + F_{5,x} = 0 \\
&F_{05,y} + F_{45,y} + F_{5,y} + G_{5,y} = 0 \\
&r_{50,x}F_{05,y} - r_{50,y}F_{05,x} + r_{54,x}F_{45,y} - r_{54,y}F_{45,x} + M_{5,z} = 0 \\
&F_{46,x} - F_{67,x} + F_{6,x} = 0 \\
&F_{46,y} - F_{67,y} + F_{6,y} + G_{6,y} = 0 \\
&r_{64,x}F_{46,y} - r_{64,y}F_{46,x} - r_{67,x}F_{67,y} + r_{67,y}F_{67,x} + M_{6,z} = 0 \\
&F_{37,x} + F_{67,x} + F_{7,x} = 0 \\
&F_{37,y} + F_{67,y} + G_{7,y} + F_{7,y} = 0 \\
&r_{73,x}F_{37,y} - r_{73,y}F_{37,x} + r_{76,x}F_{67,y} - r_{76,y}F_{67,x} + M_{7,z} + T_{spring}^{Knee} = 0
\end{aligned}
\tag{7.6}
$$

The equations can be expressed by a 21 by 21 matrix. Solving the equation, we can have the motor torque and interaction forces between the links. Details of the link parameters are provided in Table 7.2, which are obtained from the leg exoskeleton's SolidWorks model.

$$
\begin{bmatrix}
1 & 0 & -1 & 0 & -1 & 0 & 0 & 0 & 0 & 0 & 0 & 0 & 0 & 0 & 0 & 0 & 0 & 0 & 0 & 0 & 0 \\
0 & 1 & 0 & -1 & 0 & -1 & 0 & 0 & 0 & 0 & 0 & 0 & 0 & 0 & 0 & 0 & 0 & 0 & 0 & 0 & 0 \\
-r_{10,y} & r_{10,x} & r_{12,y} & -r_{12,x} & r_{14,y} & -r_{14,x} & 1 & 0 & 0 & 0 & 0 & 0 & 0 & 0 & 0 & 0 & 0 & 0 & 0 & 0 & 0 \\
0 & 0 & 1 & 0 & 0 & 0 & 0 & -1 & 0 & 0 & 0 & 0 & 0 & 0 & 0 & 0 & 0 & 0 & 0 & 0 & 0 \\
0 & 0 & 0 & 1 & 0 & 0 & 0 & 0 & -1 & 0 & 0 & 0 & 0 & 0 & 0 & 0 & 0 & 0 & 0 & 0 & 0 \\
0 & 0 & -r_{21,y} & r_{21,x} & 0 & 0 & 0 & r_{23,y} & -r_{23,x} & 0 & 0 & 0 & 0 & 0 & 0 & 0 & 0 & 0 & 0 & 0 & 0 \\
0 & 0 & 0 & 0 & 0 & 0 & 0 & 1 & 0 & 1 & 0 & -1 & 0 & 0 & 0 & 0 & 0 & 0 & 0 & 0 & 0 \\
0 & 0 & 0 & 0 & 0 & 0 & 0 & 0 & 1 & 0 & 1 & 0 & -1 & 0 & 0 & 0 & 0 & 0 & 0 & 0 & 0 \\
0 & 0 & 0 & 0 & 0 & 0 & 0 & -r_{32,y} & r_{32,x} & -r_{30,y} & r_{30,x} & r_{37,y} & -r_{37,x} & 0 & 0 & 0 & 0 & 0 & 0 & 0 & 0 \\
0 & 0 & 0 & 0 & 1 & 0 & 0 & 0 & 0 & 0 & 0 & 0 & 0 & -1 & 0 & -1 & 0 & 0 & 0 & 0 & 0 \\
0 & 0 & 0 & 0 & 0 & 1 & 0 & 0 & 0 & 0 & 0 & 0 & 0 & 0 & -1 & 0 & -1 & 0 & 0 & 0 & 0 \\
0 & 0 & 0 & 0 & -r_{41,y} & r_{41,x} & 0 & 0 & 0 & 0 & 0 & 0 & 0 & r_{45,y} & -r_{45,x} & r_{46,y} & -r_{45,x} & 0 & 0 & 0 & 0 \\
0 & 0 & 0 & 0 & 0 & 0 & 0 & 0 & 0 & 0 & 0 & 0 & 0 & 1 & 0 & 0 & 0 & 1 & 0 & 0 & 0 \\
0 & 0 & 0 & 0 & 0 & 0 & 0 & 0 & 0 & 0 & 0 & 0 & 0 & 0 & 1 & 0 & 0 & 0 & 1 & 0 & 0 \\
0 & 0 & 0 & 0 & 0 & 0 & 0 & 0 & 0 & 0 & 0 & 0 & 0 & -r_{54,y} & r_{54,x} & 0 & 0 & -r_{50,y} & r_{50,x} & 0 & 0 \\
0 & 0 & 0 & 0 & 0 & 0 & 0 & 0 & 0 & 0 & 0 & 0 & 0 & 0 & 0 & 1 & 0 & 0 & 0 & -1 & 0 \\
0 & 0 & 0 & 0 & 0 & 0 & 0 & 0 & 0 & 0 & 0 & 0 & 0 & 0 & 0 & 0 & 1 & 0 & 0 & 0 & -1 \\
0 & 0 & 0 & 0 & 0 & 0 & 0 & 0 & 0 & 0 & 0 & 0 & 0 & 0 & 0 & -r_{64,y} & r_{64,x} & 0 & 0 & r_{67,y} & -r_{67,x} \\
0 & 0 & 0 & 0 & 0 & 0 & 0 & 0 & 0 & 0 & 0 & 1 & 0 & 0 & 0 & 0 & 0 & 0 & 0 & 1 & 0 \\
0 & 0 & 0 & 0 & 0 & 0 & 0 & 0 & 0 & 0 & 0 & 0 & 1 & 0 & 0 & 0 & 0 & 0 & 0 & 0 & 1 \\
0 & 0 & 0 & 0 & 0 & 0 & 0 & 0 & 0 & 0 & 0 & -r_{73,y} & r_{73,x} & 0 & 0 & 0 & 0 & 0 & 0 & -r_{76,y} & r_{76,x}
\end{bmatrix}
\begin{bmatrix}
F_{01,x} \\ F_{01,y} \\ F_{12,x} \\ F_{12,y} \\ F_{14,x} \\ F_{14,y} \\ M_{01,z} \\ F_{23,x} \\ F_{23,y} \\ F_{03,x} \\ F_{03,y} \\ F_{37,x} \\ F_{37,y} \\ F_{45,x} \\ F_{45,y} \\ F_{46,x} \\ F_{46,y} \\ F_{05,x} \\ F_{05,y} \\ F_{67,x} \\ F_{67,y}
\end{bmatrix}
=
\begin{bmatrix}
-F_{1,x} \\
-F_{1,y} - G_{1,y} \\
-M_{1,z} \\
-F_{2,x} \\
-F_{2,y} - G_{2,y} \\
-M_{2,z} \\
-F_{3,x} \\
-F_{3,y} - G_{3,y} \\
-M_{3,z} - T_{spring}^{Hip} + T_{spring}^{Knee} \\
-F_{4,x} \\
-F_{4,y} - G_{4,y} \\
-M_{4,z} \\
-F_{5,x} \\
-F_{5,y} - G_{5,y} \\
-M_{5,z} \\
-F_{6,x} \\
-F_{6,y} - G_{6,y} \\
-M_{6,z} \\
-F_{7,x} \\
-F_{7,y} - G_{7,y} \\
-M_{7,z} - T_{spring}^{Knee}
\end{bmatrix}
\tag{7.7}
$$

Table 7.2 Link parameters for dynamic analysis

Number	Mass (kg)	Moment of inertia (10^{-3} kg·m^2)	L_i (m)	γ_i (radian)
Link 1	0.0926	0.112	0.0193	2.8765
Link 2	0.0443	0.149	0.0859	0
Link 3	9.2086	186.6	0.2248	0
Link 4	0.2724	1.7	0.0828	0.5375
Link 5	0.0472	0.127	0.0834	0
Link 6	0.0918	1.4	0.1983	0
Link 7	3.974	113.1	0.1031	-1.2470

7.4 Optimization Construction

With the results from the kinematic and force analysis, the PD optimization problem can then be constructed. Objective and constraints can be established using the joint states and torques. In the optimization problem, we investigated 4 cases: without spring, with a hip CSM, with a knee CSM and with both hip and knee CSMs.

Design variables consists of the controls points for crank angular displacement and parameters for the hip and knee clutched spring. A design variable vector for the case of adding both springs can be given as:

$$X = [Q_1, ..., Q_n, t_{on}^{hip}, t_{off}^{hip}, k_{hip}, t_{on}^{knee}, t_{off}^{knee}, k_{knee}] \tag{7.8}$$

where Q_1 to Q_n are the control points for the crank angular displacement; t_{on}^{hip} and t_{off}^{hip} the on/off timings for the hip spring; k_{hip} the spring stiffness of the hip spring;

t_{on}^{knee} and t_{off}^{knee} the on/off timings for the hip spring; k_{knee} the spring stiffness of the knee spring. Design variables for other cases need to remove the mechanism parameters for hip, or knee, or both.

We also use the mechanical energy as the objective of the optimization problem. From equation (7.7), we can have the crank joint motor torque: M_{01z}. The velocity of the crank equals $\dot{\varphi}_1$. Therefore, the objective can be expressed as:

$$J = \int_0^T | M_{01,z}\dot{\varphi}_1 | dt \tag{7.9}$$

In the leg exoskeleton, the crank rotates at a constant speed of ¼ of the normal walking speed. To make the model achieve the same motion with the designed leg exoskeleton, equality constraints on crank angular displacements are applied. The constraints can be expressed as:

$$\varphi_1^i = {}^{ref}\varphi_1^i \tag{7.10}$$

where φ_1^i is the i^{th} angular displacement point of the crank; ${}^{ref}\varphi_1^i$ its corresponding reference motion of the crank where the crank rotates at a constant speed.

Inequality constraints on the on/off timings are also applied:

$$\begin{aligned} t_{on}^{hip} - t_{off}^{hip} < 0 \\ t_{on}^{knee} - t_{off}^{knee} < 0 \end{aligned} \tag{7.11}$$

The following vectors gives the bounds for control points, on/off timings and spring stiffness.

$$\begin{aligned} LB &= [-3.5,...,-3.5,0,0,0,0,0,0] \\ UB &= [4.7,...,4.7,4T,4T,100,4T,4T,100] \end{aligned} \tag{7.12}$$

where lower bounds for control point were set as -3.5; upper bounds for control points are set as 4.7. These bounds were set according to the angular displacement of the crank. Lower bounds for on/off timings and spring stiffness have been set as 0; upper bounds for on/off time have been set as 4 times of the normal gait time; upper bounds for spring stiffness have been set as 100.

Therefore, the optimization can be constructed as:

Objective: $\min. J = \int_0^T | M_{01,z}\dot{\varphi}_1 | dt$

Design variables: $X = [Q_1,...,Q_n,t_{on}^{hip},t_{off}^{hip},k_{hip},t_{on}^{knee},t_{off}^{knee},k_{knee}]$, where the spring parameters are added accordingly.

Constraints: from equations (7.10) and (7.11).

Bounds: from equation (7.12).

7.4 Inverse Dynamics for Validation

ID on the leg exoskeleton serves two purposes. On one hand, it validates the effectiveness of PD method for generating required motion and revealing motor torque that causes the motion. On the other hand, results (torques or mechanical energy) from

PD are compared with the results of ID to evaluate the performance of the clutched-spring mechanisms.

As the crank rotates at a constant speed, its angular acceleration equals 0;

$$\ddot{\varphi}_1 = 0 \tag{7.13}$$

Its angular velocity equals:

$$\dot{\varphi}_1 = -\frac{\pi}{2T} \tag{7.14}$$

where T is the total time for a walking gait cycle.

Its angular displacement can then be given as:

$$\varphi_1 = 3.7 - \frac{\pi t}{2T} \tag{7.15}$$

where the number 3.7 is the initial angular displacement of the crank, which is obtained from the linkage design process in Chapter 4.

With the states of the input crank, we can calculate the states of all the links in the leg exoskeleton. We can then solve for the motor torque according to equation (7.7). Then mechanical can then be calculated using equation (7.9). The torque and mechanical energy are used to validate results from PD studies.

7.5 Results and Discussion

In this study, 4 cases: without spring, with a hip CSM, with a knee CSM and with hip and knee CSMs have been examined. The without-spring case aimed to examine the PD method for reproducing required motion and reveal the motor torque causing the motion. The crank angular profiles and the motor torques are compared in Fig. 7.4 with the result form ID. The PD method is able to reproduce the required crank profile in the leg exoskeleton, and the PD returned motor torque is also identical to the ID motor torque. Errors in angle and torque are small. Therefore, the PD method can be used to study the energetic performance of the clutched-spring mechanisms in the leg exoskeleton.

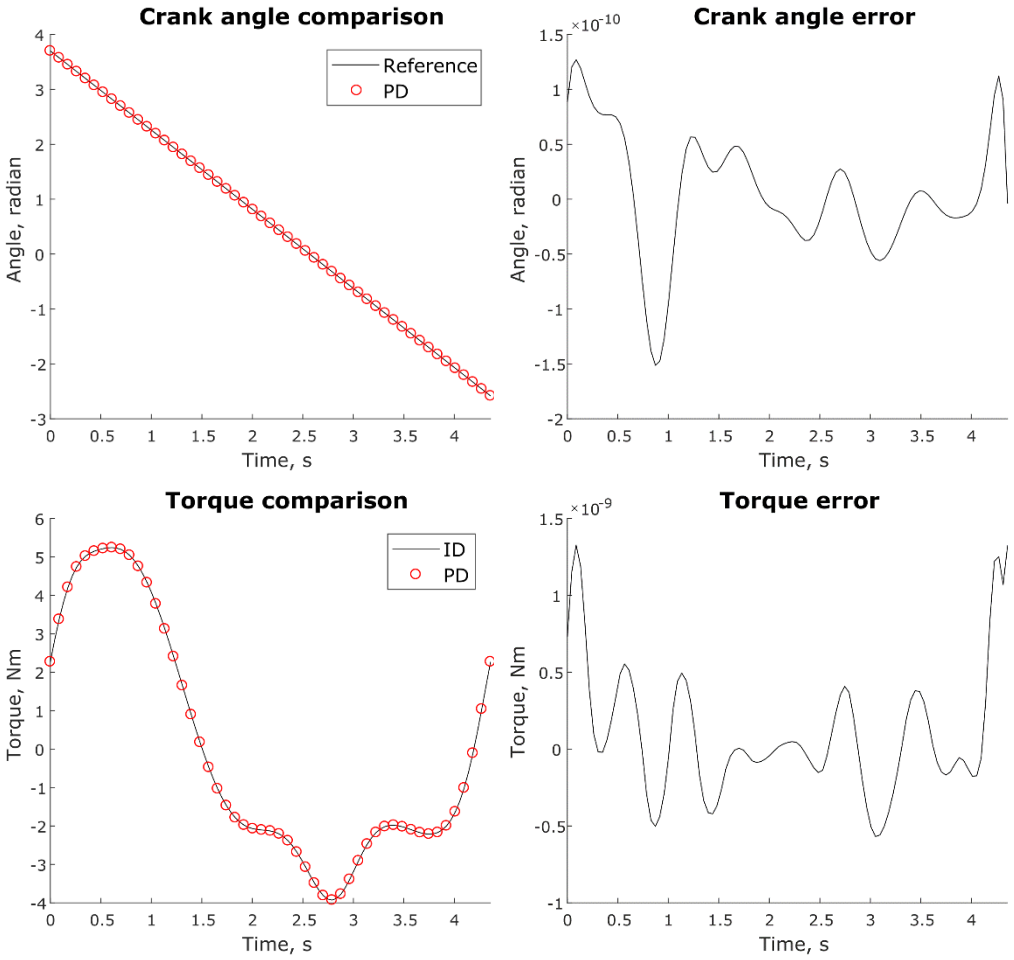

Fig. 7.4 Crank angular displacement and torque comparison

The second graph in Fig. 7.5 shows the resultant torques with a hip spring. When the spring is turned on, a reduction in motor torque occurs. This is also true with the knee spring case, as in the third graph. When both hip and knee springs are introduced in the model, the motor torque is further reduced compared with the hip or knee spring only cases.

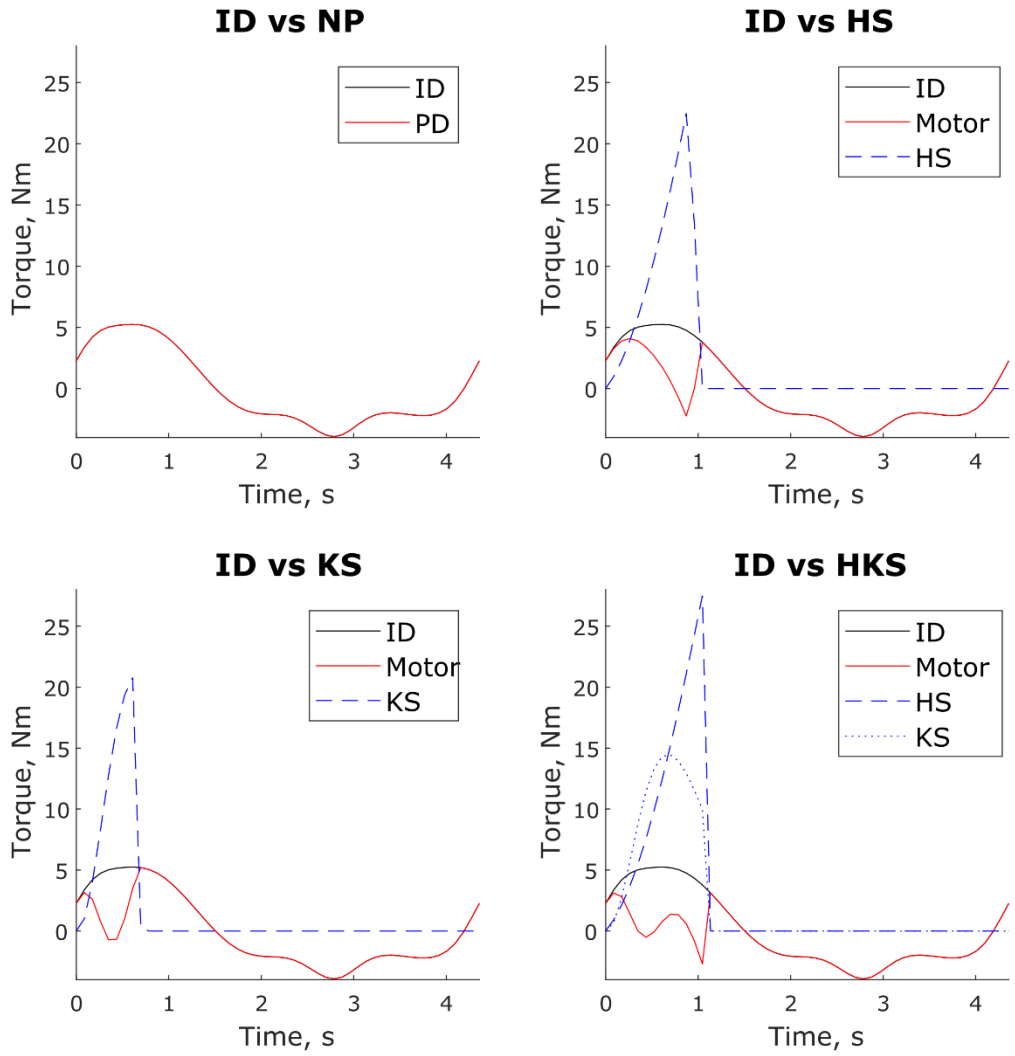

Fig. 7.5 Torque comparison

The energy consumptions in various cases are compared in Fig 7.6. In the no spring case, PD returns the same energy consumption with the ID based study. This is expected as PD precisely reveal the reference motion both kinematically and dynamically. Adding hip/knee spring saves similar energy, 17.59% and 15.26% respectively, showing the benefits of introducing clutched-spring mechanisms at the two joints. The results show the highest energy saving of 30.85% when both springs are included, which is consistent with the torque results in Fig. 7.5.

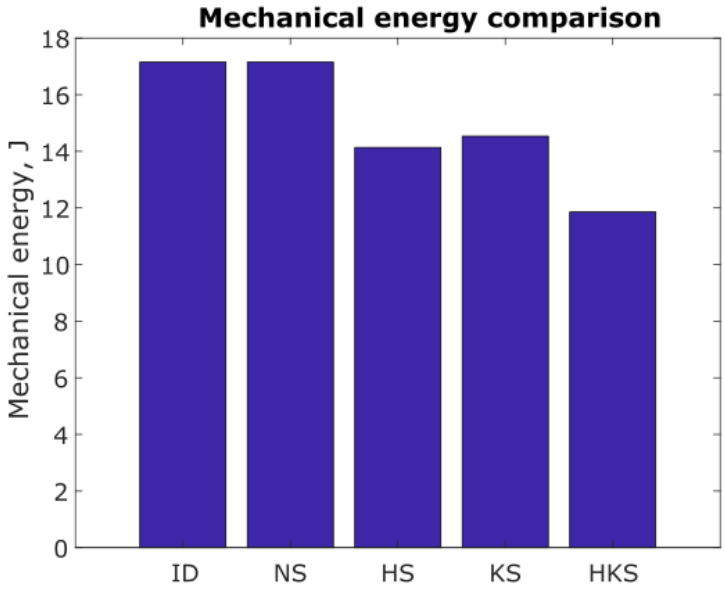

Fig. 7.6 Mechanical energy comparison

7.6 Conclusions

PD method was applied on the 1-DOF leg exoskeleton to introduce CSMs into the device at hip and knee joints. Both independent springs can reduce energy consumption. The highest energy saving has been achieved by adding both springs, with an amount of 30.85%. The results suggest the application of CSMs to lengthen the operation hours of the leg exoskeleton. The mechanisms' application is not restricted to the current device. Other exoskeleton devices involving human motion may also benefit from CSMs for better energy efficiency.

The studies also underscore the effectiveness of the PD method for obtaining the optimal design of CSMs. The method may also assist other exoskeleton designs if clutched-spring mechanisms are involved in the devices.

Physical prototypes of the CSMs are under development. Figure 7.7 gives a linear-spring version of the CSM which is for convenient implementation in both of the exoskeletons (from Chapter 5 and Chapter 7). If applied in the linkage-based leg exoskeleton, we can simply replace the torsional spring in the mathematical model. A torsional spring version will also be considered in future study.

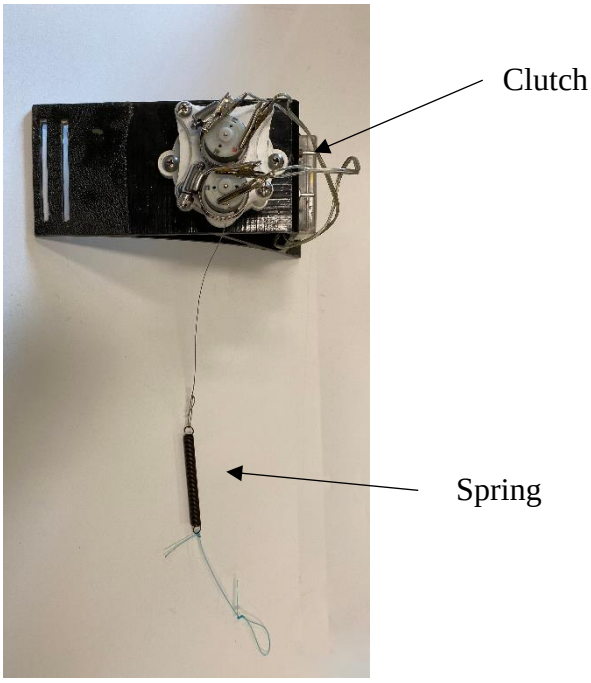

Fig. 7.7 A clutched spring mechanism prototype

Appendix A: Kinematic Analysis

A.1 Link Angular States

First, we calculated the angular velocities of the links based on our previous kinematic analysis on joint angles: In the first loop, taking the first order derivative of (4.3) gives the following equations:

$$l_1\dot{\varphi}_1 ie^{i\varphi_1} + l_2\dot{\varphi}_2 ie^{i\varphi_2} + l_3\dot{\varphi}_3 ie^{i\varphi_3} = 0 \tag{7.16}$$

Solve for $\dot{\varphi}_2$ and $\dot{\varphi}_3$ gives:

$$\dot{\varphi}_2 = -\frac{l_1\dot{\varphi}_1 \sin(\varphi_1 - \varphi_3)}{l_2 \sin(\varphi_2 - \varphi_3)} \tag{7.17}$$

$$\dot{\varphi}_3 = -\frac{l_1\dot{\varphi}_1 \sin(\varphi_1 - \varphi_2)}{l_3 \sin(\varphi_3 - \varphi_2)} \tag{7.18}$$

Taking the second derivative of (4.3) gives:

$$l_1\ddot{\varphi}_1 ie^{i\varphi_1} - l_1\dot{\varphi}_1^2 e^{i\varphi_1} + l_2\ddot{\varphi}_2 ie^{i\varphi_2} - l_2\dot{\varphi}_2^2 e^{i\varphi_2} + l_3\ddot{\varphi}_3 ie^{i\varphi_3} - l_3\dot{\varphi}_3^2 e^{i\varphi_3} = 0 \tag{7.19}$$

Solve for $\ddot{\varphi}_2$ and $\ddot{\varphi}_3$ gives:

$$\ddot{\varphi}_2 = -\frac{l_1\ddot{\varphi}_1 \sin(\varphi_1 - \varphi_3) + l_1\dot{\varphi}_1^2 \cos(\varphi_1 - \varphi_3) + l_3\dot{\varphi}_3^2 + l_2\dot{\varphi}_2^2 \cos(\varphi_2 - \varphi_3)}{l_2 \sin(\varphi_2 - \varphi_3)} \tag{7.20}$$

$$\ddot{\varphi}_3 = -\frac{l_1\ddot{\varphi}_1 \sin(\varphi_1 - \varphi_2) + l_1\dot{\varphi}_1^2 \cos(\varphi_1 - \varphi_2) + l_2\dot{\varphi}_2^2 + l_3\dot{\varphi}_3^2 \cos(\varphi_3 - \varphi_2)}{l_3 \sin(\varphi_3 - \varphi_2)} \tag{7.21}$$

In the second loop, similarly we can solve for $\dot{\varphi}_6$ and $\dot{\varphi}_7$:

$$\dot{\varphi}_6 = -\frac{l_5\dot{\varphi}_5 \sin(\varphi_5 - \varphi_7)}{l_6 \sin(\varphi_6 - \varphi_7)} \tag{7.22}$$

$$\dot{\varphi}_7 = -\frac{l_5\dot{\varphi}_5 \sin(\varphi_5 - \varphi_6)}{l_7 \sin(\varphi_7 - \varphi_6)} \tag{7.23}$$

where

$\dot{\varphi}_5 = \dot{\varphi}_1$.

Then solve for $\ddot{\varphi}_6$ and $\ddot{\varphi}_7$ yields

$$\ddot{\varphi}_6 = -\frac{l_5\ddot{\varphi}_5 \sin(\varphi_5 - \varphi_7) + l_5\dot{\varphi}_5{}^2 \cos(\varphi_5 - \varphi_7) + l_6\dot{\varphi}_6{}^2 \cos(\varphi_6 - \varphi_7) + l_7\dot{\varphi}_7{}^2}{l_6 \sin(\varphi_6 - \varphi_7)} \tag{7.24}$$

$$\ddot{\varphi}_7 = -\frac{l_5\ddot{\varphi}_5 \sin(\varphi_5 - \varphi_6) + l_5\dot{\varphi}_5{}^2 \cos(\varphi_5 - \varphi_6) + l_7\dot{\varphi}_7{}^2 \cos(\varphi_7 - \varphi_6) + l_6\dot{\varphi}_6{}^2}{l_7 \sin(\varphi_7 - \varphi_6)} \tag{7.25}$$

where

$\ddot{\varphi}_5 = \ddot{\varphi}_1$.

In the third loop, solve for $\dot{\varphi}_{10}$ and $\ddot{\varphi}_{11}$ yields:

$$\dot{\varphi}_{10} = -\frac{l_5\dot{\varphi}_5 \sin(\varphi_5 - \varphi_{11}) + l_9\dot{\varphi}_9 \sin(\varphi_9 - \varphi_{11}) + l_{12}\dot{\varphi}_{12} \sin(\varphi_{12} - \varphi_{11})}{l_{10} \sin(\varphi_{10} - \varphi_{11})} \tag{7.26}$$

$$\dot{\varphi}_{11} = -\frac{l_5\dot{\varphi}_5 \sin(\varphi_5 - \varphi_{10}) + l_9\dot{\varphi}_9 \sin(\varphi_9 - \varphi_{10}) + l_{12}\dot{\varphi}_{12} \sin(\varphi_{12} - \varphi_{10})}{l_{11} \sin(\varphi_{11} - \varphi_{10})} \tag{7.27}$$

where

$\dot{\varphi}_9 = \dot{\varphi}_6$,

$\dot{\varphi}_{12} = \dot{\varphi}_3$.

Solve for $\ddot{\varphi}_{10}$ and $\ddot{\varphi}_{11}$ yields:

$$\ddot{\varphi}_{10} = -\frac{l_5\ddot{\varphi}_5 \sin(\varphi_5 - \varphi_{11}) + l_5\dot{\varphi}_5{}^2 \cos(\varphi_5 - \varphi_{11})}{l_{10} \sin(\varphi_{10} - \varphi_{11})} - \frac{l_9\ddot{\varphi}_9 \sin(\varphi_9 - \varphi_{11}) + l_9\dot{\varphi}_9{}^2 \cos(\varphi_9 - \varphi_{11})}{l_{10} \sin(\varphi_{10} - \varphi_{11})}$$
$$- \frac{l_{10}\dot{\varphi}_{10}{}^2 \cos(\varphi_{10} - \varphi_{11}) + l_{11}\dot{\varphi}_{11}{}^2}{l_{10} \sin(\varphi_{10} - \varphi_{11})} - \frac{l_{12}\ddot{\varphi}_{12} \sin(\varphi_{12} - \varphi_{11}) + l_{12}\dot{\varphi}_{12}{}^2 \cos(\varphi_{12} - \varphi_{11})}{l_{10} \sin(\varphi_{10} - \varphi_{11})}$$

(7.28)

$$\ddot{\varphi}_{11} = -\frac{l_5\ddot{\varphi}_5 \sin(\varphi_5 - \varphi_{10}) + l_5\dot{\varphi}_5{}^2 \cos(\varphi_5 - \varphi_{10})}{l_{11} \sin(\varphi_{11} - \varphi_{10})} - \frac{l_9\ddot{\varphi}_9 \sin(\varphi_9 - \varphi_{10}) + l_9\dot{\varphi}_9{}^2 \cos(\varphi_9 - \varphi_{10})}{l_{11} \sin(\varphi_{11} - \varphi_{10})}$$
$$- \frac{l_{10}\dot{\varphi}_{10}{}^2 + l_{11}\dot{\varphi}_{11}{}^2 \cos(\varphi_{11} - \varphi_{10})}{l_{11} \sin(\varphi_{11} - \varphi_{10})} - \frac{l_{12}\ddot{\varphi}_{12} \sin(\varphi_{12} - \varphi_{10}) + l_{12}\dot{\varphi}_{12}{}^2 \cos(\varphi_{12} - \varphi_{10})}{l_{11} \sin(\varphi_{11} - \varphi_{10})}$$

(7.29)

where

$\ddot{\varphi}_5 = \ddot{\varphi}_1$,

$\ddot{\varphi}_9 = \ddot{\varphi}_6$,

$\ddot{\varphi}_{12} = \ddot{\varphi}_3$.

A.2 Link COM States

The displacements of link COMs can be expressed as the following equations:

$$\begin{aligned}
\mathrm{p}_1 &= R_1 e^{i(\varphi_1 + \gamma_1)} \\
\mathrm{p}_2 &= l_1 e^{i\varphi_1} + R_2 e^{i(\varphi_2 + \gamma_2)} \\
\mathrm{p}_3 &= l_1 e^{i\varphi_1} + l_2 e^{i\varphi_2} + R_3 e^{i(\varphi_3 + \gamma_3)} \\
\mathrm{p}_4 &= l_5 e^{i\varphi_5} + R_4 e^{i(\varphi_6 + \gamma_4)} \\
\mathrm{p}_5 &= l_5 e^{i\varphi_5} + l_6 e^{i\varphi_6} + R_5 e^{i(\varphi_7 + \gamma_5)} \\
\mathrm{p}_6 &= l_5 e^{i\varphi_5} + l_9 e^{i\varphi_9} + R_6 e^{i(\varphi_{10} + \gamma_6)} \\
\mathrm{p}_7 &= l_5 e^{i\varphi_5} + l_9 e^{i\varphi_9} + l_{10} e^{i\varphi_{10}} + R_7 e^{i(\varphi_{11} + \gamma_7)}
\end{aligned} \tag{7.30}$$

where R_i is the arm of the COM in link *i*. An illustration of R_i is given in Fig.

Expand (7.30) according to Euler's formula ($e^{ix} = \cos x + i \sin x$), the real parts represent displacements along the *x*-axis and the imaginary parts represent displacements along the *y*-axis.

$$
\begin{aligned}
\mathrm{p}_{1,x} &= R_1 \cos(\varphi_1 + \gamma_1) \\
\mathrm{p}_{1,y} &= R_1 \sin(\varphi_1 + \gamma_1) \\
\mathrm{p}_{2,x} &= l_1 \cos\varphi_1 + R_2 \cos(\varphi_2 + \gamma_2) \\
\mathrm{p}_{2,y} &= l_1 \sin\varphi_1 + R_2 \sin(\varphi_2 + \gamma_2) \\
\mathrm{p}_{3,x} &= l_1 \cos\varphi_1 + l_2 \cos\varphi_2 + R_3 \cos(\varphi_3 + \gamma_3) \\
\mathrm{p}_{3,y} &= l_1 \sin\varphi_1 + l_2 \sin\varphi_2 + R_3 \sin(\varphi_3 + \gamma_3) \\
\mathrm{p}_{4,x} &= l_5 \cos\varphi_5 + R_4 \cos(\varphi_6 + \gamma_4) \\
\mathrm{p}_{4,y} &= l_5 \sin\varphi_5 + R_4 \sin(\varphi_6 + \gamma_4) \\
\mathrm{p}_{5,x} &= l_5 \cos\varphi_5 + l_6 \cos\varphi_6 + R_5 \cos(\varphi_7 + \gamma_5) \\
\mathrm{p}_{5,y} &= l_5 \sin\varphi_5 + l_6 \sin\varphi_6 + R_5 \sin(\varphi_7 + \gamma_5) \\
\mathrm{p}_{6,x} &= l_5 \cos\varphi_5 + l_9 \cos\varphi_9 + R_6 \cos(\varphi_{10} + \gamma_6) \\
\mathrm{p}_{6,y} &= l_5 \sin\varphi_5 + l_9 \sin\varphi_9 + R_6 \sin(\varphi_{10} + \gamma_6) \\
\mathrm{p}_{7,x} &= l_5 \cos\varphi_5 + l_9 \cos\varphi_9 + l_{10} \cos\varphi_{10} + R_7 \cos(\varphi_{11} + \gamma_7) \\
\mathrm{p}_{7,y} &= l_5 \sin\varphi_5 + l_9 \sin\varphi_9 + l_{10} \sin\varphi_{10} + R_7 \sin(\varphi_{11} + \gamma_7)
\end{aligned}
\tag{7.31}
$$

where $p_{i,x}$ is the i^{th} link's COM linear displacement along *x*-axis, whereas $p_{i,y}$ along the *y*-axis.

Taking the first derivative of (7.30) gives the linear velocities of the COMs.

$$
\begin{aligned}
\dot{\mathrm{p}}_1 &= R_1\dot{\varphi}_1 e^{i(\varphi_1+\gamma_1+\frac{\pi}{2})} \\
\dot{\mathrm{p}}_2 &= l_1\dot{\varphi}_1 e^{i(\varphi_1+\frac{\pi}{2})} + R_2\dot{\varphi}_2 e^{i(\varphi_2+\gamma_2+\frac{\pi}{2})} \\
\dot{\mathrm{p}}_3 &= l_1\dot{\varphi}_1 e^{i(\varphi_1+\frac{\pi}{2})} + l_2\dot{\varphi}_2 e^{i(\varphi_2+\frac{\pi}{2})} + R_3\dot{\varphi}_3 e^{i(\varphi_3+\gamma_3+\frac{\pi}{2})} \\
\dot{\mathrm{p}}_4 &= l_5\dot{\varphi}_5 e^{i(\varphi_5+\frac{\pi}{2})} + R_4\dot{\varphi}_6 e^{i(\varphi_6+\gamma_4+\frac{\pi}{2})} \\
\dot{\mathrm{p}}_5 &= l_5\dot{\varphi}_5 e^{i(\varphi_5+\frac{\pi}{2})} + l_6\dot{\varphi}_6 e^{i(\varphi_6+\frac{\pi}{2})} + R_5\dot{\varphi}_7 e^{i(\varphi_7+\gamma_5+\frac{\pi}{2})} \\
\dot{\mathrm{p}}_6 &= l_5\dot{\varphi}_5 e^{i(\varphi_5+\frac{\pi}{2})} + l_9\dot{\varphi}_9 e^{i(\varphi_9+\frac{\pi}{2})} + R_6\dot{\varphi}_{10} e^{i(\varphi_{10}+\gamma_6+\frac{\pi}{2})} \\
\dot{\mathrm{p}}_7 &= l_5\dot{\varphi}_5 e^{i(\varphi_5+\frac{\pi}{2})} + l_9\dot{\varphi}_9 e^{i(\varphi_9+\frac{\pi}{2})} + l_{10}\dot{\varphi}_{10} e^{i(\varphi_{10}+\frac{\pi}{2})} + R_7\dot{\varphi}_{11} e^{i(\varphi_{11}+\gamma_7+\frac{\pi}{2})}
\end{aligned}
\tag{7.32}
$$

Similarly, expanding the equations according Euler' formula yields the linear velocity along the *x* and y-axis.

$$\dot{\mathrm{p}}_{1,x} = R_1\dot{\varphi}_1 \cos(\varphi_1 + \gamma_1 + \frac{\pi}{2})$$

$$\dot{\mathrm{p}}_{1,y} = R_1\dot{\varphi}_1 \sin(\varphi_1 + \gamma_1 + \frac{\pi}{2})$$

$$\dot{\mathrm{p}}_{2,x} = l_1\dot{\varphi}_1 \cos(\varphi_1 + \frac{\pi}{2}) + R_2\dot{\varphi}_2 \cos(\varphi_2 + \gamma_2 + \frac{\pi}{2})$$

$$\dot{\mathrm{p}}_{2,y} = l_1\dot{\varphi}_1 \cos(\varphi_1 + \frac{\pi}{2}) + R_2\dot{\varphi}_2 \cos(\varphi_2 + \gamma_2 + \frac{\pi}{2})$$

$$\dot{\mathrm{p}}_{3,x} = l_1\dot{\varphi}_1 \cos(\varphi_1 + \frac{\pi}{2}) + l_2\dot{\varphi}_2 \cos(\varphi_2 + \frac{\pi}{2}) + R_3\dot{\varphi}_3 \cos(\varphi_3 + \gamma_3 + \frac{\pi}{2})$$

$$\dot{\mathrm{p}}_{3,y} = l_1\dot{\varphi}_1 \sin(\varphi_1 + \frac{\pi}{2}) + l_2\dot{\varphi}_2 \sin(\varphi_2 + \frac{\pi}{2}) + R_3\dot{\varphi}_3 \sin(\varphi_3 + \gamma_3 + \frac{\pi}{2})$$

$$\dot{\mathrm{p}}_{4,x} = l_5\dot{\varphi}_5 \cos(\varphi_5 + \frac{\pi}{2}) + R_4\dot{\varphi}_6 \cos(\varphi_6 + \gamma_4 + \frac{\pi}{2})$$

$$\dot{\mathrm{p}}_{4,y} = l_5\dot{\varphi}_5 \sin(\varphi_5 + \frac{\pi}{2}) + R_4\dot{\varphi}_6 \sin(\varphi_6 + \gamma_4 + \frac{\pi}{2})$$

$$\dot{\mathrm{p}}_{5,x} = l_5\dot{\varphi}_5 \cos(\varphi_5 + \frac{\pi}{2}) + l_6\dot{\varphi}_6 \cos(\varphi_6 + \frac{\pi}{2}) + R_5\dot{\varphi}_7 \cos(\varphi_7 + \gamma_5 + \frac{\pi}{2})$$

$$\dot{\mathrm{p}}_{5,y} = l_5\dot{\varphi}_5 \sin(\varphi_5 + \frac{\pi}{2}) + l_6\dot{\varphi}_6 \sin(\varphi_6 + \frac{\pi}{2}) + R_5\dot{\varphi}_7 \sin(\varphi_7 + \gamma_5 + \frac{\pi}{2})$$

$$\dot{\mathrm{p}}_{6,x} = l_5\dot{\varphi}_5 \cos(\varphi_5 + \frac{\pi}{2}) + l_9\dot{\varphi}_9 \cos(\varphi_9 + \frac{\pi}{2}) + R_6\dot{\varphi}_{10} \cos(\varphi_{10} + \gamma_6 + \frac{\pi}{2})$$

$$\dot{\mathrm{p}}_{6,y} = l_5\dot{\varphi}_5 \sin(\varphi_5 + \frac{\pi}{2}) + l_9\dot{\varphi}_9 \sin(\varphi_9 + \frac{\pi}{2}) + R_6\dot{\varphi}_{10} \sin(\varphi_{10} + \gamma_6 + \frac{\pi}{2})$$

$$\dot{\mathrm{p}}_{7,x} = l_5\dot{\varphi}_5 \cos(\varphi_5 + \frac{\pi}{2}) + l_9\dot{\varphi}_9 \cos(\varphi_9 + \frac{\pi}{2}) + l_{10}\dot{\varphi}_{10} \cos(\varphi_{10} + \frac{\pi}{2}) + R_7\dot{\varphi}_{11} \cos(\varphi_{11} + \gamma_7 + \frac{\pi}{2})$$

$$\dot{\mathrm{p}}_{7,y} = l_5\dot{\varphi}_5 \sin(\varphi_5 + \frac{\pi}{2}) + l_9\dot{\varphi}_9 \sin(\varphi_9 + \frac{\pi}{2}) + l_{10}\dot{\varphi}_{10} \sin(\varphi_{10} + \frac{\pi}{2}) + R_7\dot{\varphi}_{11} \sin(\varphi_{11} + \gamma_7 + \frac{\pi}{2}) \tag{7.33}$$

where $\dot{p}_{i,x}$ represents the i^{th} link's COM linear velocity along the *x*-axis, whereas $\dot{p}_{i,y}$ along the *y*-axis.

Taking the second derivative of (7.30) gives the linear accelerations of the COMs:

$$\ddot{\mathrm{p}}_1 = R_1\ddot{\varphi}_1 e^{i(\varphi_1+\gamma_1+\frac{\pi}{2})} + R_1\dot{\varphi}_1^{\,2} e^{i(\varphi_1+\gamma_1+\pi)}$$

$$\ddot{\mathrm{p}}_2 = l_1\ddot{\varphi}_1 e^{i(\varphi_2+\frac{\pi}{2})} + l_1\dot{\varphi}_1^{\,2} e^{i(\varphi_2+\pi)} + R_2\ddot{\varphi}_2 e^{i(\varphi_2+\gamma_2+\frac{\pi}{2})} + R_2\dot{\varphi}_2^{\,2} e^{i(\varphi_2+\gamma_2+\pi)}$$

$$\ddot{\mathrm{p}}_3 = l_1\ddot{\varphi}_1 e^{i(\varphi_1+\frac{\pi}{2})} + l_1\dot{\varphi}_1^{\,2} e^{i(\varphi_1+\pi)} + l_2\ddot{\varphi}_2 e^{i(\varphi_2+\frac{\pi}{2})} + l_2\dot{\varphi}_2^{\,2} e^{i(\varphi_2+\pi)} + R_3\ddot{\varphi}_3 e^{i(\varphi_3+\gamma_3+\frac{\pi}{2})} + R_3\dot{\varphi}_3^{\,2} e^{i(\varphi_3+\gamma_3+\pi)}$$

$$\ddot{\mathrm{p}}_4 = l_5\ddot{\varphi}_5 e^{i(\varphi_5+\frac{\pi}{2})} + l_5\dot{\varphi}_5^{\,2} e^{i(\varphi_5+\pi)} + R_4\ddot{\varphi}_6 e^{i(\varphi_6+\gamma_4+\frac{\pi}{2})} + R_4\dot{\varphi}_6^{\,2} e^{i(\varphi_6+\gamma_4+\pi)}$$

$$\ddot{\mathrm{p}}_5 = l_5\ddot{\varphi}_5 e^{i(\varphi_5+\frac{\pi}{2})} + l_5\dot{\varphi}_5^{\,2} e^{i(\varphi_5+\pi)} + l_6\ddot{\varphi}_6 e^{i(\varphi_6+\frac{\pi}{2})} + l_6\dot{\varphi}_6^{\,2} e^{i(\varphi_6+\pi)} + R_5\ddot{\varphi}_7 e^{i(\varphi_7+\gamma_5+\frac{\pi}{2})} + R_5\dot{\varphi}_7^{\,2} e^{i(\varphi_7+\gamma_5+\pi)}$$

$$\ddot{\mathrm{p}}_6 = l_5\ddot{\varphi}_5 e^{i(\varphi_5+\frac{\pi}{2})} + l_5\dot{\varphi}_5^{\,2} e^{i(\varphi_5+\pi)} + l_9\ddot{\varphi}_9 e^{i(\varphi_9+\frac{\pi}{2})} + l_9\dot{\varphi}_9^{\,2} e^{i(\varphi_9+\pi)} + R_6\ddot{\varphi}_{10} e^{i(\varphi_{10}+\gamma_6+\frac{\pi}{2})} + R_6\dot{\varphi}_{10}^{\,2} e^{i(\varphi_{10}+\gamma_6+\pi)}$$

$$\ddot{\mathrm{p}}_7 = l_5\ddot{\varphi}_5 e^{i(\varphi_5+\frac{\pi}{2})} + l_5\dot{\varphi}_5^{\,2} e^{i(\varphi_5+\pi)} + l_9\ddot{\varphi}_9 e^{i(\varphi_9+\frac{\pi}{2})} + l_9\dot{\varphi}_9^{\,2} e^{i(\varphi_9+\pi)} + l_{10}\ddot{\varphi}_{10} e^{i(\varphi_{10}+\frac{\pi}{2})} + l_{10}\dot{\varphi}_{10}^{\,2} e^{i(\varphi_{10}+\pi)} + R_7\ddot{\varphi}_{11} e^{i(\varphi_{11}+\gamma_7+\frac{\pi}{2})} + R_7\dot{\varphi}_{11}^{\,2} e^{i(\varphi_{11}+\gamma_7+\pi)}$$

(7.34)

Similarly, expanding the equations according Euler' formula yields the linear accelerations along the *x* and y-axis.

$$\ddot{\mathrm{p}}_{1,x} = R_1\ddot{\varphi}_1 \cos(\varphi_i + \gamma_1 + \frac{\pi}{2}) + R_1\dot{\varphi}_1^{\,2} \cos(\varphi_i + \gamma_1 + \pi)$$

$$\ddot{\mathrm{p}}_{1,y} = R_1\ddot{\varphi}_1 \sin(\varphi_i + \gamma_1 + \frac{\pi}{2}) + R_1\dot{\varphi}_1^{\,2} \sin(\varphi_i + \gamma_1 + \pi)$$

$$\ddot{\mathrm{p}}_{2,x} = l_1\ddot{\varphi}_1 \cos(\varphi_2 + \frac{\pi}{2}) + l_1\dot{\varphi}_1^{\,2} \cos(\varphi_2 + \pi) + R_2\ddot{\varphi}_2 \cos(\varphi_2 + \gamma_2 + \frac{\pi}{2})$$
$$+ R_2\dot{\varphi}_2^{\,2} \cos(\varphi_2 + \gamma_2 + \pi)$$

$$\ddot{\mathrm{p}}_{2,y} = l_1\ddot{\varphi}_1 \sin(\varphi_2 + \frac{\pi}{2}) + l_1\dot{\varphi}_1^{\,2} \sin(\varphi_2 + \pi) + R_2\ddot{\varphi}_2 \sin(\varphi_2 + \gamma_2 + \frac{\pi}{2})$$
$$+ R_2\dot{\varphi}_2^{\,2} \sin(\varphi_2 + \gamma_2 + \pi)$$

$$\ddot{\mathrm{p}}_{3,x} = l_1\ddot{\varphi}_1 \cos(\varphi_1 + \frac{\pi}{2}) + l_1\dot{\varphi}_1^{\,2} \cos(\varphi_1 + \pi) + l_2\ddot{\varphi}_2 \cos(\varphi_2 + \frac{\pi}{2}) + l_2\dot{\varphi}_2^{\,2} \cos(\varphi_2 + \pi)$$
$$+ R_3\ddot{\varphi}_3 \cos(\varphi_3 + \gamma_3 + \frac{\pi}{2}) + R_3\dot{\varphi}_3^{\,2} \cos(\varphi_3 + \gamma_3 + \pi)$$

$$\ddot{\mathrm{p}}_{3,y} = l_1\ddot{\varphi}_1 \sin(\varphi_1 + \frac{\pi}{2}) + l_1\dot{\varphi}_1^{\,2} \sin(\varphi_1 + \pi) + l_2\ddot{\varphi}_2 \sin(\varphi_2 + \frac{\pi}{2}) + l_2\dot{\varphi}_2^{\,2} \sin(\varphi_2 + \pi)$$
$$+ R_3\ddot{\varphi}_3 \sin(\varphi_3 + \gamma_3 + \frac{\pi}{2}) + R_3\dot{\varphi}_3^{\,2} \sin(\varphi_3 + \gamma_3 + \pi)$$

$$\ddot{\mathrm{p}}_{4,x} = l_5\ddot{\varphi}_5 \cos(\varphi_5 + \frac{\pi}{2}) + l_5\dot{\varphi}_5^{\,2} \cos(\varphi_5 + \pi) + R_4\ddot{\varphi}_6 \cos(\varphi_6 + \gamma_4 + \frac{\pi}{2})$$
$$+ R_4\dot{\varphi}_6^{\,2} \cos(\varphi_6 + \gamma_4 + \pi)$$

$$\ddot{\mathrm{p}}_{4,y} = l_5\ddot{\varphi}_5 \sin(\varphi_5 + \frac{\pi}{2}) + l_5\dot{\varphi}_5^{\,2} \sin(\varphi_5 + \pi) + R_4\ddot{\varphi}_6 \sin(\varphi_6 + \gamma_4 + \frac{\pi}{2})$$
$$+ R_4\dot{\varphi}_6^{\,2} \sin(\varphi_6 + \gamma_4 + \pi)$$

$$\ddot{\mathrm{p}}_{5,x} = l_5\ddot{\varphi}_5 \cos(\varphi_5 + \frac{\pi}{2}) + l_5\dot{\varphi}_5^{\,2} \cos(\varphi_5 + \pi) + l_6\ddot{\varphi}_6 \cos(\varphi_6 + \frac{\pi}{2}) + l_6\dot{\varphi}_6^{\,2} \cos(\varphi_6 + \pi)$$
$$+ R_5\ddot{\varphi}_7 \cos(\varphi_7 + \gamma_5 + \frac{\pi}{2}) + R_5\dot{\varphi}_7^{\,2} \cos(\varphi_7 + \gamma_5 + \pi)$$

$$\ddot{\mathrm{p}}_{5,y} = l_5\ddot{\varphi}_5 \sin(\varphi_5 + \frac{\pi}{2}) + l_5\dot{\varphi}_5^{\,2} \sin(\varphi_5 + \pi) + l_6\ddot{\varphi}_6 \sin(\varphi_6 + \frac{\pi}{2}) + l_6\dot{\varphi}_6^{\,2} \sin(\varphi_6 + \pi)$$
$$+ R_5\ddot{\varphi}_7 \sin(\varphi_7 + \gamma_5 + \frac{\pi}{2}) + R_5\dot{\varphi}_7^{\,2} \sin(\varphi_7 + \gamma_5 + \pi)$$

$$\ddot{\mathrm{p}}_{6,x} = l_5\ddot{\varphi}_5 \cos(\varphi_5 + \frac{\pi}{2}) + l_5\dot{\varphi}_5^{\,2} \cos(\varphi_5 + \pi) + l_9\ddot{\varphi}_9 \cos(\varphi_9 + \frac{\pi}{2}) + l_9\dot{\varphi}_9^{\,2} \cos(\varphi_9 + \pi)$$
$$+ R_6\ddot{\varphi}_{10} \cos(\varphi_{10} + \gamma_6 + \frac{\pi}{2}) + R_6\dot{\varphi}_{10}^{\,2} \cos(\varphi_{10} + \gamma_6 + \pi)$$

$$\ddot{\mathrm{p}}_{6,y} = l_5\ddot{\varphi}_5 \sin(\varphi_5 + \frac{\pi}{2}) + l_5\dot{\varphi}_5^{\,2} \sin(\varphi_5 + \pi) + l_9\ddot{\varphi}_9 \sin(\varphi_9 + \frac{\pi}{2}) + l_9\dot{\varphi}_9^{\,2} \sin(\varphi_9 + \pi)$$
$$+ R_6\ddot{\varphi}_{10} \sin(\varphi_{10} + \gamma_6 + \frac{\pi}{2}) + R_6\dot{\varphi}_{10}^{\,2} \sin(\varphi_{10} + \gamma_6 + \pi)$$

$$
\begin{aligned}
\ddot{p}_{7,x} &= l_5\ddot{\varphi}_5\cos(\varphi_5+\frac{\pi}{2}) + l_5\dot{\varphi}_5{}^2\cos(\varphi_5+\pi) + l_9\ddot{\varphi}_9\cos(\varphi_9+\frac{\pi}{2}) + l_9\dot{\varphi}_9{}^2\cos(\varphi_9+\pi) \\
&\quad + l_{10}\ddot{\varphi}_{10}\cos(\varphi_{10}+\frac{\pi}{2}) + l_{10}\dot{\varphi}_{10}{}^2\cos(\varphi_{10}+\pi) + R_7\ddot{\varphi}_{11}\cos(\varphi_{11}+\gamma_7+\frac{\pi}{2}) \\
&\quad + R_7\dot{\varphi}_{11}{}^2\cos(\varphi_{11}+\gamma_7+\pi) \\
\ddot{p}_{7,y} &= l_5\ddot{\varphi}_5\cos(\varphi_5+\frac{\pi}{2}) + l_5\dot{\varphi}_5{}^2\cos(\varphi_5+\pi) + l_9\ddot{\varphi}_9\cos(\varphi_9+\frac{\pi}{2}) + l_9\dot{\varphi}_9{}^2\cos(\varphi_9+\pi) \\
&\quad + l_{10}\ddot{\varphi}_{10}\cos(\varphi_{10}+\frac{\pi}{2}) + l_{10}\dot{\varphi}_{10}{}^2\cos(\varphi_{10}+\pi) + R_7\ddot{\varphi}_{11}\cos(\varphi_{11}+\gamma_7+\frac{\pi}{2}) \\
&\quad + R_7\dot{\varphi}_{11}{}^2\cos(\varphi_{11}+\gamma_7+\pi)
\end{aligned}
\tag{7.35}
$$

where $\ddot{p}_{i,x}$ represents the i^{th} link's COM linear acceleration along the *x*-axis, whereas $\ddot{p}_{i,y}$ along the *y*-axis.

Appendix B: Force Analysis

Force analysis was conducted using the Newton-Euler formation, based on the free-body diagram in Fig 7.2.

In all the links we have

$$\begin{aligned} \boldsymbol{G}_i &= m_i \boldsymbol{g} \\ \boldsymbol{F}_i &= m_i \ddot{\boldsymbol{p}}_i \\ \boldsymbol{M}_i &= I_i \ddot{\boldsymbol{\varphi}}_i \end{aligned} \tag{7.36}$$

where G_i is the gravitational force of link *i*, **g** the gravitational acceleration, F_i the inertial force of link *i*, $\ddot{p}_i$ linear acceleration of , I_i the moment inertia of link *i*, $\ddot{\varphi}_i$ the angular acceleration of link *i*.

The Newton-Euler formulation are given as follows.

For link 1,

$$\begin{aligned} &\boldsymbol{F}_{01} + \boldsymbol{F}_{21} + \boldsymbol{F}_{41} + \boldsymbol{F}_1 + \boldsymbol{G}_1 = 0 \\ &\boldsymbol{r}_{10} \times \boldsymbol{F}_{01} + \boldsymbol{r}_{12} \times \boldsymbol{F}_{21} + \boldsymbol{r}_{14} \times \boldsymbol{F}_{41} + \boldsymbol{M}_{01} + \boldsymbol{M}_1 = 0 \end{aligned} \tag{7.37}$$

where

$\boldsymbol{r}_{10} = \boldsymbol{p}_A - \boldsymbol{p}_1$,

$\boldsymbol{r}_{12} = \boldsymbol{p}_B - \boldsymbol{p}_1$,

$\boldsymbol{r}_{14} = \boldsymbol{p}_D - \boldsymbol{p}_1$.

For link 2,

$$\begin{aligned} &\boldsymbol{F}_{12} + \boldsymbol{F}_{32} + \boldsymbol{F}_2 + \boldsymbol{G}_2 = 0 \\ &\boldsymbol{r}_{21} \times \boldsymbol{F}_{12} + \boldsymbol{r}_{23} \times \boldsymbol{F}_{32} + \boldsymbol{M}_2 = 0 \end{aligned} \tag{7.38}$$

where

$\boldsymbol{r}_{21} = \boldsymbol{p}_{\boldsymbol{B}} - \boldsymbol{p}_2$,

$\boldsymbol{r}_{23} = \boldsymbol{p}_{\boldsymbol{C}} - \boldsymbol{p}_2$.

For link 3,

$$\begin{aligned} &\boldsymbol{F}_{23} + \boldsymbol{F}_{03} + \boldsymbol{F}_{73} + \boldsymbol{F}_3 + \boldsymbol{G}_3 = 0 \\ &\boldsymbol{r}_{32} \times \boldsymbol{F}_{23} + \boldsymbol{r}_{30} \times \boldsymbol{F}_{03} + \boldsymbol{r}_{37} \times \boldsymbol{F}_{73} + \boldsymbol{M}_3 + \boldsymbol{T}_{\boldsymbol{spring}}^{\boldsymbol{hip}} - \boldsymbol{T}_{\boldsymbol{spring}}^{\boldsymbol{knee}} = 0 \end{aligned} \tag{7.39}$$

where

$\boldsymbol{r}_{32} = \boldsymbol{p}_{\boldsymbol{C}} - \boldsymbol{p}_3$,

$\boldsymbol{r}_{30} = \boldsymbol{p}_{\boldsymbol{H}} - \boldsymbol{p}_3$,

$\boldsymbol{r}_{37} = \boldsymbol{p}_{\boldsymbol{K}} - \boldsymbol{p}_3$.

For link 4,

$$\begin{aligned} &\boldsymbol{F}_{14} + \boldsymbol{F}_{54} + \boldsymbol{F}_{64} + \boldsymbol{F}_4 + \boldsymbol{G}_4 = 0 \\ &\boldsymbol{r}_{41} \times \boldsymbol{F}_{14} + \boldsymbol{r}_{45} \times \boldsymbol{F}_{54} + \boldsymbol{r}_{46} \times \boldsymbol{F}_{64} + \boldsymbol{M}_4 = 0 \end{aligned} \tag{7.40}$$

where

$\boldsymbol{r}_{41} = \boldsymbol{p}_{\boldsymbol{D}} - \boldsymbol{p}_4$,

$\boldsymbol{r}_{45} = \boldsymbol{p}_{\boldsymbol{E}} - \boldsymbol{p}_4$,

$\boldsymbol{r}_{46} = \boldsymbol{p}_{\boldsymbol{I}} - \boldsymbol{p}_4$.

For link 5,

$$\begin{aligned} &\boldsymbol{F}_{05} + \boldsymbol{F}_{45} + \boldsymbol{F}_5 + \boldsymbol{G}_5 = 0 \\ &\boldsymbol{r}_{50} \times \boldsymbol{F}_{05} + \boldsymbol{r}_{54} \times \boldsymbol{F}_{45} + \boldsymbol{M}_5 = 0 \end{aligned} \tag{7.41}$$

where

$\boldsymbol{r}_{50} = \boldsymbol{p}_{\boldsymbol{G}} - \boldsymbol{p}_5$,

$\boldsymbol{r}_{54} = \boldsymbol{p}_{\boldsymbol{E}} - \boldsymbol{p}_5$.

For link 6,

$$\begin{aligned} &\boldsymbol{F}_{46} + \boldsymbol{F}_{76} + \boldsymbol{F}_6 + \boldsymbol{G}_6 = 0 \\ &\boldsymbol{r}_{64} \times \boldsymbol{F}_{46} + \boldsymbol{r}_{67} \times \boldsymbol{F}_{76} + \boldsymbol{M}_6 = 0 \end{aligned} \tag{7.42}$$

where

$\boldsymbol{r}_{64} = \boldsymbol{p}_{\boldsymbol{I}} - \boldsymbol{p}_6$,

$\boldsymbol{r}_{67} = \boldsymbol{p}_{\boldsymbol{J}} - \boldsymbol{p}_6$.

For link 7,

$$\begin{aligned} &\boldsymbol{F}_{37} + \boldsymbol{F}_{67} + \boldsymbol{F}_7 + \boldsymbol{G}_7 = 0 \\ &\boldsymbol{r}_{73} \times \boldsymbol{F}_{37} + \boldsymbol{r}_{76} \times \boldsymbol{F}_{67} + \boldsymbol{M}_7 + \boldsymbol{T}_{\boldsymbol{spring}}^{\boldsymbol{knee}} = 0 \end{aligned} \tag{7.43}$$

where

$\boldsymbol{r}_{73} = \boldsymbol{p}_{\boldsymbol{K}} - \boldsymbol{p}_7$,

$\boldsymbol{r}_{76} = \boldsymbol{p}_{\boldsymbol{J}} - \boldsymbol{p}_7$.

Expanding and simplifying the equations yield the following 21 equations:

$$
\begin{aligned}
&F_{01,x} - F_{12,x} - F_{14,x} + F_{1,x} = 0 \\
&F_{01,y} - F_{12,y} - F_{14,y} + F_{1,y} + G_{1,y} = 0 \\
&r_{10,x}F_{01,y} - r_{10,y}F_{01,x} - r_{12,x}F_{12,y} + r_{12,y}F_{12,x} - r_{14,x}F_{14,y} + r_{14,y}F_{14,x} + M_{01,z} + M_{1,z} = 0 \\
&F_{12,x} - F_{23,x} + F_{2,x} = 0 \\
&F_{12,y} - F_{23,y} + F_{2,y} + G_{2,y} = 0 \\
&r_{21,x}F_{12,y} - r_{21,y}F_{12,x} - r_{23,x}F_{23,y} + r_{23,y}F_{23,x} + M_{2,z} = 0 \\
&F_{23,x} + F_{03,x} - F_{37,x} + F_{3,x} = 0 \\
&F_{23,y} + F_{03,y} - F_{37,y} + F_{3,y} + G_{3,y} = 0 \\
&r_{32,x}F_{23,y} - r_{32,y}F_{23,x} + r_{30,x}F_{03,y} - r_{30,y}F_{03,x} - r_{37,x}F_{37,y} + r_{37,y}F_{37,x} + M_{3,z} + T_{spring}^{Hip} - T_{spring}^{Knee} = 0 \\
&F_{14,x} - F_{45,x} - F_{46,x} + F_{4,x} = 0 \\
&F_{14,y} - F_{45,y} - F_{46,y} + F_{4,y} + G_{4,y} = 0 \\
&r_{41,x}F_{14,y} - r_{41,y}F_{14,x} - r_{45,x}F_{45,y} + r_{45,y}F_{45,x} - r_{46,x}F_{46,y} + r_{46,y}F_{46,x} + M_{4,z} = 0 \\
&F_{05,x} + F_{45,x} + F_{5,x} = 0 \\
&F_{05,y} + F_{45,y} + F_{5,y} + G_{5,y} = 0 \\
&r_{50,x}F_{05,y} - r_{50,y}F_{05,x} + r_{54,x}F_{45,y} - r_{54,y}F_{45,x} + M_{5,z} = 0 \\
&F_{46,x} - F_{67,x} + F_{6,x} = 0 \\
&F_{46,y} - F_{67,y} + F_{6,y} + G_{6,y} = 0 \\
&r_{64,x}F_{46,y} - r_{64,y}F_{46,x} - r_{67,x}F_{67,y} + r_{67,y}F_{67,x} + M_{6,z} = 0 \\
&F_{37,x} + F_{67,x} + F_{7,x} = 0 \\
&F_{37,y} + F_{67,y} + G_{7,y} + F_{7,y} = 0 \\
&r_{73,x}F_{37,y} - r_{73,y}F_{37,x} + r_{76,x}F_{67,y} - r_{76,y}F_{67,x} + M_{7,z} + T_{spring}^{Knee} = 0
\end{aligned}
\tag{7.44}
$$

where $F_{ij,x}$ is the force exerted on link *j* from link *i* along the x-axis, whereas $F_{ij,y}$ along the y-axis; $G_{i,y}$ the gravitational force of link *i*; T_{spring}^{Hip} and T_{spring}^{Knee} the spring torques at hip and knee joints respectively; $M_{01,z}$ the motor torque; $M_{i,z}$ torque due to moment of inertia in link *i* along z-axis.

Part IV Conclusions

Chapter 8 Conclusions and Future work

8.1 Summaries and Conclusions

This thesis exploited planar 1-DOF linkages with only revolute joints for leg exoskeletons design. The design problem challenges 1-DOF linkages for multiple successive angular outputs, which has not been addressed in the literature. In addition, design requirements on 1-DOF linkages for exoskeletons have not been discussed in the literature. In order to solve the linkage design problem and address the requirements for exoskeletons. A systematic linkage design methodology was proposed to address.

The methodology consists of problem definition, type synthesis, and dimensional synthesis. Problem definition discusses issues for developing 1-DOF linkage for exoskeletons and sums up several requirements. Proper functionality is guaranteed by demanding the linkage to generate human-like motions; safety is ensured by considering angular output limits and linkage singularities. Compactness can be achieved by limiting the dimensions of the links.

Type synthesis proposes candidate linkages for generating multiple successive angular outputs. A four-bar linkage is first used to generate the first angular output. Then the following angular outputs can be realized by adding dyad in sequence. Linkage types are proposed according the options to add the dyads.

The type synthesis method is able to propose a number of candidate linkages for the required number of angular outputs. Though in this study, we focused on 1-DOF linkage for 2 or 3 angular outputs, the method can be used to propose 1-DOF linkages for a required number of outputs greater than 3.

As the type synthesis method generates candidate linkage by adding dyads in sequence, it does not enumerate the designs with a given number of links. For example, it cannot enumerate all the designs for 1-DOF-6-bar linkages. Therefore, the type synthesis method would miss out several a number of designs. In addition, the method attempts to achieve complicated angular outputs by increasing the number of dyads. The design method may lead to more complicated designs.

Dimensional synthesis exploits the candidate linkages for reproducing human-like motions. It employs an optimization-based method to achieve the optimal design of a linkage. The cost function is the structure error between the reference motion and the exoskeleton outputs; constraints address the design requirements, such as functionality, joint limits, singularity, etc.; bounds make the exoskeleton compact and wearable. The optimization problem is solved using a global optimization algorithm: genetic algorithm. The method is able to address the design requirements. The framework of the optimization problem can also be used for designing planar 1-DOF linkages for other purposes.

A design procedure was proposed to integrate the type and dimensional synthesis method. Dimensional synthesis employs computational power to obtain optimal

parameters of a linkage. As type synthesis method proposes a great number of candidate linkages, examining all the candidates one by one can be time consuming and computationally expensive. The proposed design procedure can effectively reduce the number of linkages to be examined. It helps to find a functional linkage efficiently.

A leg exoskeleton is then developed based on the proposed 1-DOF linkage design methodology. The aimed leg exoskeleton is for generating human-walking gait pattern at the hip and knee joints. The ankle joint is neglected due to its complex motion pattern, which may lead to overall complicated linkage design.

Using the method, for the first time, we achieved a 1-DOF-8-bar-10-joint linkage design to reproduce the angular outputs at hip and knee joints. A prototype was then developed based on the linkage, which involved actuation design, control system design, and harness design. The achieved leg exoskeleton is able to generate a human-like gait pattern at hip and knee joints. The leg exoskeleton can run forward and backward safely, no singularities occurred during operation. The open-loop control system is able to drive the device, and it is easy to operate. Therefore, the leg exoskeleton can provide CPM based rehabilitation.

A recent breakthrough on saving human walking energy cost proposes a CSM applied at the ankle joint. The study showed energy saving with the passive clutched-spring mechanism. From the energetic perspective, the mechanism utilizes the negative-positive energetic pattern during walking. It harvests energy during the negative-energy phase and returns energy in the following positive energy phase. The negative-

positive energy pattern also exists in the hip and knee joints. Therefore, we can hypothesise that the clutched-spring mechanism may also be applied to hip and knee joints.

This thesis employed OpenSim to evaluate the mechanism at hip and knee joints for saving walking energy cost. An indirect method is introduced to achieve the optimal spring on/off timings and stiffness. A leg exoskeleton for mounting the springs was first designed and imported into OpenSim. Then the optimal virtual muscle force for maximum energy saving at each joint was achieved using OpenSim built-in features: ID and CMC. We then used spring forces to approximate the tension forces, which was achieved in MATLAB via optimization. In the end, we tested the optimal spring stiffness and compared with neighbouring spring stiffness.

The results showed energy saving at the ankle, knee and hip joints with optimal spring stiffness and on/off timings. Therefore, we conclude that with proper spring stiffness and on/off timings the clutched-spring mechanism can save walking energy cost at all the leg joints.

Though the simulation study proves the effectiveness of the clutched-spring mechanism, the platform has its limitations. OpenSim cannot conduct optimization on an imported leg exoskeleton for optimal parameters. PD was then introduced to address the issue. PD utilizes optimization to reproduce/predict human motions. It enables cause and effect study in human motions such as walking, running, lifting, etc.

Previous application of PD mainly focuses on human motions, this thesis extended its application to exoskeleton design. It was used to achieve the optimal parameters of the CSMs. The method was first tested on a pendulum leg model. PD could track the required motion of the leg and reveal joint torque that causes the motion when spring is not considered. It also returned optimal spring parameters when a spring/clutched-spring mechanism was added. In both cases, motor energy was reduced, while the clutched ones saved more.

The pendulum leg study validated the effectiveness of the PD method for obtaining the optimal design of a CSM. In addition, the study shows the CSMs' potential for energy saving in a dynamic system.

The PD method was then applied on the 1-DOF leg exoskeleton. Both hip and knee CSMs improved the energy efficiency. An energy saving of 30.85% was achieved when both of the hip and knee joints are assisted by CSM. The study demonstrated the energetic saving potential of CSMs in leg exoskeleton devices. Such springs can be used to extend the battery life of leg exoskeletons for longer working hours.

8.2 Main Contributions

This thesis systematically solves the problem of generating multiple successive function generation outputs using 1-DOF linkages for the first time. Problem definition, type synthesis, and dimensional synthesis were discussed in detail. Though the method

has been tailored for developing 1-DOF linkage based exoskeletons, it can serve beyond exoskeleton design where multiple function generation outputs are required from a 1-DOF linkage.

A leg exoskeleton for CPM-based rehabilitation have been achieved based on the 1-DOF linkage design method. The leg exoskeleton can produce a gait pattern at hip and knee joint. The device is lightweight and portable. It may provide rehabilitation services beyond clinical settings.

CSMs have been proved effective for saving human locomotion energy if applied at hip or knee joint, while previous studies focused on ankle joint. Though human walking is believed to be energy efficient, the simulation study in OpenSim shows the potential to further reduce the metabolic cost of walking. Clutched-springs mechanisms may also benefit other daily tasks such as running, stair ascending and descending. The study hints lightweight portable devices assisting healthy individuals in daily life.

The PD method was originally used for simulating human motions. This thesis extended its application for leg exoskeleton design. CSMs in a pendulum leg and the exoskeleton were optimized using the PD method. The method was able to return optimal parameters for maximum energy saving. The method can be used for exoskeleton design where dynamics of the device is considered.

The studies on pendulum leg and leg exoskeleton further proved the effectiveness of CSMs for improving the energy efficiency of a dynamic system. Energy has been saved in both studies. CSMs may also serve multibody dynamic systems beyond exoskeletons.

8.3 Future Work

The 1-DOF linkage design method in the thesis builds up candidate linkage types for multiple function generation outputs by simply adding RRR dyads in sequence. This cannot guarantee enumeration of all the possible linkage designs. Graph-based methods can enumerate 1-DOF linkage types with a given number of links. The problem of generating multiple successive angular outputs can be considered as finding successive links in the graphs. Therefore, a method to enumerate all the linkage designs based on graphs is possible. Further study would investigate the graph-based method for type synthesis.

Current leg exoskeleton utilizes an open-loop control system to activate the device, which can only provide CPM-based rehabilitation. However, studies show that interactive rehabilitation produces better rehabilitative effects compared with CPM based rehabilitation. To enable interactive rehabilitation, a more complex control and sensing system is needed to detect a user's movement intention and provide assistance when required. Further development of the leg exoskeleton will also include implementation of CSMs to improve its energy efficiency for longer working hours.

The OpenSim simulation studies on the CSMs has proved the effectiveness of the mechanism for saving walking energy cost and returned the optimal mechanism parameters. The results can be used to develop a passive exoskeleton that saves the metabolic cost for healthy users.

The CSM studies only uses a single spring and the spring is only turned on/off once in a cyclic motion. However, pendulum study and the human walking energetic pattern indicates that multiple springs and multiple on/off are also possible for a better energetic performance. In addition, the studies only considered a constant spring stiffness, while it is possible for better energy saving with varying spring stiffness. Further study will investigate using multiple springs in a joint and turn on/off a spring for multiple times, and the use of varying stiffness springs.

The predictive dynamic method can serve beyond the application of the proposed 1-DOF linkage-based leg exoskeleton. It can be used to conduct simulation on human and leg exoskeleton together to facilitate leg exoskeleton development. This thesis only tested PD for leg exoskeleton design on a case of swing the leg. However, it has the potential for developing or improving leg exoskeletons that assist daily motions, such as walking, running, lifting, etc. Future study will apply the PD method on human-exoskeleton systems for other tasks such as running, stand-sit transition, and stair ascending and descending.

This thesis first conducted optimization on a 1-DOF linkage for producing a human-like gait, then optimized CSMs for a better energetic performance. However, the

linkage parameters may also affect the motor energy cost. Future work can integrate the optimization problems into a multi-objective one to simultaneously obtain linkage and CSM designs.

List of Publications Arisen from This PhD Study

Journal Papers

Z. Shen, G. Allison, and L. Cui, "An Integrated Type and Dimensional Synthesis Method to Design One Degree-of-Freedom Planar Linkages With Only Revolute Joints for Exoskeletons," *Journal of Mechanical Design*, vol. 140, no. 9, p. 092302, 2018. (**Featured Article, 2018 JMD Editors' Choice Award**).

I would like to thank The American Society of Mechanical Engineers for permission to include this paper for parts in Chapter 3 (P.40-53) of my thesis.

Z. Shen, S. Sam, G. Allison, and L. Cui, "A Simulation-Based Study on a Clutch-Spring Mechanism Reducing Human Walking Metabolic Cost," *International Journal Of Mechanical Engineering And Robotics Research*, vol. 7, no. 1, pp. 55-60, 2018.

I would like to thank the International Journal of Mechanical Engineering and Robotics Research for permission to include this paper for Chapter 5 (Page 91 to 105) in my thesis.

Book Chapter

Z. Shen, T. Tan, G. Allison, and L. Cui, "A Customized One-Degree-of-Freedom Linkage Based Leg Exoskeleton for Continuous Passive Motion Rehabilitation," in *The International Conference of IFToMM ITALY*, 2018, pp. 518-526: Springer.

I would like to thank Spring Nature for permissions to include this paper as parts in Chapter 4 (Page 62 to 75) of my thesis.

Reference

[1] T. Vos *et al.*, "Global, regional, and national incidence, prevalence, and years lived with disability for 328 diseases and injuries for 195 countries, 1990–2016: a systematic analysis for the Global Burden of Disease Study 2016," *The Lancet,* vol. 390, no. 10100, pp. 1211-1259, 2017.

[2] B. Chen *et al.*, "Recent developments and challenges of lower extremity exoskeletons," *Journal of Orthopaedic Translation,* vol. 5, pp. 26-37, 2016.

[3] W. H. Organization and I. S. C. Society, *International perspectives on spinal cord injury*. World Health Organization, 2013.

[4] T. H. Murphy and D. Corbett, "Plasticity during stroke recovery: from synapse to behaviour," *Nature reviews neuroscience,* vol. 10, no. 12, p. 861, 2009.

[5] P. Langhorne, J. Bernhardt, and G. Kwakkel, "Stroke rehabilitation," *The Lancet,* vol. 377, no. 9778, pp. 1693-1702, 2011.

[6] P. Langhorne, F. Coupar, and A. Pollock, "Motor recovery after stroke: a systematic review," *The Lancet Neurology,* vol. 8, no. 8, pp. 741-754, 2009.

[7] V. Sirtori, D. Corbetta, L. Moja, and R. Gatti, "Constraint-induced movement therapy for upper extremities in stroke patients," *Cochrane Database Syst Rev,* vol. 4, no. 4, 2009.

[8] I. G. van de Port, S. Wood-Dauphinee, E. Lindeman, and G. Kwakkel, "Effects of exercise training programs on walking competency after stroke: a systematic review," *American Journal of Physical Medicine & Rehabilitation,* vol. 86, no. 11, pp. 935-951, 2007.

[9] D. R. Louie, J. J. Eng, and T. Lam, "Gait speed using powered robotic exoskeletons after spinal cord injury: a systematic review and correlational

study," *Journal of neuroengineering and rehabilitation*, vol. 12, no. 1, p. 82, 2015.

[10] N. Sezer, S. Akkuş, and F. G. Uğurlu, "Chronic complications of spinal cord injury," *World journal of orthopedics*, vol. 6, no. 1, p. 24, 2015.

[11] J. J. Adriaansen *et al.*, "Secondary health conditions in persons with spinal cord injury: a longitudinal study from one to five years post-discharge," *Journal of rehabilitation medicine*, vol. 45, no. 10, pp. 1016-1022, 2013.

[12] A. Curt, H. J. Van Hedel, D. Klaus, V. Dietz, and E.-S. s. group, "Recovery from a spinal cord injury: significance of compensation, neural plasticity, and repair," *Journal of neurotrauma*, vol. 25, no. 6, pp. 677-685, 2008.

[13] A. L. Behrman, M. G. Bowden, and P. M. Nair, "Neuroplasticity after spinal cord injury and training: an emerging paradigm shift in rehabilitation and walking recovery," *Physical therapy*, vol. 86, no. 10, pp. 1406-1425, 2006.

[14] T. Kitago and J. W. Krakauer, "Motor learning principles for neurorehabilitation," in *Handbook of clinical neurology*, vol. 110: Elsevier, 2013, pp. 93-103.

[15] K. Y. Nam, H. J. Kim, B. S. Kwon, J.-W. Park, H. J. Lee, and A. Yoo, "Robot-assisted gait training (Lokomat) improves walking function and activity in people with spinal cord injury: a systematic review," *Journal of neuroengineering and rehabilitation*, vol. 14, no. 1, p. 24, 2017.

[16] J. Mehrholz and M. Pohl, "Electromechanical-assisted gait training after stroke: a systematic review comparing end-effector and exoskeleton devices," *J Rehabil Med*, vol. 44, no. 3, pp. 193-9, Mar 2012.

[17] J. Mehrholz, M. Pohl, T. Platz, J. Kugler, and B. Elsner, "Electromechanical and robot‐assisted arm training for improving activities of daily living, arm

function, and arm muscle strength after stroke," *Cochrane Database of Systematic Reviews,* no. 11, 2015.

[18] J. M. Hidler and D. A. Brown, "Robotic Devices for Overground Gait and Balance Training," in *Neurorehabilitation Technology*: Springer, 2012, pp. 397-409.

[19] K. Low, "Robot-assisted gait rehabilitation: From exoskeletons to gait systems," in *2011 Defense Science Research Conference and Expo (DSR)*, 2011, pp. 1-10: IEEE.

[20] W. Huo, S. Mohammed, J. C. Moreno, and Y. Amirat, "Lower limb wearable robots for assistance and rehabilitation: A state of the art," *IEEE systems Journal,* vol. 10, no. 3, pp. 1068-1081, 2016.

[21] W. Meng, Q. Liu, Z. Zhou, Q. Ai, B. Sheng, and S. S. Xie, "Recent development of mechanisms and control strategies for robot-assisted lower limb rehabilitation," *Mechatronics,* vol. 31, pp. 132-145, 2015.

[22] S. Hesse and D. Uhlenbrock, "A mechanized gait trainer for restoration of gait," *Journal of rehabilitation research and development,* vol. 37, no. 6, pp. 701-708, 2000.

[23] H. Schmidt, "HapticWalker-A novel haptic device for walking simulation," in *Proceedings of EuroHaptics,* 2004, vol. 2, pp. 60-67: Citeseer.

[24] H. Yano, S. Tamefusa, N. Tanaka, H. Saitou, and H. Iwata, "Gait rehabilitation system for stair climbing and descending," in *2010 IEEE Haptics Symposium,* 2010, pp. 393-400: IEEE.

[25] J. Yoon, B. Novandy, C.-H. Yoon, and K.-J. Park, "A 6-DOF gait rehabilitation robot with upper and lower limb connections that allows

walking velocity updates on various terrains," *IEEE/ASME Transactions on Mechatronics,* vol. 15, no. 2, pp. 201-215, 2010.

[26] K. Homma, O. Fukuda, J. Sugawara, Y. Nagata, and M. Usuba, "A wire-driven leg rehabilitation system: Development of a 4-DOF experimental system," in *Proceedings 2003 IEEE/ASME International Conference on Advanced Intelligent Mechatronics (AIM 2003)*, 2003, vol. 2, pp. 908-913: IEEE.

[27] G. Abbasnejad, J. Yoon, and H. Lee, "Optimum kinematic design of a planar cable-driven parallel robot with wrench-closure gait trajectory," *Mechanism and Machine Theory,* vol. 99, pp. 1-18, 2016.

[28] V. Bartenbach, K. Schmidt, M. Naef, D. Wyss, and R. Riener, "Concept of a soft exosuit for the support of leg function in rehabilitation," in *2015 IEEE International Conference on Rehabilitation Robotics (ICORR)*, 2015, pp. 125-130: IEEE.

[29] K. Homma, O. Fukuda, and Y. Nagata, "Study of a wire-driven leg rehabilitation system," in *IEEE/RSJ international conference on intelligent robots and systems*, 2002, vol. 2, pp. 1451-1456: IEEE.

[30] Y. Li, Y. Maeda, and M. Hashimoto, "Lightweight, Soft Variable Stiffness Gel Spats for Walking Assistance," *INTERNATIONAL JOURNAL OF ADVANCED ROBOTIC SYSTEMS,* vol. 12, 2015.

[31] A. T. Asbeck, S. M. De Rossi, K. G. Holt, and C. J. Walsh, "A biologically inspired soft exosuit for walking assistance," *The International Journal of Robotics Research,* p. 0278364914562476, 2015.

[32] A. T. Asbeck, R. J. Dyer, A. F. Larusson, and C. J. Walsh, "Biologically-inspired soft exosuit," in *Rehabilitation robotics (ICORR), 2013 IEEE international conference on*, 2013, pp. 1-8: IEEE.

[33] Y. Ding, I. Galiana, A. T. Asbeck, B. Quinlivan, S. M. De Rossi, and C. Walsh, "Multi-joint actuation platform for lower extremity soft exosuits," in *Robotics and automation (ICRA), 2014 IEEE international conference on*, 2014, pp. 1327-1334: IEEE.

[34] R. Bogue, "Exoskeletons and robotic prosthetics: a review of recent developments," *Industrial Robot: An International Journal,* vol. 36, no. 5, pp. 421-427, 2009.

[35] L. Mertz, "The next generation of exoskeletons: Lighter, cheaper devices are in the works," *Pulse, IEEE,* vol. 3, no. 4, pp. 56-61, 2012.

[36] B. Makinson, "Research and development prototype for machine augmentation of human strength and endurance. hardiman i project," DTIC Document1971.

[37] A. B. Zoss, H. Kazerooni, and A. Chu, "Biomechanical design of the Berkeley lower extremity exoskeleton (BLEEX)," *Mechatronics, IEEE/ASME Transactions on,* vol. 11, no. 2, pp. 128-138, 2006.

[38] S. Yu, H. Lee, S. Lee, W. Kim, J. Han, and C.-S. Han, "Design of an under-actuated exoskeleton system for walking assist while load carrying," *Advanced Robotics*, vol. 26, no. 5-6, pp. 561-580, 2012.

[39] W. Kim, H. Lee, D. Kim, J. Han, and C. Han, "Mechanical design of the Hanyang Exoskeleton Assistive Robot (HEXAR)," in *Control, Automation and Systems (ICCAS), 2014 14th International Conference on*, 2014, pp. 479-484: IEEE.

[40] K. Yamamoto, M. Ishii, H. Noborisaka, and K. Hyodo, "Stand alone wearable power assisting suit-sensing and control systems," in *Robot and Human Interactive Communication, 2004. ROMAN 2004. 13th IEEE International Workshop on*, 2004, pp. 661-666: IEEE.

[41] T. Kawabata, H. Satoh, and Y. Sankai, "Working posture control of robot suit HAL for reducing structural stress," in *Robotics and Biomimetics (ROBIO), 2009 IEEE International Conference on*, 2009, pp. 2013-2018: IEEE.

[42] Y. Mori, J. Okada, and K. Takayama, "Development of a standing style transfer system" ABLE" for disabled lower limbs," *Mechatronics, IEEE/ASME Transactions on,* vol. 11, no. 4, pp. 372-380, 2006.

[43] R. J. Farris, H. A. Quintero, and M. Goldfarb, "Preliminary evaluation of a powered lower limb orthosis to aid walking in paraplegic individuals," *Neural Systems and Rehabilitation Engineering, IEEE Transactions on,* vol. 19, no. 6, pp. 652-659, 2011.

[44] D. Sanz-Merodio, M. Cestari, J. C. Arevalo, X. Carrillo, and E. Garcia, "Generation and control of adaptive gaits in lower-limb exoskeletons for motion assistance," *Advanced Robotics,* vol. 28, no. 5, pp. 329-338, 2014.

[45] T.-J. Yeh, M.-J. Wu, T.-J. Lu, F.-K. Wu, and C.-R. Huang, "Control of McKibben pneumatic muscles for a power-assist, lower-limb orthosis," *Mechatronics,* vol. 20, no. 6, pp. 686-697, 2010.

[46] B. Chen *et al.*, "Design of a lower extremity exoskeleton for motion assistance in paralyzed individuals," in *2015 IEEE International Conference on Robotics and Biomimetics (ROBIO)*, 2015, pp. 144-149: IEEE.

[47] K. A. Strausser and H. Kazerooni, "The development and testing of a human machine interface for a mobile medical exoskeleton," in *Intelligent Robots*

and Systems (IROS), 2011 IEEE/RSJ International Conference on, 2011, pp. 4911-4916: IEEE.

[48] A. Esquenazi, M. Talaty, A. Packel, and M. Saulino, "The ReWalk powered exoskeleton to restore ambulatory function to individuals with thoracic-level motor-complete spinal cord injury," *American journal of physical medicine & rehabilitation,* vol. 91, no. 11, pp. 911-921, 2012.

[49] G. Colombo, M. Joerg, R. Schreier, and V. Dietz, "Treadmill training of paraplegic patients using a robotic orthosis," *Journal of rehabilitation research and development,* vol. 37, no. 6, p. 693, 2000.

[50] J. F. Veneman, R. Kruidhof, E. E. Hekman, R. Ekkelenkamp, E. H. Van Asseldonk, and H. Van Der Kooij, "Design and evaluation of the LOPES exoskeleton robot for interactive gait rehabilitation," *Neural Systems and Rehabilitation Engineering, IEEE Transactions on*, vol. 15, no. 3, pp. 379-386, 2007.

[51] R. Riener, "Technology of the robotic gait orthosis Lokomat," in *Neurorehabilitation technology*: Springer, 2016, pp. 395-407.

[52] P. Metrailler, R. Brodard, Y. Stauffer, R. Clavel, and R. Frischknecht, "Cyberthosis: Rehabilitation robotics with controlled electrical muscle stimulation," Sashi S Kommu, Published by I-Tech Education and Publishing2007.

[53] S. Slavnic, A. Leu, D. Ristic-Durrant, and A. Gräser, "Concept of a mobile robot-assisted gait rehabilitation system—Simulation study," in *Intelligent Robots and Systems (IROS), 2010 IEEE/RSJ International Conference on*, 2010, pp. 6022-6027: IEEE.

[54] H. B. Lim, T. P. Luu, K. H. Hoon, and K. Low, "Natural gait parameters prediction for gait rehabilitation via artificial neural network," in *Intelligent Robots and Systems (IROS), 2010 IEEE/RSJ International Conference on*, 2010, pp. 5398-5403: IEEE.

[55] T. P. Luu, K. H. Low, X. Qu, H. B. Lim, and K. H. Hoon, "Hardware Development and Locomotion Control Strategy for an Over-Ground Gait Trainer: NaTUre-Gaits," *Translational Engineering in Health and Medicine, IEEE Journal of,* vol. 2, pp. 1-9, 2014.

[56] S. A. Kolakowsky-Hayner, J. Crew, S. Moran, and A. Shah, "Safety and feasibility of using the Ekso™ bionic exoskeleton to aid ambulation after spinal cord injury," *J Spine,* vol. 4, p. 003, 2013.

[57] I. Díaz, J. J. Gil, and E. Sánchez, "Lower-limb robotic rehabilitation: literature review and challenges," *Journal of Robotics,* vol. 2011, 2011.

[58] S. J. Ball, I. E. Brown, and S. H. Scott, "A planar 3DOF robotic exoskeleton for rehabilitation and assessment," in *Engineering in Medicine and Biology Society, 2007. EMBS 2007. 29th Annual International Conference of the IEEE*, 2007, pp. 4024-4027: IEEE.

[59] S. Christensen and S. Bai, "Kinematic analysis and design of a novel shoulder exoskeleton using a double parallelogram linkage," *Journal of Mechanisms and Robotics,* vol. 10, no. 4, p. 041008, 2018.

[60] E. G. Xydas, L. S. Louca, and A. Mueller, "Analysis and Passive Control of a Four-bar Linkage for the Rehabilitation of Upper-limb Motion," in *ASME 2015 Dynamic Systems and Control Conference*, 2015, pp. V003T42A006-V003T42A006: American Society of Mechanical Engineers.

[61] A. Otten, C. Voort, A. Stienen, R. Aarts, E. van Asseldonk, and H. van der Kooij, "LIMPACT: A hydraulically powered self-aligning upper limb exoskeleton," *IEEE/ASME transactions on mechatronics*, vol. 20, no. 5, pp. 2285-2298, 2015.

[62] J. Ngeo *et al.*, "Control of an optimal finger exoskeleton based on continuous joint angle estimation from EMG signals," in *Engineering in Medicine and Biology Society (EMBC), 2013 35th Annual International Conference of the IEEE*, 2013, pp. 338-341: IEEE.

[63] B. Choi and H. R. Choi, "SKK hand master-hand exoskeleton driven by ultrasonic motors," in *Proceedings. 2000 IEEE/RSJ International Conference on Intelligent Robots and Systems (IROS 2000)(Cat. No. 00CH37113)*, 2000, vol. 2, pp. 1131-1136: IEEE.

[64] M. M. Foumashi, M. Troncossi, and V. P. Castelli, "Design of a new hand exoskeleton for rehabilitation of post-stroke patients," in *Romansy 19–Robot Design, Dynamics and Control*: Springer, 2013, pp. 159-166.

[65] S. K. Banala *et al.*, "Gravity-balancing leg orthosis and its performance evaluation," *Robotics, IEEE Transactions on*, vol. 22, no. 6, pp. 1228-1239, 2006.

[66] K. Kim, M. Kang, Y. Choi, H. Jang, J. Han, and C. Han, "Development of the exoskeleton knee rehabilitation robot using the linear actuator," *International Journal of Precision Engineering and Manufacturing*, vol. 13, no. 10, pp. 1889-1895, 2012.

[67] C. Copilusi, M. Ceccarelli, N. Dumitru, and G. Carbone, "Design and simulation of a leg exoskeleton linkage for a human rehabilitation system," in

The 11th IFToMM international symposium on science of mechanisms and machines, 2014, pp. 117-125: Springer.

[68] A. Bataller, J. Cabrera, M. Clavijo, and J. Castillo, "Evolutionary synthesis of mechanisms applied to the design of an exoskeleton for finger rehabilitation," *Mechanism and Machine Theory*, vol. 105, pp. 31-43, 2016.

[69] E. T. Wolbrecht, D. J. Reinkensmeyer, and A. Perez-Gracia, "Single degree-of-freedom exoskeleton mechanism design for finger rehabilitation," in *Rehabilitation Robotics (ICORR), 2011 IEEE International Conference on*, 2011, pp. 1-6: IEEE.

[70] L. Cui, A. Phan, and G. Allison, "Design and fabrication of a three dimensional printable non-assembly articulated hand exoskeleton for rehabilitation," in *2015 37th Annual International Conference of the IEEE Engineering in Medicine and Biology Society (EMBC)*, 2015, pp. 4627-4630: IEEE.

[71] N. Robson and G. S. Soh, "Geometric design of eight-bar wearable devices based on limb physiological contact task," *Mechanism and Machine Theory*, vol. 100, pp. 358-367, 2016.

[72] D. Giesbrecht, "Design and optimization of a one-degree-of-freedom eight-bar leg mechanism for a walking machine," The University of Manitoba, 2010.

[73] L. Birglen and C. Ruella, "Analysis and optimization of one-degree of freedom robotic legs," *Journal of Mechanisms and Robotics*, vol. 6, no. 4, p. 041004, 2014.

[74] S. Nansai, N. Rojas, M. R. Elara, R. Sosa, and M. Iwase, "On a Jansen leg with multiple gait patterns for reconfigurable walking platforms," *Advances in Mechanical Engineering*, vol. 7, no. 3, p. 1687814015573824, 2015.

[75] H. FUNABASHI, K. OGAWA, Y. GOTOH, and F. KOJIMA, "Synthesis of Leg-Mechanisms of Biped Walking Machines: Part I, Synthesis of Ankle-Path-Generator," *Bulletin of JSME*, vol. 28, no. 237, pp. 537-543, 1985.

[76] H. Funabashi, K. Ogawa, I. Honda, and N. Iwatsuki, "Synthesis of Leg-Mechanisms of Biped Walking Machines: Part II, Synthesis of Foot-Driving Mechanism," *Bulletin of JSME*, vol. 28, no. 237, pp. 544-549, 1985.

[77] K. Deb and S. Tiwari, "Multi-objective optimization of a leg mechanism using genetic algorithms," *Engineering Optimization*, vol. 37, no. 4, pp. 325-350, 2005.

[78] H. Mehdigholi and S. Akbarnejad, "Optimization of Watt's Six-bar Linkage to Generate Straight and Parallel Leg Motion," *International Journal of Advanced Robotic Systems*, vol. 9, 2012.

[79] W. B. O. Al-Araidah, T. Darabseh, S. M. BaniHani, "Conceptual Design of a Single DOF Human-Like Eight-Bar Leg Mechanism," *Jordan Journal of Mechanical and Industrial Engineering*, Journal vol. Volume 5, p. 5, 2011.

[80] W.-B. Shieh, L.-W. Tsai, S. Azarm, and A. Tits, "Multiobjective optimization of a leg mechanism with various spring configurations for force reduction," *Journal of Mechanical Design*, vol. 118, no. 2, pp. 179-185, 1996.

[81] W. B. Shieh, L. W. Tsai, and S. Azarm, "Design and optimization of a one‐degree‐of‐freedom six‐bar leg mechanism for a walking machine," *Journal of Robotic systems*, vol. 14, no. 12, pp. 871-880, 1997.

[82] W. Batayneh, O. Al-Araidah, and S. Malkawi, "Biomimetic Design of a Single DOF Stephenson III Leg Mechanism," *Mechanical Engineering Research,* vol. 3, no. 2, 2013.

[83] S. Nansai, M. R. Elara, and M. Iwase, "Dynamic analysis and modeling of Jansen mechanism," *Procedia Engineering*, vol. 64, pp. 1562-1571, 2013.

[84] K. Komoda and H. Wagatsuma, "A proposal of the extended mechanism for theo jansen linkage to modify the walking elliptic orbit and a study of cyclic base function," in *Proceedings of the 7th Annual Dynamic Walking Conference (DWC'12)*, 2012.

[85] C. Liang, M. Ceccarelli, and Y. Takeda, "Operation analysis of a one-DOF pantograph leg mechanisms," *Proceedings of the RAAD,* pp. 15-17, 2008.

[86] D. G. Olson, A. G. Erdman, and D. R. Riley, "A systematic procedure for type synthesis of mechanisms with literature review literaturbe-sprechung," *Mechanism and Machine Theory*, vol. 20, no. 4, pp. 285-295, 1985.

[87] F. Buchsbaum and F. Freudenstein, "Synthesis of kinematic structure of geared kinematic chains and other mechanisms," *Journal of mechanisms*, vol. 5, no. 3, pp. 357-392, 1970.

[88] F. Freudenstein and L. Dobjansky, "Some applications of graph theory to the structural analysis of mechanisms," *ASME Transaction Journal of Engineering for Industry,* vol. 89, no. 1, pp. 153-158, 1967.

[89] H. Ding, F. Hou, A. Kecskeméthy, and Z. Huang, "Synthesis of the whole family of planar 1-DOF kinematic chains and creation of their atlas database," *Mechanism and Machine Theory,* vol. 47, pp. 1-15, 2012.

[90] N. Manolescu, "A method based on Baranov trusses, and using graph theory to find the set of planar jointed kinematic chains and mechanisms," *Mechanism and Machine Theory,* vol. 8, no. 1, pp. 3-22, 1973.

[91] I. Popescu and D. B. Marghitu, "Structural design of planar mechanisms with dyads," *Multibody System Dynamics,* vol. 19, no. 4, pp. 407-425, 2008.

[92] C. Zhang, P. R. Norton, and T. Hammonds, "Optimization of parameters for specified path generation using an atlas of coupler curves of geared five-bar linkages," *Mechanism and machine theory,* vol. 19, no. 6, pp. 459-466, 1984.

[93] J.-W. Kim, T. Seo, and J. Kim, "A new design methodology for four-bar linkage mechanisms based on derivations of coupler curve," *Mechanism and Machine Theory,* vol. 100, pp. 138-154, 2016.

[94] F. Freudenstein, "Approximate Synthesis of Four-Bar Linkages*[1, 2]," *Resonance,* 2010.

[95] A. Kunjur and S. Krishnamurty, "Genetic algorithms in mechanism synthesis," *Journal of Applied Mechanisms and Robotics,* vol. 4, no. 2, pp. 18-24, 1997.

[96] A. G. Erdman, "Three and four precision point kinematic synthesis of planar linkages," *Mechanism and Machine Theory,* vol. 16, no. 3, pp. 227-245, 1981.

[97] F. Freudenstein, "Approximate synthesis of four-bar linkages," *Resonance,* vol. 15, no. 8, pp. 740-767, 2010.

[98] F. Y. Chen, "Algebraic synthesis of a class of four-bar linkages and their equivalent mechanisms," *Journal of Mechanisms,* vol. 6, no. 2, pp. 213-230, 1971.

[99] F. Y. Chen, "An analytical method for synthesizing the four-bar crank-rocker mechanism," *Journal of Engineering for Industry*, vol. 91, no. 1, pp. 45-54, 1969.

[100] E. Pennestrì and P. P. Valentini, "A review of simple analytical methods for the kinematic synthesis of four-bar and slider-crank function generators for two and three prescribed finite positions," *Buletin Stiintific Seria Mecanica Aplicata; University of Pitesti: Pites, ti, Romania,* pp. 128-143, 2009.

[101] C. McLarnan, "Synthesis of six-link plane mechanisms by numerical analysis," *Journal of Engineering for Industry*, vol. 85, no. 1, pp. 5-10, 1963.

[102] C.-F. Chang and W.-M. Hwang, "Kinematic synthesis of Watt-I mechanisms generating closed coupler curves with up to four cusps," *Mechanism and machine theory,* vol. 29, no. 4, pp. 501-511, 1994.

[103] K. Watanabe and H. Katoh, "Identification of motion domains of planar six-link mechanisms of the Stephenson-type," *Mechanism and Machine Theory*, vol. 39, no. 10, pp. 1081-1099, 2004.

[104] C. Chen and J. Angeles, "Kinematic Synthesis of an eight bar linkage to visit eleven poses exactly," in *International Federation for the Promotion of Mechanism and Machine Science World Congress (IFToMM 2007),* 2007, pp. 1-6: International Federation for the promotion of mechanism and machine science.

[105] G. Cui and J. Han, "The solution region-based synthesis methodology for a 1-DOF eight-bar linkage," *Mechanism and Machine Theory,* vol. 98, pp. 231-241, 2016.

[106] J. B. Rosen, "The gradient projection method for nonlinear programming. Part I. Linear constraints," *Journal of the society for industrial and applied mathematics,* vol. 8, no. 1, pp. 181-217, 1960.

[107] J. Rosen, "The gradient projection method for nonlinear programming. Part II. Nonlinear constraints," *Journal of the Society for Industrial and Applied Mathematics,* vol. 9, no. 4, pp. 514-532, 1961.

[108] P. Wolfe, "Recent developments in nonlinear programming," in *Advances in computers*, vol. 3: Elsevier, 1962, pp. 155-187.

[109] J. C. Oliva and E. D. Goodman, "Simultaneous Type and Dimensional Synthesis of Planar 1DOF Mechanisms Using Evolutionary Search and Convertible Agents (DETC2009-86722)," *Journal of Mechanisms and Robotics,* vol. 2, no. 3, p. 031001, 2010.

[110] J. Cabrera, F. Nadal, J. Munoz, and A. Simon, "Multiobjective constrained optimal synthesis of planar mechanisms using a new evolutionary algorithm," *Mechanism and machine theory,* vol. 42, no. 7, pp. 791-806, 2007.

[111] S. Acharyya and M. Mandal, "Performance of EAs for four-bar linkage synthesis," *Mechanism and Machine Theory,* vol. 44, no. 9, pp. 1784-1794, 2009.

[112] R. R. Bulatović and S. R. Dordević, "On the optimum synthesis of a four-bar linkage using differential evolution and method of variable controlled deviations," *Mechanism and Machine Theory,* vol. 44, no. 1, pp. 235-246, 2009.

[113] P. Shiakolas, D. Koladiya, and J. Kebrle, "On the optimum synthesis of four-bar linkages using differential evolution and the geometric centroid of

precision positions," *Inverse Problems in Engineering,* vol. 10, no. 6, pp. 485-502, 2002.

[114] J. Cabrera, A. Simon, and M. Prado, "Optimal synthesis of mechanisms with genetic algorithms," *Mechanism and machine theory,* vol. 37, no. 10, pp. 1165-1177, 2002.

[115] G. Renner and A. Ekárt, "Genetic algorithms in computer aided design," *Computer-Aided Design,* vol. 35, no. 8, pp. 709-726, 2003.

[116] A. Wall and T. Board, "The biological effect of continuous passive motion on the healing of full-thickness defects in articular cartilage. An experimental investigation in the rabbit," in *Classic Papers in Orthopaedics*: Springer, 2014, pp. 437-439.

[117] R. B. Salter *et al.,* "Clinical application of basic research on continuous passive motion for disorders and injuries of synovial joints: a preliminary report of a feasibility study," *Journal of orthopaedic research,* vol. 1, no. 3, pp. 325-342, 1983.

[118] P. J. Mcnair, E. W. Dombroski, D. J. Hewson, and S. N. Stanley, "Stretching at the ankle joint: viscoelastic responses to holds and continuous passive motion," *Medicine & Science in Sports & Exercise,* vol. 33, no. 3, pp. 354-358, 2001.

[119] X. L. Hu, K.-y. Tong, R. Song, X. J. Zheng, and W. W. Leung, "A comparison between electromyography-driven robot and passive motion device on wrist rehabilitation for chronic stroke," *Neurorehabilitation and Neural Repair,* vol. 23, no. 8, pp. 837-846, 2009.

[120] T. Breen, R. Gelberman, and G. Ackerman, "Elbow flexion contractures: treatment by anterior release and continuous passive motion," *Journal of Hand Surgery,* vol. 13, no. 3, pp. 286-287, 1988.

[121] U. Dundar, H. Toktas, T. Cakir, D. Evcik, and V. Kavuncu, "Continuous passive motion provides good pain control in patients with adhesive capsulitis," *International Journal of Rehabilitation Research,* vol. 32, no. 3, pp. 193-198, 2009.

[122] R. Garofalo, M. Conti, A. Notarnicola, L. Maradei, A. Giardella, and A. Castagna, "Effects of one-month continuous passive motion after arthroscopic rotator cuff repair: results at 1-year follow-up of a prospective randomized study," *Musculoskeletal surgery,* vol. 94, no. 1, pp. 79-83, 2010.

[123] B. G. Lee, N. S. Cho, and Y. G. Rhee, "Effect of two rehabilitation protocols on range of motion and healing rates after arthroscopic rotator cuff repair: aggressive versus limited early passive exercises," *Arthroscopy: The Journal of Arthroscopic & Related Surgery,* vol. 28, no. 1, pp. 34-42, 2012.

[124] J. Dent, "Continuous passive motion in hand rehabilitation," *Prosthetics and orthotics international,* vol. 17, no. 2, pp. 130-135, 1993.

[125] T. B. Thien, J. H. Becker, and J. C. Theis, "Rehabilitation after surgery for flexor tendon injuries in the hand," *Cochrane Database of Systematic Reviews,* no. 4, 2004.

[126] J. W. Strickland and S. V. Glogovac, "Digital function following flexor tendon repair in zone II: a comparison of immobilization and controlled passive motion techniques," *The Journal of hand surgery,* vol. 5, no. 6, pp. 537-543, 1980.

[127] D. Lynch, M. Ferraro, J. Krol, C. M. Trudell, P. Christos, and B. T. Volpe, "Continuous passive motion improves shoulder joint integrity following stroke," *Clinical rehabilitation,* vol. 19, no. 6, pp. 594-599, 2005.

[128] Y.-J. Chang, C.-Y. Fang, M.-J. Hsu, H.-Y. Lien, and M.-K. Wong, "Decrease of hypertonia after continuous passive motion treatment in individuals with spinal cord injury," *Clinical rehabilitation,* vol. 21, no. 8, pp. 712-718, 2007.

[129] Y.-J. Chang, J.-N. Liang, M.-J. Hsu, H.-Y. Lien, C.-Y. Fang, and C.-H. Lin, "Effects of continuous passive motion on reversing the adapted spinal circuit in humans with chronic spinal cord injury," *Archives of physical medicine and rehabilitation,* vol. 94, no. 5, pp. 822-828, 2013.

[130] W. van Dijk and H. Van der Kooij, "XPED2: A passive exoskeleton with artificial tendons," *Robotics & Automation Magazine, IEEE,* vol. 21, no. 4, pp. 56-61, 2014.

[131] H. J. Ralston, "Energy-speed relation and optimal speed during level walking," *European Journal of Applied Physiology and Occupational Physiology,* vol. 17, no. 4, pp. 277-283, 1958.

[132] M. Srinivasan and A. Ruina, "Computer optimization of a minimal biped model discovers walking and running," *Nature,* vol. 439, no. 7072, pp. 72-75, 2006.

[133] J. Maxwell Donelan, R. Kram, and K. Arthur D, "Mechanical and metabolic determinants of the preferred step width in human walking," *Proceedings of the Royal Society of London. Series B: Biological Sciences,* vol. 268, no. 1480, pp. 1985-1992, 2001.

[134] J. E. Bertram and A. Ruina, "Multiple walking speed–frequency relations are predicted by constrained optimization," *Journal of theoretical Biology*, vol. 209, no. 4, pp. 445-453, 2001.

[135] M. Zarrugh, F. Todd, and H. Ralston, "Optimization of energy expenditure during level walking," *European Journal of Applied Physiology and Occupational Physiology*, vol. 33, no. 4, pp. 293-306, 1974.

[136] K. Sasaki and R. R. Neptune, "Muscle mechanical work and elastic energy utilization during walking and running near the preferred gait transition speed," *Gait & posture,* vol. 23, no. 3, pp. 383-390, 2006.

[137] A. J. Van den Bogert, "Exotendons for assistance of human locomotion," *Biomedical engineering online,* vol. 2, no. 17, pp. 1-8, 2003.

[138] S. H. Collins, M. B. Wiggin, and G. S. Sawicki, "Reducing the energy cost of human walking using an unpowered exoskeleton," *Nature,* vol. 522, no. 7555, pp. 212-5, Jun 11 2015.

[139] A. Valiente, "Design of a quasi-passive parallel leg exoskeleton to augment load carrying for walking," DTIC Document2005.

[140] C. J. Walsh, K. Endo, and H. Herr, "A quasi-passive leg exoskeleton for load-carrying augmentation," *International Journal of Humanoid Robotics,* vol. 4, no. 03, pp. 487-506, 2007.

[141] L. Roussel, C. Canudas-de-Wit, and A. Goswami, "Generation of energy optimal complete gait cycles for biped robots," in *Proceedings. 1998 IEEE International Conference on Robotics and Automation (Cat. No. 98CH36146)*, 1998, vol. 3, pp. 2036-2041: IEEE.

[142] C. Chevallereau, A. Formal'Sky, and B. Perrin, "Low energy cost reference trajectories for a biped robot," in *Proceedings. 1998 IEEE International*

Conference on Robotics and Automation (Cat. No. 98CH36146), 1998, vol. 2, pp. 1398-1404: IEEE.

[143] F. C. Anderson and M. G. Pandy, "Static and dynamic optimization solutions for gait are practically equivalent," *Journal of biomechanics,* vol. 34, no. 2, pp. 153-161, 2001.

[144] F. C. Anderson and M. G. Pandy, "Dynamic optimization of human walking," *Journal of biomechanical engineering,* vol. 123, no. 5, pp. 381-390, 2001.

[145] M. De Zee, M. Lund, C. Schwartz, C. Olesen, and J. Rasmussen, "Validation of musculoskeletal models: the importance of trend validations," 2010.

[146] S. L. Delp and J. P. Loan, "A graphics-based software system to develop and analyze models of musculoskeletal structures," *Computers in biology and medicine,* vol. 25, no. 1, pp. 21-34, 1995.

[147] S. L. Delp *et al.*, "OpenSim: open-source software to create and analyze dynamic simulations of movement," *IEEE transactions on biomedical engineering,* vol. 54, no. 11, pp. 1940-1950, 2007.

[148] J. Muller, "Simulating in-vivo tibiofemoral loads with the aid of a customised Life-Modeler musculoskeletal system," in *ASME 2012 Summer Bioengineering Conf*, 2012, pp. 195-196.

[149] Y. Xiang *et al.*, "Predictive dynamics: an optimization-based novel approach for human motion simulation," *Structural and Multidisciplinary Optimization,* vol. 41, no. 3, pp. 465-479, 2010.

[150] A. Murray and P. Larochelle, "A classification scheme for planar 4r, spherical 4r, and spatial rccc linkages to facilitate computer animation," *ASME Paper No. DETC98/MECH-5887,* 1998.

[151] Z. Shen, G. Allison, and L. Cui, "An Integrated Type and Dimensional Synthesis Method to Design One Degree-of-Freedom Planar Linkages With Only Revolute Joints for Exoskeletons," *Journal of Mechanical Design,* vol. 140, no. 9, p. 092302, 2018.

[152] D. A. Winter, *Biomechanics and motor control of human movement*. John Wiley & Sons, 2009.

[153] G. Bovi, M. Rabuffetti, P. Mazzoleni, and M. Ferrarin, "A multiple-task gait analysis approach: kinematic, kinetic and EMG reference data for healthy young and adult subjects," *Gait & posture,* vol. 33, no. 1, pp. 6-13, 2011.

[154] M. P. Murray, A. B. Drought, and R. C. Kory, "Walking patterns of normal men," *J Bone Joint Surg Am,* vol. 46, no. 2, pp. 335-360, 1964.

[155] D. A. Winter, "Biomechanical motor patterns in normal walking," *Journal of motor behavior,* vol. 15, no. 4, pp. 302-330, 1983.

[156] P. De Leva, "Adjustments to Zatsiorsky-Seluyanov's segment inertia parameters," *Journal of biomechanics,* vol. 29, no. 9, pp. 1223-1230, 1996.

[157] OpenSim, "OpenSim Core Models," 2019.

[158] C. J. Walsh, K. Pasch, and H. Herr, "An autonomous, underactuated exoskeleton for load-carrying augmentation," in *Intelligent Robots and Systems, 2006 IEEE/RSJ International Conference on*, 2006, pp. 1410-1415: IEEE.

[159] P. Malcolm, W. Derave, S. Galle, and D. De Clercq, "A simple exoskeleton that assists plantarflexion can reduce the metabolic cost of human walking," *PloS one,* vol. 8, no. 2, p. e56137, 2013.

[160] P.-C. Kao, C. L. Lewis, and D. P. Ferris, "Invariant ankle moment patterns when walking with and without a robotic ankle exoskeleton," *Journal of biomechanics*, vol. 43, no. 2, pp. 203-209, 2010.

[161] L. Biagiotti and C. Melchiorri, *Trajectory planning for automatic machines and robots*. Springer Science & Business Media, 2008.

[162] K. Abdel-Malek and J. S. Arora, *Human Motion Simulation: Predictive Dynamics*. Academic Press, 2013.

Appendix: Author Contribution Statements and Publisher Permissions

Author Contribution Statements

A. Z. Shen, G. Allison, and L. Cui, "An Integrated Type and Dimensional Synthesis Method to Design One Degree-of-Freedom Planar Linkages With Only Revolute Joints for Exoskeletons," *Journal of Mechanical Design*, vol. 140, no. 9, p. 092302, 2018.

Authors and full affiliations:

	Conception & design	**Theoretical study & programming**	**Prototype development & validation**	**Manuscript Writing, revision, and finalisation**
Garry Allison	☒	☒	☒	☒
I acknowledge that Zefang Shen made above contributions in this paper and agree that the paper can be incorporated as part of his thesis. Signature:				
Lei Cui	☒	☒	☒	☒
I acknowledge that Zefang Shen made above contributions in this paper and agree that the paper can be incorporated as part of his thesis. Signature:				

B. Z. Shen, S. Sam, G. Allison, and L. Cui, "A Simulation-Based Study on a Clutch-Spring Mechanism Reducing Human Walking Metabolic Cost," *International Journal Of Mechanical Engineering And Robotics Research*, vol. 7, no. 1, pp. 55-60, 2018.

Authors and full affiliations:

<table>
<tr><th></th><th>Conception & design</th><th>Theoretical study & optimization</th><th>Interpretation & discussion</th><th>Manuscript Writing, revision, and finalisation</th></tr>
<tr><td>Scott Sam</td><td>☒</td><td>☒</td><td>☒</td><td>☒</td></tr>
<tr><td colspan="5">I acknowledge that Zefang Shen made above contributions in this paper and agree that the paper can be incorporated as part of his thesis.

Signature:</td></tr>
<tr><td>Garry Allison</td><td>☒</td><td>☒</td><td>☒</td><td>☒</td></tr>
<tr><td colspan="5">I acknowledge that Zefang Shen made above contributions in this paper and agree that the paper can be incorporated as part of his thesis.

Signature:</td></tr>
<tr><td>Lei Cui</td><td>☒</td><td>☒</td><td>☒</td><td>☒</td></tr>
<tr><td colspan="5">I acknowledge that Zefang Shen made above contributions in this paper and agree that the paper can be incorporated as part of his thesis.

Signature:</td></tr>
</table>

C. Z. Shen, T. Tan, G. Allison, and L. Cui, "A Customized One-Degree-of-Freedom Linkage Based Leg Exoskeleton for Continuous Passive Motion Rehabilitation," in *The International Conference of IFToMM ITALY*, 2018, pp. 518-526: Springer.

Authors and full affiliations:

	Conception and design	**Theoretical study & programming**	**Prototype development & validation**	**Manuscript Writing, revision, and finalisation**
Tele Tan	☒	☒	☒	☒
I acknowledge that Zefang Shen made above contributions in this paper and agree that the paper can be incorporated as part of his thesis. Signature:				
Garry Allison	☒	☒	☒	☒
I acknowledge that Zefang Shen made above contributions in this paper and agree that the paper can be incorporated as part of his thesis. Signature:				
Lei Cui	☒	☒	☒	☒
I acknowledge that Zefang Shen made above contributions in this paper and agree that the paper can be incorporated as part of his thesis. Signature:				

Zefang Shen

From: Beth Darchi <DarchiB@asme.org>
Sent: Saturday, 18 May 2019 3:19 AM
To: Zefang Shen
Subject: RE: Include paper in Thesis

Dear Mr. Shen,
It is our pleasure to grant you permission to use **all or any part of** the ASME paper "An Integrated Type and Dimensional Synthesis Method to Design One Degree-of-Freedom Planar Linkages With Only Revolute Joints for Exoskeletons," by Zefang Shen, Garry Allison and Lei Cui, J. Mech. Des 140(9), 2018, cited in your letter for inclusion in a PhD. Thesis entitled Design and development of a 1-degree-of-freedom leg exoskeleton for rehabilitation to be published by Curtin University.

Permission is granted for the specific use as stated herein and does not permit further use of the materials without proper authorization. Proper attribution must be made to the author(s) of the materials. **Please note**: if any or all of the figures and/or Tables are of another source, permission should be granted from that outside source or include the reference of the original source. ASME does not grant permission for outside source material that may be referenced in the ASME works.

As is customary, we request that you ensure full acknowledgment of this material, the author(s), source and ASME as original publisher. Acknowledgment must be retained on all pages where figure is printed and distributed.

Many thanks for your interest in ASME publications.

Sincerely,

Beth Darchi
Publishing Administrator
ASME
2 Park Avenue
New York, NY 10016-5990
Tel 1.212.591.7700
darchib@asme.org

From: Zefang Shen [mailto:zefang.shen@postgrad.curtin.edu.au]
Sent: Thursday, May 16, 2019 11:49 AM
To: permissions@asme.org
Cc: Beth Darchi <DarchiB@asme.org>
Subject: RE: Include paper in Thesis

Hi,

Can you please help me with the permission to use my published paper in my PhD thesis?
The following is the filled **PUBLICATIONS PERMISSION REQUEST FORM.**

Many thanks for your time.

ASME Publication Title

(Conference/Journal/Book)*: Journal of Mechanical

Design

Complete List of ASME Authors*: Zefang Shen,

Garry Allison, Lei Cui

ASME Paper Title (Conference or Journal) *: An Integrated Type and Dimensional Synthesis Method to Design One Degree-of-Freedom Planar Linkages With Only Revolute Joints for Exoskeletons

(Journal) paper number *: MD-18-1008

Volume Number: Vol. 140

DOI Number: 10.1115/1.4040486

Indicate Page(s) in the ASME publication: 092302

Year of Publication*: 2018

Usage (Please check box): ☐ Print ☒ Academic ☐ Online ☐ Intranet

Title of outside publication / Thesis*: Design and development of a 1-degree-of-freedom leg exoskeleton for rehabilitation

Outside Publisher or University*: Curtin University

Explanation of Usage: Including the paper in my PhD. Thesis

First Name*: Zefang
Last Name*: Shen
Address Line 1*: Kent Street, Bentley

Address Line 2: City*:

Perth
State*: WA

Zip *: 6102

Email*:
zefang.shen@postgrad.curtin.edu.au

Regards
Zefang

From: Beth Darchi <DarchiB@asme.org>
Sent: Thursday, May 16, 2019 11:11 PM
To: Zefang Shen <zefang.shen@postgrad.curtin.edu.au>
Subject: FW: Include paper in Thesis

In order for us to address permission requests to use ASME material, please be sure to fill out all required fields (*) to complete the form. Please send the form to permissions@asme.org.

Upon receipt of this form, I will be happy to give this matter my immediate attention and consideration.

ASME CONFERENCE/JOURNAL /BOOKS PUBLICATIONS PERMISSION REQUEST FORM:
*Please **TYPE** in all required fields. Please do not write in.

ASME Publication Title (Conference/Journal/Book)*:

Complete List of ASME Authors*:

ASME Paper Title (Conference or Journal) *:

Conference Paper Number (if conference)*:
(Journal) paper number *:
Volume Number
DOI Number:
Indicate Page(s) in the ASME publication:
Year of Publication*:
List ASME Figure Numbers:
List ASME Table Numbers:
Number of Copies:

Usage (Please check box): ☐ **Print** ☐ **Academic** ☐ **Online** ☐ **Intranet**

Title of outside publication / Thesis*:

Outside Publisher or University*:

Explanation of Usage:

First Name*:
Last Name*:
Address Line 1*:

Address Line

2: City*:
State*:
Zip*:
Phone:
Fax:
Email*:

Regards,

Beth Darchi
Publishing Administrator
ASME
2 Park Avenue
New York, NY 10016-5990
Tel 1.212.591.7700
darchib@asme.org

Begin forwarded message:

From: Zefang Shen <zefang.shen@postgrad.curtin.edu.au>
Subject: Include paper in Thesis
Date: May 16, 2019 at 2:02:39 AM EDT
To: "assistant@asmejmd.org" <assistant@asmejmd.org>

Hi,

I would like to enquire if I can include my published paper in my thesis?
Do I need permission from the Journal/publisher? And how can I get the permissions if the permission is needed?

Here is my published work in JMD.

Z. Shen, G. Allison, and L. Cui, "An Integrated Type and Dimensional Synthesis Method to Design One Degree-of-Freedom Planar Linkages With Only Revolute Joints for Exoskeletons," *Journal of Mechanical Design,* vol. 140, no. 9, p. 092302, 2018.

Many thanks for your time.

Regards

Zefang

Zefang Shen

From: ijmerr <ijmerr@ejournal.net>
Sent: Thursday, 16 May 2019 2:29 PM
To: Zefang Shen
Subject: Re:Include papers in Thesis

Dear Zefang Shen,

Thanks for your support to IJMERR. Since the journal is open-access, you could archive the paper through our website. Please cite IJMERR as reference source in your thesis.

--
Warm Regards,
--
Shira W. Lu
IJMERR Associate Executive Editor
Email: ijmerr@ejournal.net; Website: http://www.ijmerr.com

在2019-05-16，Zefang Shen <zefang.shen@postgrad.curtin.edu.au> 写道:

-----原始邮件-----

发件人: Zefang Shen <zefang.shen@postgrad.curtin.edu.au>

发送时间: 2019年5月16日 星期四

收件人: "ijmerr@ejournal.net" <ijmerr@ejournal.net>

主题: Include papers in Thesis

Hi,

I would like to enquire if I can include my published paper in my thesis?

Do I need permission from the Journal/publisher? And how can I get the permissions if the permission is needed?

Here is my published work in IJMERR.

Z. Shen, S. Sam, G. Allison, and L. Cui, "A Simulation-Based Study on a Clutch-Spring Mechanism Reducing Human Walking Metabolic Cost," *International Journal Of Mechanical Engineering And Robotics Research,* vol. 7, no. 1, pp. 55-60, 2018.

Many thanks for your time.

SPRINGER NATURE LICENSE TERMS AND CONDITIONS

May 16, 2019

This Agreement between Zefang Shen ("You") and Springer Nature ("Springer Nature") consists of your license details and the terms and conditions provided by Springer Nature and Copyright Clearance Center.

License Number	4590640552249
License date	May 16, 2019
Licensed Content Publisher	Springer Nature
Licensed Content Publication	Springer eBook
Licensed Content Title	A Customized One-Degree-of-Freedom Linkage Based Leg Exoskeleton for Continuous Passive Motion Rehabilitation
Licensed Content Author	Zefang Shen, Tele Tan, Garry Allison et al
Licensed Content Date	Jan 1, 2019
Type of Use	Thesis/Dissertation
Requestor type	academic/university or research institute
Format	electronic
Portion	full article/chapter
Will you be translating?	no
Circulation/distribution	<501
Author of this Springer Nature content	yes
Title	design and development of a 1-degree-of-freedom leg exoskeleton for rehabilitation
Institution name	Curtin University
Expected presentation date	May 2019
Requestor Location	Zefang Shen Curtin University Bentley, Perth WA Bentley, Perth, WA 6102 Australia Attn:
Total	0.00 AUD
Terms and Conditions	

Springer Nature Terms and Conditions for RightsLink Permissions

Springer Nature Customer Service Centre GmbH (the Licensor) hereby grants you a non-exclusive, world-wide licence to reproduce the material and for the purpose and requirements specified in the attached copy of your order form, and for no other use, subject to the conditions below:

1. The Licensor warrants that it has, to the best of its knowledge, the rights to license reuse of this material. However, you should ensure that the material you are requesting is original to the Licensor and does not carry the copyright of another entity (as credited in the published version).

   If the credit line on any part of the material you have requested indicates that it was

reprinted or adapted with permission from another source, then you should also seek permission from that source to reuse the material.

2. Where **print only** permission has been granted for a fee, separate permission must be obtained for any additional electronic re-use.

3. Permission granted **free of charge** for material in print is also usually granted for any electronic version of that work, provided that the material is incidental to your work as a whole and that the electronic version is essentially equivalent to, or substitutes for, the print version.

4. A licence for 'post on a website' is valid for 12 months from the licence date. This licence does not cover use of full text articles on websites.

5. Where **'reuse in a dissertation/thesis'** has been selected the following terms apply: Print rights of the final author's accepted manuscript (for clarity, NOT the published version) for up to 100 copies, electronic rights for use only on a personal website or institutional repository as defined by the Sherpa guideline (www.sherpa.ac.uk/romeo/).

6. Permission granted for books and journals is granted for the lifetime of the first edition and does not apply to second and subsequent editions (except where the first edition permission was granted free of charge or for signatories to the STM Permissions Guidelines http://www.stm-assoc.org/copyright-legal-affairs/permissions/permissions-guidelines/), and does not apply for editions in other languages unless additional translation rights have been granted separately in the licence.

7. Rights for additional components such as custom editions and derivatives require additional permission and may be subject to an additional fee. Please apply to Journalpermissions@springernature.com/bookpermissions@springernature.com for these rights.

8. The Licensor's permission must be acknowledged next to the licensed material in print. In electronic form, this acknowledgement must be visible at the same time as the figures/tables/illustrations or abstract, and must be hyperlinked to the journal/book's homepage. Our required acknowledgement format is in the Appendix below.

9. Use of the material for incidental promotional use, minor editing privileges (this does not include cropping, adapting, omitting material or any other changes that affect the meaning, intention or moral rights of the author) and copies for the disabled are permitted under this licence.

10. Minor adaptations of single figures (changes of format, colour and style) do not require the Licensor's approval. However, the adaptation should be credited as shown in Appendix below.

Appendix — Acknowledgements:

For Journal Content:
Reprinted by permission from [**the Licensor**]: [**Journal Publisher** (e.g. Nature/Springer/Palgrave)] [**JOURNAL NAME**] [**REFERENCE CITATION** (Article name, Author(s) Name), [**COPYRIGHT**] (year of publication)

For **Advance Online Publication papers:**
Reprinted by permission from [**the Licensor**]: [**Journal Publisher** (e.g. Nature/Springer/Palgrave)] [**JOURNAL NAME**] [**REFERENCE CITATION** (Article name, Author(s) Name), [**COPYRIGHT**] (year of publication), advance online publication, day month year (doi: 10.1038/sj.[JOURNAL ACRONYM].)

For Adaptations/Translations:
Adapted/Translated by permission from [**the Licensor**]: [**Journal Publisher** (e.g.

Nature/Springer/Palgrave)] [**JOURNAL NAME**] [**REFERENCE CITATION** (Article name, Author(s) Name), [**COPYRIGHT**] (year of publication)

Note: For any republication from the British Journal of Cancer, the following credit line style applies:

Reprinted/adapted/translated by permission from [**the Licensor**]: on behalf of Cancer Research UK: : [**Journal Publisher** (e.g. Nature/Springer/Palgrave)] [**JOURNAL NAME**] [**REFERENCE CITATION** (Article name, Author(s) Name), [**COPYRIGHT**] (year of publication)

For **Advance Online Publication** papers:
Reprinted by permission from The [**the Licensor**]: on behalf of Cancer Research UK: [**Journal Publisher** (e.g. Nature/Springer/Palgrave)] [**JOURNAL NAME**] [**REFERENCE CITATION** (Article name, Author(s) Name), [**COPYRIGHT**] (year of publication), advance online publication, day month year (doi: 10.1038/sj. [JOURNAL ACRONYM])

For Book content:
Reprinted/adapted by permission from [**the Licensor**]: [**Book Publisher** (e.g. Palgrave Macmillan, Springer etc) [**Book Title**] by [**Book author**(s)] [**COPYRIGHT**] (year of publication)

Other Conditions:

Version 1.1